FORSCHUNGSZENTRUM ROSSENDORF
Mitglied der Wissenschaftsgemeinschaft Gottfried Wilhelm Leibniz

WISSENSCHAFTLICH-TECHNISCHE BERICHTE
FZR-362
Januar 2003
ISSN 1437-322X

Institute of Ion Beam Physics and Materials Research

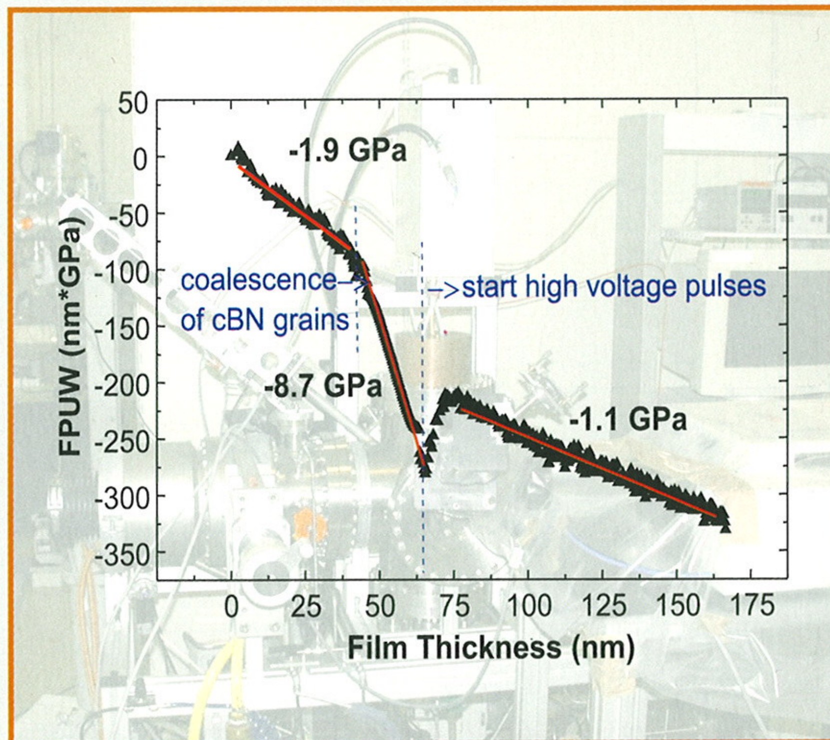

Annual Report 2002

FORSCHUNGSZENTRUM ROSSENDORF
Mitglied der Wissenschaftsgemeinschaft Gottfried Wilhelm Leibniz

WISSENSCHAFTLICH-TECHNISCHE BERICHTE
FZR-362
January 2003

Annual Report 2002

Institut für Ionenstrahlphysik und Materialforschung

Editors:

J. von Borany, M. Helm, H.-U. Jäger,
W. Möller, E. Wieser

Bibliothek FZ Rossendorf

01259339

Preface

The Forschungszentrum Rossendorf (FZR) represents the largest governmental research institution in the "new" states of the Federal Republic of Germany, with R&D activities in the fields of the structure of matter, life sciences, and environment and safety. Its presently about 600 employees are organized in five institutes. FZR is a member of the "Leibniz Society" (WGL), with the federal government and the state of Saxony each contributing 50 % of the basic funding.

The Institute of Ion Beam Physics and Materials Research (IIM) employs more than 100 scientists, engineers, technicians and PhD and diploma students. The institute combines basic research and application-oriented studies in the fields of ion beam applications to materials and semiconductor research. The institute constitutes a national and international ion beam center, which, in addition to its own scientific activities, offers services and transfers know-how on ion beam techniques to universities, other research institutes, and industry.

For these purposes, a broad range of ion-related equipment is available, delivering ions with energies from about 10 eV (plasma treatment) to several 10 MeV (electrostatic accelerators), which are used for thin film synthesis, modification and analysis. In 2002, the focused ion beam has been upgraded with a new column, which will enable focusing to few tens of nm for a large number of different ions. For the diagnostics of ion-treated surfaces, other standard analytical techniques are available such as transmission electron microscopy, X-ray diffraction, Auger and photoelectron spectroscopy, and a number of chemical, mechanical, electrical and optical diagnostics. The latter facilities have been expanded recently to enable various kinds of ultrafast and stationary optical investigations over a wide frequency range. Exciting new possibilities will be soon provided by the infrared free-electron laser, which is presently under construction at the FZR. Sample processing is routinely done in a class 100 clean-room.

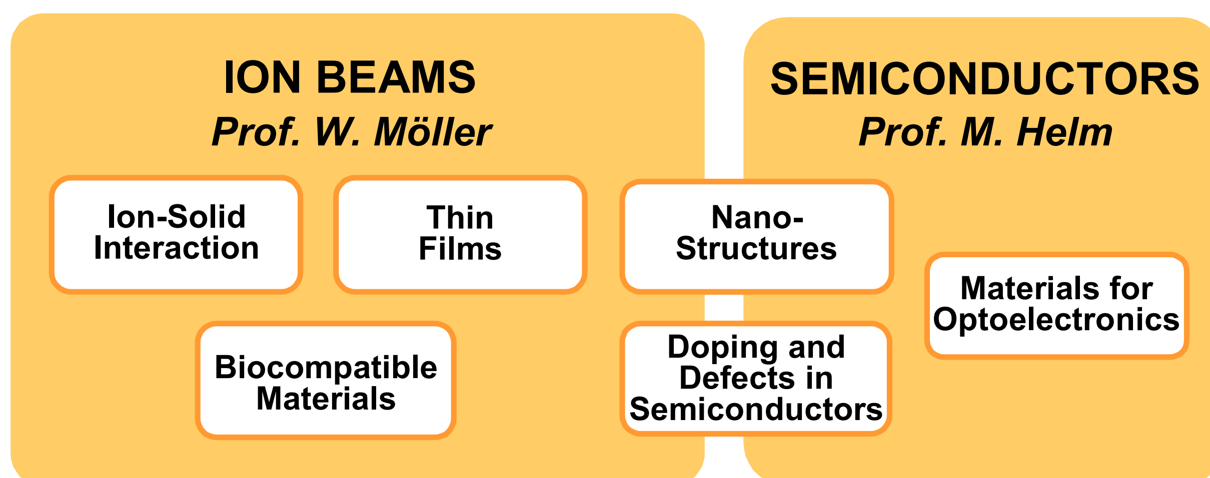

The diagram displays the main R&D activities of the institute. It is the purpose of the present Annual Report to document its scientific progress in 2002 by a few selected extended contributions, numerous short contributions, and a statistical overview on publications, conference contributions and lectures given by members of the institute. It also reports on the training of young scientists and on external and collaborative actions.

In addition to the European Large Scale Facility "Center for Application of Ion Beams in Materials Research" ("AIM"), under which more than 35 different groups from all over Europe were hosted, the "Synchrotron Radiation Beamline for Radiochemistry and Materials Research (ROBL)" at the ESRF in Grenoble is operated as a European Large Scale Facility. In this program 11 European user groups

took advantage of the respective materials research facilities. In addition, the institute has been selected as "Marie-Curie Training Site" of the European Union, named "Development of Functional Layers Using Ion Beam Techniques". By its support, five foreign PhD students performed part of their work at Rossendorf.

In 2002, one diploma student and four PhD students finished their theses at the institute and their examinations at the Technical University of Dresden. The institute (co-)organized a workshop on “Nanostructures for Electronics and Optics (NEOP)” and “The 6th Int. Conference on Computer Simulation of Radiation Effects in Solids (COSIRES)”, among others.

The institute would like to thank all partners and friends, and the organizations who supported its progress in 2002. Special thanks are due to the Executive Board of the Forschungszentrum Rossendorf, the Minister of Science and Arts of the Free State of Saxony, and the Minister of Education and Research of the Federal Government of Germany. Our partners from universities, industry and research institutes all around the world contribute essentially to the success of the institute, and play a crucial role for its further development. Last but not least, the directors would like to thank all members and guests of the institute for their active and excellent contributions in 2002.

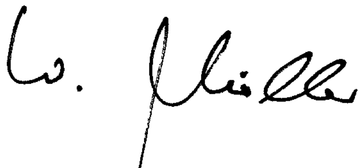

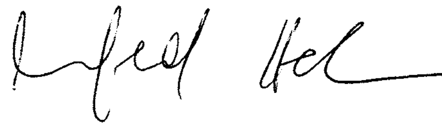

Prof. Wolfhard Möller

Prof. Manfred Helm

Contents

Selected Reports

Page

B. Abendroth and A. Kolitsch 9
Growth of Low Stress Cubic Boron Nitride with Magnetron Sputtering Using Combined Low and High Voltage Substrate Bias

C. Klein, M. Mäder, R. Grötzschel and A. Mücklich 13
High Resolution Rutherford Backscattering with Heavy Ions

M.F. Maitz, I. Tsyganov, M.T. Pham and E. Wieser 17
Blood Compatibility of Titanium Oxides with Various Crystal Structures and Element Doping

V. Heera, K.N. Madhusoodanan, A. Mücklich, D. Panknin and W. Skorupa 21
Low-Resistivity, p-Type SiC Layers Produced by Al Implantation and Ion-Beam-Induced Crystallization

R. Kögler, F. Eichhorn, J.R. Kaschny, A. Mücklich, H. Reuther, W. Skorupa, C. Serre and A. Perez-Rodriguez 25
Synthesis of Nano-Sized SiC Precipitates in Si by Simultaneous Dual Beam Implantation of C^+ and Si^+ Ions

T. Müller, K.-H. Heinig and W. Möller 29
Size and Location Control of Si Nanocrystals at Ion Beam Synthesis in Thin SiO_2 Films

J.U. Schmidt and B. Schmidt 33
Silicon Nanocrystal Memory Devices Prepared by Magnetron Sputtering

T. Gebel, L. Rebohle, W. Skorupa, A.N. Nazarov, I.N. Osiyuk and V.S. Lysenko 37
Charge Trapping in Ge-Implanted Light Emitting SiO_2 Layers

J. M. Sun, T. Dekorsy, W. Skorupa, B. Schmidt and M. Helm 40
Current Bistability in an Efficient Silicon Light-Emitting Diode

T. Dekorsy, N. Georgiev, M. Helm and O.V. Misochko 43
Femtosecond Electron and Phonon Dynamics in High-Temperature Superconductors: New Insight into the Pseudogap Regime

Short Contributions

Ion-Solid-Interaction 51

Thin Films 55

Biotechnological Materials 62

Nanostructures 65

Doping and Defects in Semiconductors 69

Materials for Optoelectronics 73

Others 77

Equipment 79

Glossary 81

Statistics

Editorships 85

Publications 85

Invited Talks 94

Conference Contributions 96

Lectures 107

Reports 110

Patents 110

Diploma Theses 111

PhD Theses 111

Awards 111

Organization of Meetings 111

Laboratory Visits 112

Guests 114

EU supported Users of AIM-LSF 117

EU supported Users of ROBL-LSF 119

Marie Curie Trainig Site 120

Institute Seminars 120

Other Seminars 122

Projects 124

Experimental Equipment 127

Organigram 129

List of Personnel 130

Growth of Low Stress Cubic Boron Nitride with Magnetron Sputtering Using Combined Low and High Voltage Substrate Bias

B. Abendroth and A. Kolitsch

Cubic boron nitride is known as the second hardest material after diamond. Superior to diamond, it does not react with ferrous materials and is resistant to oxidation up to 1300 °C. It is therefore a very promising material for hard coatings. So far industrial application of cBN thin films has been inhibited by the high intrinsic compressive stress that builds up in the films during deposition using conventional techniques like ion beam assisted deposition (IBAD) [1], magnetron sputtering [2] or laser ablation [3]. As a consequence the films delaminate when a critical thickness of some hundred nanometers is exceeded.

Several approaches to relax the stress have been published including deposition at high temperatures [4], post deposition annealing [5], or adding third elements like C [6] or Si [7]. Also buffer layers improving the adhesion to the substrate have been successfully applied [8]. Most promising results were obtained with IBAD combined with ion implantation using ion energies between 35 keV and 300 keV. The stress in the cBN films was significantly reduced in post deposition implantation experiments [9], in a sequential growth and implantation process [10], and in simultaneous growth and implantation experiments [11]. Drawbacks of these techniques are the need of a linear accelerator providing ions at adequate energies and the low growth rates that are obtained with IBAD. Additionally, growth of thick films with IBAD is restricted in some cases due to an unstable boron evaporation rate during long-time deposition.

To overcome these shortcomings, in the present work cBN films were deposited using magnetron sputtering with simultaneous stress release by energetic ion bombardment. This principle of simultaneous growth and stress relaxation is, to our knowledge, successfully applied for the first time to a plasma assisted deposition process. The ion bombardment is realised by applying a combination of negative high and low voltage bias pulses to the substrate. The substrate voltage sequence including high voltage pulses is schematically shown in Fig. 1, where the low voltage (growth) is set to –150 V and the high voltage (stress relaxation) is –8 keV. Short intermediate pulses of a positive voltage (+80 V) are used to discharge the surface. Varying the repetition rate of low-voltage cycles between the high voltage pulses, the ratio of high energy to low energy ions impinging on the substrate can be controlled.

The films were grown on silicon substrates by unbalanced radio frequency magnetron sputtering from an hBN target in an Ar/N_2 discharge. The Ar/N_2 ratio was 2:1 and the total ion flux to the substrate was approximately $1.5 \cdot 10^{15}$ ions/cm^{2}s. The substrate temperature was 350 °C.

The stress evolution was monitored by optical cantilever bending measurements during deposition. The method is described in more detail in reference [12]. Using this technique, the film force that causes the cantilever to bend, the so-called force per unit width (FPUW), can be derived in situ. The characteristic FPUW evolution during the deposition of an hBN/cBN layered film [1] has been used to determine the point when cBN nucleation is completed by coalescence of cBN grains and a pure cBN film begins to grow. In situ spectroscopic ellipsometry was additionally used to obtain the actual film thickness and growth rate that are required for a depth resolved stress analysis.

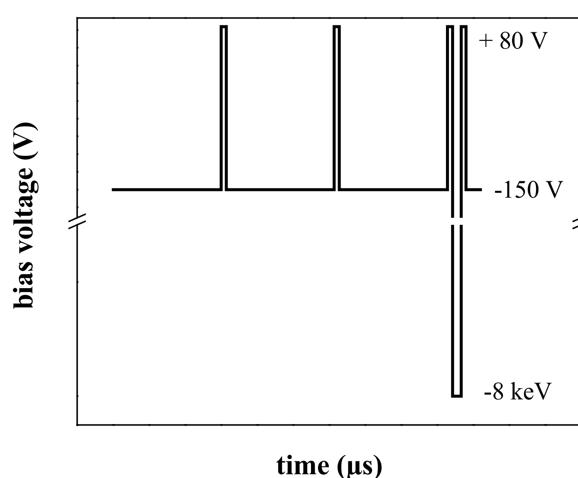

Fig. 1: Schematic of the substrate bias voltage sequence.

The average global stress S in a film of a thickness d_f is calculated by

$$S = \frac{FPUW}{d_f}.$$

More information on the stress behavior in the hBN/cBN layered structure is given by the instantaneous stress σ, which is obtained by the first derivative of the FPUW with respect to the film thickness d_f.

The evolution of the FPUW as a function of film thickness during a cBN deposition is shown in Fig. 2. The instantaneous stress is obtained from the slope of the linear regression. Negative values denote compressive stress. Throughout the deposition, the low voltage substrate bias was set to -150 V in order to enable cBN nucleation and growth of an hBN/cBN layered film [1]. In the hBN nucleation layer σ is -2 GPa. After the cBN nucleation and grain coalescence, the instantaneous stress increases up to –8.7 GPa. Eyhusen et al. found that the hBN/cBN interface is unstable upon energetic ion bombardment and cBN is transformed back to hBN [13]. Therefore, before starting the high voltage pulses, another 20 nm cBN have been grown at a bias voltage of -150 V after grain coalescence was accomplished. The mean projected range of 8 keV Ar ions is about 15 nm (calculated with SRIM 2000-40 [14]), therefore the hBN/cBN interface is not irradiated. With the starting of the high voltage pulses the FPUW decreases immediately. After a few nanometers growth a steady state is reached and the film grows further with an instantaneous stress of –1.1 GPa.

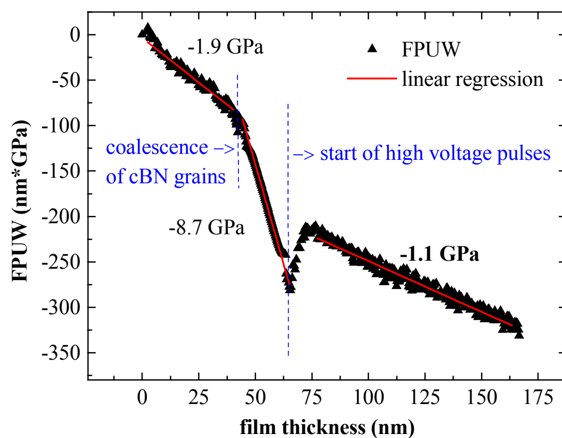

Fig. 2: FPUW evolution during a cBN deposition. The straight lines mark linear regressions, the slope of the lines gives the instantaneous stress at that film thickness.

Unfortunately the films deposited in this way delaminate nevertheless. Since the delaminated pieces roll up, one can conclude that a stress gradient exists in the layers. This can be attributed to the fact that the energetic ion bombardment affects only the surface of the growing film. The underlying hBN and non-irradiated parts of the cBN remain under high stress. This suggests to grow a buffer layer in order to minimize the stress gradient. For this reason, an extended hBN buffer layer was deposited with gradually increasing bias voltage prior to the cBN nucleation. The resulting FPUW evolution is shown in Fig. 3. The deposition can be divided into 4 parts:

(1) High voltage pulses of –2 kV. The ions penetrate the growing film and reach the substrate. This leads to interface mixing and improves adhesion. In this stage the low voltage is set to 0 V.

(2) Gradually increase of the low voltage from 0 V to –180 V until cBN nucleates. High voltage is suspended.

(3) 20 nm cBN growth under constant low voltage bias of –180 V.

(4) Start of high voltage pulses with –4 kV. Low voltage is kept at -150 V.

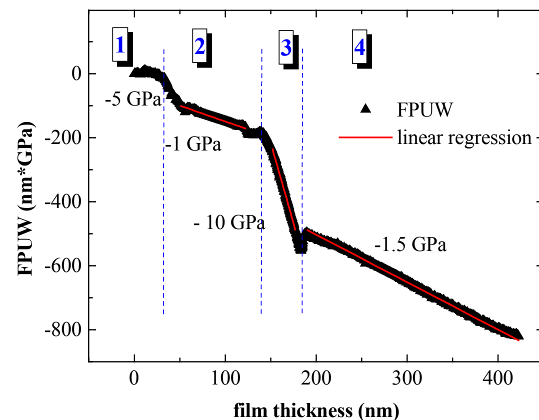

Fig. 3: FPUW evolution during the deposition of 125 nm buffer layer and 300 nm cBN.

In stage (1) no stress builds up in the film. During step (2) the instantaneous stress increases up to –5 GPa for a bias voltage of –50 V. During the further stepwise increase of the bias voltage up to –180 V the instantaneous stress is constant at approximately –1 GPa. This behavior may be explained by a change of the orientation of the hBN basal planes. It is known that for ion bombardment with energies lower than some tens of electron volts, the hBN planes are oriented preferentially parallel to the surface, whereas at higher ion energy the planes are oriented preferentially perpendicular to the surface [15]. The high stress in the beginning of stage (2) might therefore arise from a transition of the orientation of the hBN planes. At the end of stage (2), the ion energies are sufficient to initiate cBN nucleation. The very high stress of –10 GPa that builds up in stage (3), is similar to the stress that was observed after cBN grain coalescence when no buffer layer was deposited, as shown in Fig 2. Also the relaxation of the stress upon high-energy ion bombardment that begins

with stage (4) is comparable to the cBN deposition described before. By the deposition of about 125 nm hBN buffer layer, it was possible to deposit 300 nm cBN on top without delamination.

In order to investigate the influence of the bombarding ion species, experiments were carried out using $Ar^+ + N_2^+$ bombardment and pure N_2^+ bombardment only. In the latter case, the gas composition was changed to pure nitrogen after cBN nucleation. The resulting bonding structures of the deposited layers are summarized in Fig 4. In Fig. 4(a) the FTIR spectrum of a cBN film that was deposited without energetic ion irradiation is shown as a reference. In this sample 35 nm cBN were deposited on top of 120 nm hBN buffer layer. The phonons at 1400 cm^{-1} and 780 cm^{-1} are the stretching and bending mode of the hBN of the buffer layer. The peak at 1090 cm^{-1} is the cBN Reststrahlen region. The spectra of the samples which were grown under 4 keV $Ar^+ + N_2^+$ or 8 keV N_2^+ irradiation are shown in Figs. 4(b) and 4(c), respectively. From the ratio of the peak intensities at 1400 cm^{-1} and 1090 cm^{-1} the cBN content was estimated to be approximately 40% in Fig. 4(b) and 55% in Fig. 4(c). It has to be considered that the hBN buffer layer is 125 nm thick in both samples and contributes to the peak intensity of the stretching mode in Figs. 4(b) and 4(c) with approximately 30%. This leads to the conclusion, that during the energetic ion bombardment the films do not grow as pure cBN, or some cBN is transformed back to hBN.

Comparing the spectra of the implanted samples with the non-implanted reference sample, a broadening of the cBN peak and a peak shift is observed. Taking a closer look at the shape of the cBN peak, a very interesting peak splitting is observed that cannot be explained only by a simple peak broadening due to smaller grain sizes and higher defect concentration but may be due to incomplete stress relaxation.

The instantaneous stresses that were measured during 4 keV $Ar^+ + N_2^+$ and 8 keV N_2^+ implantation were -1.5 and -1.6 GPa, respectively. That means that the amount of stress relaxation does not depend on the ion species, if the ions impact with same energy (N_2 dissociates upon the impact and each N atom receives then 4 keV), although the projected range and the deposited energy are different for 4 keV Ar and 4 keV N. In both cases, the damage of the growing film is well below 1 displacement per atom.

The presented technique of growing thin films with low intrinsic stress has the advantage that it can be easily integrated into any plasma based deposition process. It allows deposition of cBN (but also other materials) with reasonable and stable growth rates and simultaneously allows to relax the stress in the films at low temperatures, which expected to be advantageous for many substrate/film combinations.

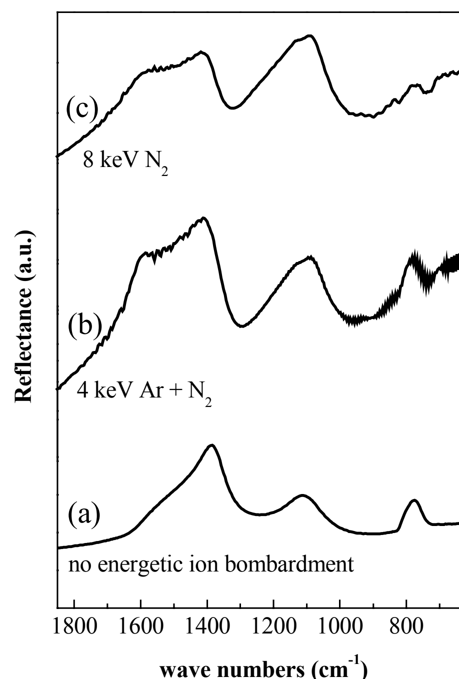

Fig. 4: FTIR spectra of layers consisting of (a) 125 nm hBN + 35 nm cBN grown only under low voltage bias, (b) 125 nm hBN + 300 nm cBN irradiated with 4 keV Ar^+ and N_2^+, (c) 125 nm hBN + 300 nm cBN irradiated with 8 keV N_2^+.

Acknowledgements

The authors gratefully acknowledge Dr. R. Gago for valuable discussions. The financial support of this work by Deutsche Forschungsgemeinschaft under contract No. FU 303/2-2 is gratefully acknowledged.

References

[1] W. Fukarek, J. Vac. Sci. Technol. A **19** (2001) 2017

[2] S. Ulrich, H. Erhardt, J. Schwan, W. Donner, H. Dosch, P. Widmayer, P. Ziemann, Surf. Coat. Technol. **166-199** (1999) 269

[3] G. Reisse, S. Weissmantel, D. Rost, Diam. Relat. Mater. **11** (2002) 1276

[4] W.J. Zhang, S. Matsumoto, Phys. Rev. B 63 (2001) 073201

[5] C. Fitz, A. Kolitsch, W. Fukarek, Thin Solid Films **389** (2001) 173

[6] M.P. Johansson, I. Ivanov, L. Hultman, E.P. Münger, A. Schütze, J. Vac. Sci. Technol. A **14** (1996) 3100

[7] C. Ronning, H. Feldermann, H. Hofsäss, Diam. Relat. Mater. **9** (2000) 1767

[8] K. Yamamoto, M Keunecke, K. Bewilogua, Thin Solid Films **377-378** (2001) 331

[9] C. Fitz, W. Fukarek, W. Möller, Thin Solid Films **408** (2002) 155

[10] H.-G. Boyen, P. Widmayer, D. Schwertber ger, N. Deyneka, P. Ziemann, Appl. Phys. Lett. **76** (2000) 709

[11] C. Fitz, A. Kolitsch, W. Möller, W. Fukarek, Appl. Phys. Lett. **80** (2002) 55

[12] C. Fitz, W. Fukarek, A. Kolitsch, W. Möller, Surf. Coat. Technol. **128-129** (2000) 474

[13] S. Eyhusen, I. Gerhards, H. Hofsäss, C. Ron ning, Phase stability of cubic boron nitride upon ion impact, Presentation at the 9th cBN Expertentreffen, Bonn, 9.-11.10 2002

[14] J.F. Ziegler, J.P. Biersack, U. Littmark, The Stopping and Range of Ions in Solids, Per gamon Press, New York, 1985

[15] M. Schubert, B. Rheinländer, E. Franke, H. Neumann, J. Hahn, M. Röder, F. Richter, Appl. Phys. Lett. **70** (1997) 1819

High Resolution Rutherford Backscattering with Heavy Ions

C. Klein, M. Mäder, R. Grötzschel and A. Mücklich

Ultra-thin films play a crucial role in the design of new materials. Their structural and compositional characterization requires several complementary methods of analysis, with the special interest in an utmost high depth resolution. For this purpose, the various tools of high-energy ion beam analysis are well suited for elemental analysis. In particular, Rutherford Backscattering (RBS) can be employed as a reliable, element-specific and quantitative tool for determining concentration depth profiles of heavy elements in a light matrix.

In order to meet the requirement of a depth resolution below one nanometer, an energy resolution *dE/E* of the backscattered particle detector of the order of 10^{-3} is required. Such a high resolution is only provided by magnetic spectrometers or electrostatic analysers, that focus particles with different momenta or energies onto different positions on a focal plane and detect them with a position sensitive detector. If heavy ions such as Li, C, or F are used as primary ions, the depth resolution can be improved even further.

However, the use of magnetic or electrostatic spectrometers also raises new questions. As the depth resolution approaches the nanometer region, it becomes comparable to the typical length scale of charge state equilibration. It is well known that the charge state distribution (CSD) of ions obtained directly after a single scattering event can be different from the equilibrium CSD [1]. Under these circumstances, the depth scale that converts the energy of a scattered particle to its scattering depth may no longer be determined from tabulated stopping powers, which are valid for charge state equilibrium. As a consequence, a good knowledge of the CSDs resulting from a backscattering collision is imperative both for the understanding of the spectra and for the choice of the primary ions.

Together with a demonstration of the performance of the Rossendorf high resolution RBS setup, the present contribution will discuss the possible influence of charge-state dependent stopping on spectra from layers deeper than about 2 nm below the surface. In addition, single collision and equilibrium CSDs for ions of the second row of the periodic table will be compared.

The experiments were carried out at the Rossendorf Browne-Buechner spectrometer that was recently installed at the 3 MV Tandetron. The spectrometer, described in detail in [2], is particularly well suited for high resolution RBS (HRBS) and NRA and provides depth resolutions in the order of one monolayer in silicon [3].

Sample	d_1 (nm)	d_2 (nm)	method
Si/30×(Mo/B_4C)	1.9	2.33	XRD[4]
Si/5×(Mo/Si)	5.6	2.5	HRBS
Si/5×($Ta_{0.1}Si_{0.9}$/Si)	0.57	5.17	deposition time (calibrated with TEM)[5]

Table 1: Samples investigated. The thicknesses quoted were determined with the methods indicated in the last column.

Three model samples have been examined as listed in Table 1. In order to demonstrate the excellent depth resolution of the Browne-Buechner spectrometer, Fig. 1 shows two spectra from one of the samples. The top spectrum was obtained by Medium Energy Ion Scattering (MEIS) using 100 keV H^+ at normal incidence and a scattering angle of 130°. The peaks at high energies are related to the 0.57 nm thin layers containing Ta. The edge at low energies is due to scattering from the Si surface. While the first two Ta layers are resolved, the third, fourth and fifth Ta layers are obscured by the poor counting statistics and the deterioration of the depth resolution caused by straggling. For comparison, the bottom part of Fig. 1 shows a spectrum as measured by heavy-ion HRBS with 2 MeV C^{2+} ions at a scattering angle of 35.5° and an incidence angle of 17.5° with respect to the surface (in the following, all incidence and exit angles are measured with respect to the surface). The energy of 2 MeV was chosen, as at this energy the equilibrium charge state fraction of C^{3+} ions varies only by about 2% over an energy range of several hundred keV. In that case, the spectra of detected C^{3+} ions can be expected to reflect the sample composition with reasonable

accuracy. Hence, only one charge state needs to be measured in order to obtain all desired information. Here, all five Ta layers are clearly resolved. Due to the higher stopping power and the smaller incidence and exit angles, the depth resolution is clearly improved as compared to the MEIS case. The area under the peaks is constant within an error of 5% as obtained from the multiple Gaussian fit also shown in Fig. 1. It has to be borne in mind that in this case the outermost layer is a Si layer, so that the peaks corresponding to the highest energy belong to layers several nm below the surface. In this case, the CSDs of the scattered ions approach charge state equilibrium.

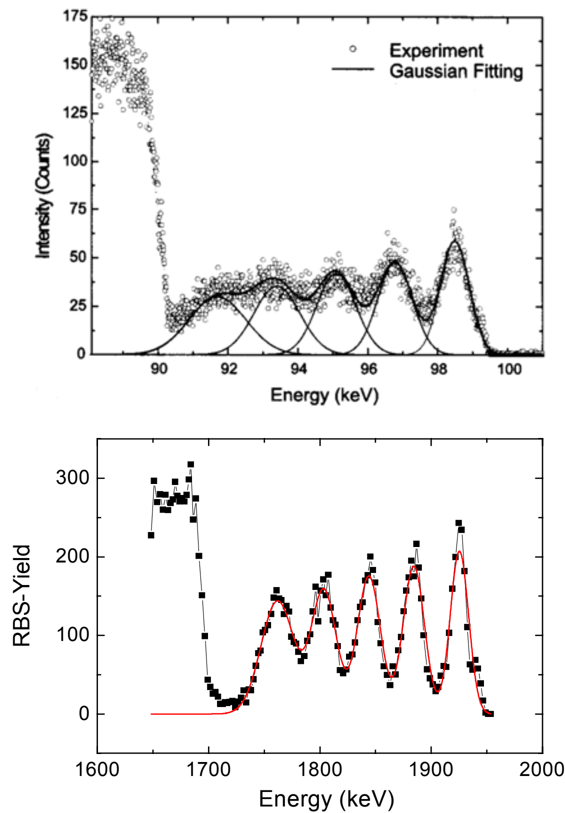

Fig. 1: Comparison of MEIS and RBS applied to a multilayer system (5 double layers of 0.57 nm $Ta_{0.1}Si_{0.9}$ and 5.17 nm Si on a Si substrate). Top: MEIS spectrum obtained with 100 keV protons at a scattering angle of 130° (from [6]). Bottom: RBS spectrum measured with 2 MeV C ions at a scattering angle of 35.5°.

The same holds for the example shown in Fig. 2. The upper part shows a TEM image of the Si/30×(Mo/B_4C) sample demonstrating the high regularity of the alternating layers. The lower part shows a spectrum obtained with 2 MeV C ions under the same conditions as in the previous example. Only the Mo layers can be seen. This spectrum was used to extract straggling data from the increase of the minima between the peaks as a function of increasing scattering depth. As long as the interface width between all layers is equal and the layers do not show thickness variations, the fit can be described with a function of the form

$$f(E) = \sum_i f_i(E) \quad (1)$$

with

$$f_i(E) = \frac{A_i}{E_{i1} - E_{i2}} \left(g(\frac{E - E_{i2}}{w_{i2}}) - g(\frac{E - E_{i1}}{w_{i1}}) \right) \quad (2)$$

where $g(E) = G(2\sqrt{\ln 2}E)$ with G denoting the Gaussian error function. Eq. (2) describes a box whose edges are located at E_{i1} and E_{i2} and smeared out with widths w_{i2} and w_{i1}. The area under the box is A_i. For the fit the A_i were assumed to be equal for each peak except for a small correction due to the increasing cross section. Also the energy width of the Mo peaks, and the energy separation of the peaks was held fixed as the effective stopping power differs by less than 3% between the first and the fifth layer. The widths can be described by

$$w_{ij} = \sqrt{w_0^2 + w_{Is}^2 + w^2 t_{ij}}, i = 1-5, j = 1,2 \quad (3)$$

where w_{ij} denotes the widths of the jth edge of the

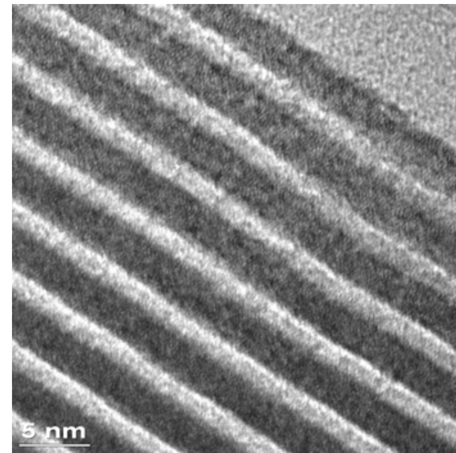

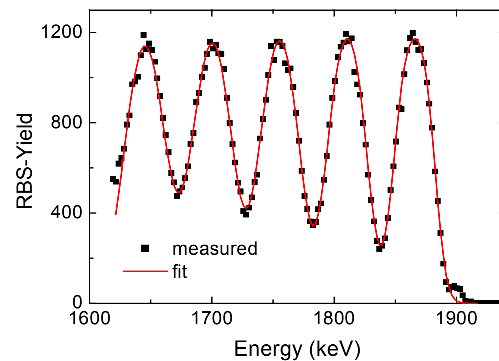

Fig. 2: Top: TEM-image of a Si/30×(Mo/B_4C) multilayer. The dark and bright layers show Mo and B_4C, respectively. Bottom: RBS spectrum of the multilayer as measured with 2 MeV C-ions at an incidence angle of 17.5° and a scattering angle of 35.5°.

*i*th peak, w_{Is} the isotopic broadening, $w^2 t_{ij}$ the broadening due to straggling at depth t_{ij}, and w_0 incorporates the broadening due to the interface width and the spectrometer resolution. For t_{ij} the XRD data were used (see Table 1). The parameter w_{Is} amounts to 7.5 keV.

The fit shown in Fig. 2 yields w_0 = 11.0 keV and w = 5.3 keV/nm$^{1/2}$. The latter value can be considered to describe the straggling of the compound $Mo_{0.3}B_{0.56}C_{0.14}$, with the same average composition as Mo/B_4C. It can be compared to the semi-empirical Yang straggling data [6], yielding 4.6 keV/nm$^{1/2}$. The agreement is satisfactory in view of the scatter in the experimental data, on which the Yang fit is based. The interface width can be estimated from the parameter w_0, from which the spectrometer resolution of 5 keV must be subtracted. This yields 9.8 keV, which, assuming an effective stopping power of 16.9 keV/nm in Mo, corresponds to a thickness of 6 Å. This is in good agreement with the interface width as obtained by XRD [4]. For the energy widths of the Mo and the B_4C layers, 33.9 keV and 21.2 keV are obtained, respectively. These values correspond to thicknesses of 2.0 nm and 1.8 nm, respectively. The thickness of the double layer Mo/B_4C can be determined with high accuracy by XRD (see Table 1). The thickness obtained by HRBS in the present study exceeds the XRD result by about 10%. A similar deviation was found for Si/5×($Ta_{0.1}Si_{0.9}$/Si) and Mo/Si-multilayers as well as for W/B_4 multilayers (not shown here). This deviation is most likely of systematic origin, being related to a systematic error in stopping power data of heavy ions at low energies. Recently such an error was suggested in [7].

Fig. 3 shows a HRBS spectrum of Si/5×(Mo/Si), measured with 3 MeV Li ions. Here, both the Mo and the Si layers show up in the spectrum. The last Mo peak and the first Si peak overlap. The dependence of the charge state on energy was corrected by using the data from [8]. The thin line shows a fit according to Eq. (1). As in the case of C ions, there is excellent agreement between the fit and the measured data, with a straggling parameter w = 4.0 keV/nm$^{1/2}$, compared to 3.0 keV/nm$^{1/2}$ according to Yang [6]. The discrepancy is somewhat larger than for C ions, which is not surprising, as the fewer experimental data for Li ions than for C ions form the base of the semi-empirical fit.

All the spectra shown above refer to scattering at a depth of at least 2 nm below the surface. The fits to the spectra demonstrate that for these depths reliable information can be well extracted without assuming any specific charge-state related effects. There is no indication of any influence of charge-state dependent stopping power. In particular, all peak widths can be well described with one value for each spectrum.

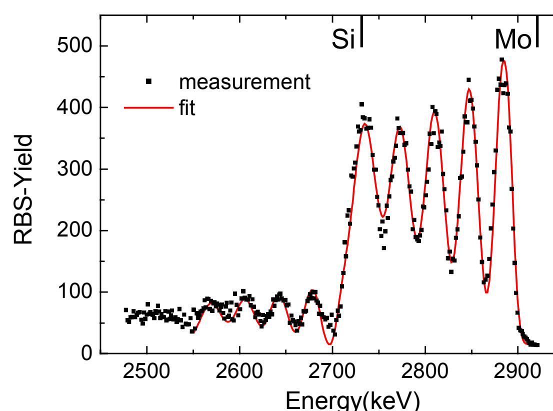

Fig. 3: HRBS spectrum of Si/5×(Mo/Si), measured with 3 MeV Li ions at a scattering angle of 35.5° and an incidence angle of 17.5°. The lines on the upper axis indicate the position of surface Si and Mo, respectively.

For a scattering that occurs immediately at the surface the situation can be more complicated. The key question concerns the difference in the CSD of ions immediately after the backscattering and the CSD in equilibrium. To obtain the CSD in equilibrium, HRBS spectra of thick Au films were measured with Li, C, and F ions at various energies in the MeV range. The single-collision CSDs were obtained by measuring spectra of monolayer samples for the same ions. To make sure that only one backscattering collision takes place, Si substrates covered with a monolayer of Au atoms were prepared in-situ in the scattering chamber. Details about the production of these samples are described in [9].

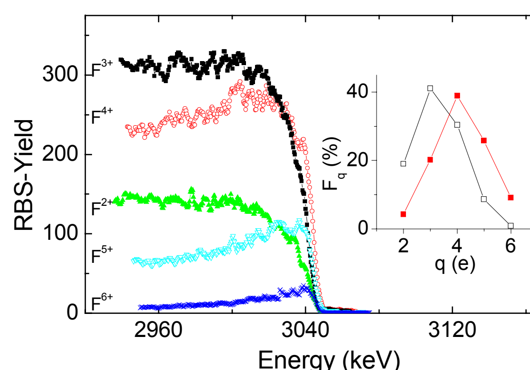

Fig. 4: Spectrum of a thick Au layer, measured with 3.15 MeV F ions at a scattering angle of 35.5° and an incidence angle of 17.5°. The inset shows the CSDs obtained for the equilibrium case (open symbols) compared to the single-collision CSD (full symbols).

Fig. 4 shows an example of 3.15 MeV F spectra for several detected charge states. The

spectral shape depends significantly on the charge state. This demonstrates that the average charge state of F ions scattered from atoms close to the surface is different from the charge state of ions scattered from atoms deeper inside the sample. While low charge states produce spectra with a broad high energy edge, high charge states result in a sharp increase of the yield at high energies, followed by a decrease towards the equilibrium value. The corresponding single collision CSDs show a marked difference of about one unit charge.

Fig. 5 shows the mean charge states of Li, C, and F ions for the equilibrium and single-collision cases at various energies. For Li and C ions, the equilibrium and single-collision CSDs are very similar. For Li ions, the latter leads to slightly lower average charge states than the former. For C, the situation is reversed. For F ions, there is a marked difference over a wide range of energies. A trend to higher charge states after a single collision with increasing nuclear charge Z is clearly visible. This result is consistent with the finding that the Li and C spectra shown in Figs. 1-3 do not feature any influence of charge state effects. F ions, on the other hand, are less suited for routine HRBS measurements.

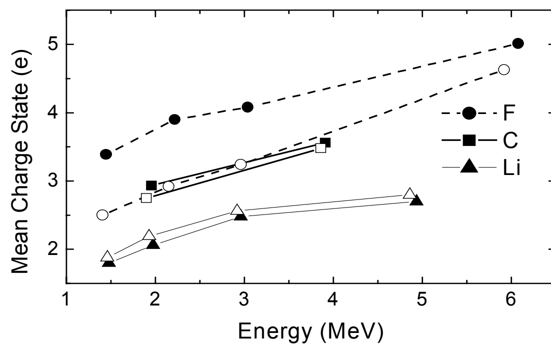

Fig. 5: Mean charge states for Li (Δ), C (□) and F (○) ions for the single collision case (full symbols) and for the equilibrium case (open symbols) in dependence on the energy of incidence.

Acknowledgements

The authors thank S. Braun, D. Strivay, and D. W. Moon for providing the multilayer samples.

References

[1] S. Jamecsny, Dissertation, Max-Planck-Institut für Metallforschung, Stuttgart, 1998

[2] R. Grötzschel, C. Klein, O. Kruse, Nucl. Instr. Meth. B **183** (2001) 3

[3] C. Klein, R. Grötzschel, M. Mäder, F. Hermann, Annual Report IIM 2000, FZR-**314** (2000) 27

[4] S. Braun, private communication

[5] D.W. Moon, H.I. Lee, K.J. Kim, T. Nishimu ra, Y. Kido, Nucl. Instr. Meth. B **183** (2001) 10

[6] Q Yang, D.J. O'Connor, Z. Wang, Nucl. Instr. Meth. B **61** (1991) 149

[7] W. Trzaska, V. Lyapin, T. Alanko, M. Mutterer, J. Räisänen, G. Tjurin, M. Wojdyr, Nucl. Instr. Meth. B **195** (2002) 147

[8] W. Jiang, R. Grötzschel, W. Pilz, W. Möller, Phys. Rev. B **59** (1999) 226

[9] C. Klein, R. Grötzschel, M. Mäder, W. Möller, Nucl. Instr. Meth. B **190** (2002) 122

Blood Compatibility of Titanium Oxides with Various Crystal Structures and Element Doping

M.F. Maitz, I. Tsyganov[1], M.T. Pham and E. Wieser

[1]*Lipetsk State Technical University, Moscowskaya 30, 398055 Lipetsk, Russia*

Medical implants in contact with blood, like heart valves or vascular stents, must be blood compatible, that means, they should show only minimum induction of blood clot formation, so that *in vivo* the fibrinolytic system can compete the fibrinogenic system. As a consequence, both the blood platelets as well as the blood clotting cascade in the plasma should be minimally activated by the surface.

Several steps of the clotting cascade can be activated by foreign surfaces. The most prominent is Factor XII at the initial step of the intrinsic pathway of the clotting cascade. It changes its conformation upon adsorption to a surface, leading to a self-activation [1]. From the biochemical point of view all clotting factors contributing to the fibrin formation are serine proteases. The limited proteolysis by the clotting factors is no chemical oxidation process, and the clotting factors do not require any coenzymes. In the case of fibrinogen, thrombin cleaves off four highly negative charged fibrinopeptides, which reduces the electrostatic repulsion of the peptides and allows their spontaneous association to a fibrin clot. However, an alternative mechanism has been suggested, by which fibrinogen can be oxidized at a surface which accepts electrons. This should lead to a destabilization of the molecule and cleavage of the fibrinopeptides [2]. According to this theory, a surface which prevents the acceptance of electrons in this energy range, but does not build up surface charges, should induce least blood clot formation. Even though this concept still has several open questions and the reaction mechanism suggested is not proven on a molecular basis, there are several studies at different systems showing a good correlation between semiconductive properties and hemocompatibility [2,3].

Besides the fibrinogenic cascade, also blood platelets can become activated by surface interactions. They become activated by negatively charged surfaces or via the von Willebrand factor/ Factor VIII complex, which adsorbs to hydrophobic surfaces [4]. Signs of activation are the adhesion at a surface, change of shape, expressions of activation markers and cytokine release.

Titanium oxides were selected as a test surface for this study. They are known to be in general well hemocompatible [5], however the effect of the different crystal structures on the hemocompatibility has not been investigated in detail. This is one subject of the present investigation. The other topic is the impact of a possible electron transfer from fibrinogen into the surface on the blood compatibility. The crystalline modifications of TiO_2, anatase and rutile, are semiconductors with band gap energies of approximately 3.0 eV. Therefore, by ion implantation of n-doping elements it is possible to inhibit an electron acceptance of the surface. An alternative way to inhibit the electron acceptance is the chemical effect obtained by implantation of an element acting as a strong electron donor in a redox system.

Various titanium oxides for this study were synthesised by metal plasma immersion ion implantation and deposition (MePIIID) on thermally oxidised silicon. By varying the substrate bias and oxygen flow the crystal structures rutile, crystalline and nanocrystalline anatase + brookite and amorphous TiO_2 were produced, as confirmed by X-ray diffraction measurements [6].

The Fermi level of the semiconductive rutile was modified by low dose implantation of phosphorous (P) ions into selected rutile samples (30 keV, 5×10^{15} cm^{-2}), and the redox potential of the non-conducting amorphous TiO_2 surface was reduced by high dose ion implantation of chromium (Cr) (30 keV, 5×10^{17} cm^{-2}). The low dose P implantation is typical for semiconductor purposes. For P-implanted samples the effect of post-implantation annealing (900 °C, 1 h in vacuum) was also studied. By the annealing process, phosphorous becomes integrated in the crystal lattice to induce the changes in the semiconductive properties. The efficiency of the process has been shown by an increased conductivity of the surface [6]. On the other hand, for the Cr implantation a high ion dose was chosen because here a chemical effect is intended, what generally requires high doses.

AFM measurements show that the amorphous and nanocrystalline surfaces are substantially smoother than the crystalline or the amor-

phous and the Cr-implanted surfaces. The roughness values are 4-6 nm and 30-40 nm, respectively.

The hemocompatibility of the layers was determined both for the cellular and plasmatic clotting system. In all biocompatibility tests the polyethylene Thermanox® (Nunc) was used as a reference.

The number of adherent blood platelets on the surface was used as a measure of blood platelet activation. The principle of this test is the measurement of the lactate dehydrogenase (LDH) activity after lysis of adherent blood platelets with a detergent. This is proportional to the number of platelets [7]. Platelet rich plasma was prepared from citrate anticoagulated human blood donations. An aliquot was incubated on the test surfaces for 45 min at 37 °C in humidified air. Non-adherent platelets were removed from the samples by gently washing in phosphate buffered saline (PBS). Then the adherent platelets were lysed with 1% Triton X in PBS.

The LDH activity in these lysates was determined photometrically by following the NADH consumption in the LDH catalysed reaction: NADH + Pyruvate $\Leftrightarrow$ Lactate + NAD + H^+. The values are standardized to the LDH activity in the lysates of the platelets in the whole aliquot platelet rich plasma.

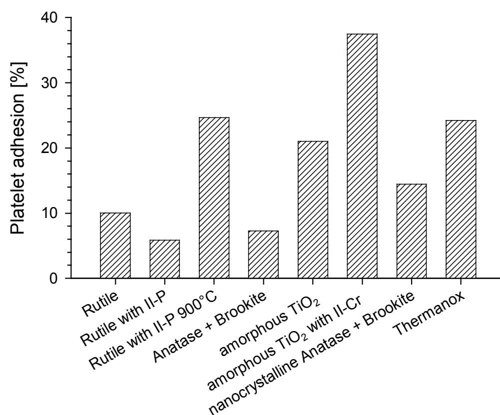

Fig. 1: Blood platelet adhesion on titanium oxide films with various crystal structures and ion implantation of phosphorous (II-P) or chromium (II-Cr). The bars indicate the median of three experiments. P implantation into rutile reduces the platelet adhesion, but this effect is inverted after annealing at 900 °C. Cr implantation strongly increases the platelet adhesion.

Among the titanium oxides not modified by subsequent implantation there is no obvious difference in the platelet adherence between the crystalline phases and the nanocrystalline or amorphous phases. The doping of rutile with P ions clearly reduces the platelet adherence on this surface, an effect which disappears after the annealing at 900 °C. This contrasts with the effect of Cr ion implantation into amorphous TiO_2, where more thrombocytes adhere on the surface than on the non-implanted titanium oxide (Fig. 1).

The fibrinogenic system was tested by measuring the time needed for clot formation of a recalcified standard human plasma on the samples at 37 °C.

The time for the clotting of plasma on the surfaces is shown in Fig. 2. Also for the activation of the plasmatic clotting system, there is no clear difference between crystalline, nanocrystalline and amorphous titanium oxides. The crystalline rutile shows the highest activation of the clotting cascade of all samples investigated, but this is strongly reduced after the doping with phosphorous ions, that means the phosphorous reduces the clotting activation. The same is true for Cr implantation into amorphous TiO_2. After tempering the effect of phosphorous ions becomes less prominent.

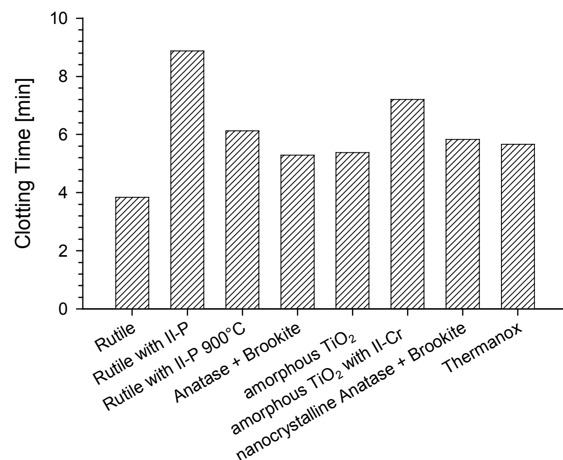

Fig. 2: Clotting time of recalcified standard human plasma on titanium oxide surfaces. The bars indicate the mean of two measurements. Both P and Cr ion implantation prolongs the clotting time, i.e. reduces the clotting activation.

The experiments in this study do not show any major difference in platelet adherence or in the activation of the clotting cascade for the different oxide structures investigated here. However, any effect of crystal structure on the hemocompatibility in this study could be overlaid by effects of the surface roughness. The amorphous TiO_2 and nanocrystalline anatase + brookite surfaces had only about one tenth of the roughness of the crystalline titanium oxides, so separate effects of crystallinity or roughness could not be identified. The surface roughness is stated to be an important factor for thrombogenicity [8], but it was found

that this is mainly true for flow conditions in the test, where shear stresses are active. Under static conditions, as in this study, a rough surface should have much less influence [9]. Further, all studies are dealing with roughness values clearly above 100 nm, so that all surfaces used in this experiment can be considered as smooth.

The adsorption of plasma proteins on a surface is a central point for blood compatibility. In general, the adsorption of proteins on a surface is driven mainly by electrostatic interactions between a protein and the surface and by hydrophilic-hydrophobic interactions. This also leads to conformational changes of the protein. At physiological pH values titanium oxide has a net charge near zero, so proteins on it will be minimally affected. This has been demonstrated for proteins like albumin adsorbed on titanium with the native oxide layer [10]. The conformational integrity of proteins is one of the prerequisites for blood compatibility and biocompatibility in general, because conformation change is one way for activation of the clotting Factor XII [1].

This study should go beyond the pure protein adsorption and check whether the inhibition of an electron transfer from fibrinogen to the surface could improve the hemocompatibility. For this titanium oxides were ion implanted either with Cr or with P ions. Chromium is an effective electron donor in a redox system (normal potential $E^0(Cr/Cr^{3+}) = -0.744$ V). It was implanted in a high dose of 5 x 10^{17} cm^{-2} into the isolating amorphous TiO_2 to exhibit the chemical effect. Its presence in the surface prevents the oxidation of fibrinogen on the surface. Phosphorous ions were implanted into semiconducting rutile with a dose of 5 x 10^{15} cm^{-2}, where a direct chemical effect is doubtful. Ion doses in this range are typical to modify the electrical properties of semiconductors, if the implanted ions are incorporated into the crystal lattice. P is an electron donor, what means it is an n-doping element for TiO_2. The elevation of the Fermi niveau inhibits an electron transfer from proteins to the surface.

In this study, the implantation of both ions in TiO_2 clearly prolongs the clotting time. However for P this is mainly true for the as-implanted samples, not after the tempering process. This contrasts the theory that a reduced electron transfer in the surface inhibits the blood clotting activity. The as-implanted coatings have the P ions incorporated in a disturbed surrounding; only after tempering the phosphorous is incorporated onto lattice sites, where it can show the properties as electron donor. The low fibrinogenic activity of the P implanted rutile seems to have other reasons.

Only for the P ion implantation the low activation of the clotting cascade is associated also with a reduced adherence of blood platelets. This especially was not the case for the Cr ion implantation, where a strongly increased adherence and activation was found. Also for the native rutile a contrasting trend was found with low platelet adherence but high activation of the clotting cascade. An opposite behavior in the activation of the humoral and the cellular clotting system by foreign surfaces frequently has been described by others [11]. Therefore the concordant low activation of blood platelets as well as of the clotting cascade in the case of P ion implantation has to be pointed out.

In this study it has been shown that low dose phosphorous ion implantation into rutile TiO_2 can reduce the activation of both haemostatic systems, the clotting cascade and blood platelets.

For this action the phosphorous is required to be accessible and not integrated in the crystal lattice of titanium oxide, what makes a biological reason more likely than an influence on redox processes of the fibrinogen.

Currently complex functional groups with biological meaning are regarded as more important for platelet adhesion than simple surface characteristics like the surface charge or surface free energy. This also is a possible mechanism for the action of the implanted P ions in TiO_2. Good hemocompatibility, i.e. low protein adsorption and low platelet adhesion, has already been proven for other phosphate containing compounds like phospholipids, phosphorylcholine and phosphazenes [12-14]. They all simulate biomolecules, especially those of the cell membrane. As a speculation, phosphorous and phosphate groups generated by ion implantation might exhibit this function, whereas phosphorous which is incorporated into the crystal lattice after the heat treatment is inactive.

Further experiments will be performed to test whether the low dose phosphorous in titanium oxide is already sufficient for a similar biological activity like the other compounds mentioned above or whether the reaction mechanism is more based on physical changes or associated to the electron densities of the surfaces.

References

[1] J. Sánchez, P.B. Lundquista, G. Elgueb, R. Larssonb, P. Olsson, Thromb. Res. **105** (2002) 407

[2] A. Bolz, M. Schaldach, Biomed. Tech. (Berl.) **37** (1992) 244

[3] J.Y. Chen, Y.X. Leng, X.B. Tian, L.P. Wang, N. Huang, P.K. Chu, P. Yang, Biomaterials **23** (2002) 2545

[4] M. Broberg, H. Nygren, Biomaterials **22** (2001) 2403

[5] N. Huang, P. Yang, X. Chen, Y. Leng, X. Zeng, G. Jun, Z. Zheng, F. Zhang, Y. Chen, X. Liu, T. Xi, Biomaterials **19** (1998) 771

[6] I. Tsyganov, M.F. Maitz, E. Wieser, F. Prokert, E. Richter, A. Rogozin, Surf. Coat. Techn. (submitted).

[7] J.M. Grunkemeier, W.B. Tsai, T.A. Horbett, J. Biomed. Mater. Res. **41** (1998) 657

[8] G. Clarotti, F. Schue, J. Sledz, A. Ait Ben Aoumar, K.E. Geckeler, A. Orsetti, G. Paleirac, Biomaterials **13** (1992) 832

[9] W. Zingg, A.W. Neumann, A.B. Strong, O.S. Hum, D.R. Absolom, Biomaterials **2** (1981) 156

[10] R. Thull, Biomol. Eng. **19** (2002) 43

[11] D.L. Coleman, D.E. Gregonis, J.D. Andrade, J. Biomed. Mater. Res. **16** (1982) 381

[12] M. Galli, L. Sommariva, F. Prati, S. Zerboni, A. Politi, R. Bonatti, S. Mameli, E. Butti, A. Pagano, G. Ferrari, Catheter Cardiovasc. Interv. **53** (2001) 182

[13] Y. Iwasaki, A. Mikami, K. Kurita, N. Yui, K. Ishihara, N. Nakabayashi, J. Biomed. Mater. Res. **36** (1997) 508

[14] A. Welle, M. Grunze, D. Tur, J. Colloid. Interface Sci. **197** (1998) 263

Low-Resistivity, p-Type SiC Layers Produced by Al Implantation and Ion-Beam-Induced Crystallization

V. Heera, K.N. Madhusoodanan[1], A. Mücklich, D. Panknin and W. Skorupa

[1]*Cochin University of Science and Technology, Cochin - 682022, India*

SiC is the most promising semiconducting material for an upcoming new generation of very robust and compact high power and high frequency electronics. A significant progress in the understanding of the SiC materials properties, in the growth of single crystals and in the development of a specific SiC device technology has been made in recent years [1,2]. Nevertheless, there are some obstacles to be overcome before SiC can be widely used in devices. Some of these obstacles are related to problems with the annealing of crystal damage produced by ion beam doping [3] and with the electrical activation of acceptor atoms in SiC [4]. In contrast to the commonly used nitrogen donor, all known acceptor atoms have relatively deep levels in SiC. Therefore, it is very difficult to produce low resistivity, p-type SiC layers, which are necessary e.g. for the formation of good Ohmic contacts to p-type material. The best acceptor atom in SiC is Al with an ionization energy of about 200 meV. Using the ionization model of noninteracting acceptors and hole mobilities observed in defect-free epi-layers the minimum resistivity can be calculated as function of the Al concentration [4]. According to this calculation Al concentrations higher than 2×10^{20} cm^{-3} are necessary in order to obtain resistivities below 0.1 Ωcm at room temperature (RT). For ion implantation doping even higher Al concentrations are necessary, because of incomplete acceptor activation and reduced hole mobilities due to radiation damage. This situation is illustrated in Fig. 1, where experimental results from Wirth et al. [5] and Bluet et al. [6] are shown together with the calculated minimum resistivity [4]. It is evident that annealing temperatures above 1600 °C are required to achieve optimum results for p-type doping of single crystalline layers. Unfortunately, annealing at such high temperatures is difficult to control and can lead to surface erosion [3,4]. Therefore, doping processes are desirable which would enable efficient acceptor activation at lower thermal budget.

The results of flash lamp annealing [5] (Fig. 1) have demonstrated that resistivities below the theoretical limit for noninteracting acceptors can be achieved at Al concentrations above 5×10^{20} cm^{-3}. This is possible because the effective acceptor ionization energy decreases as the acceptor states start to overlap [7] or influence the band structure of the SiC [8]. Above a critical acceptor concentration an impurity band is formed. This process is associated with a nonmetal-metal transition. Calculated values for the critical Al concentration range from 8.8×10^{19} cm^{-3} up to 6.5×10^{20} cm^{-3} depending on the underlying model and the SiC-polytype [9]. In practice, it is difficult to achieve this critical concentration because only a fraction of the implanted Al atoms is electrically active. Above the Al equilibrium solubility of 2×10^{20} cm^{-3} in single crystalline SiC [10] the electrically active fraction is further reduced by Al precipitation during annealing. Obviously, this precipitation can be prevented by the extremely short annealing time of 20 ms during flash lamp annealing [5].

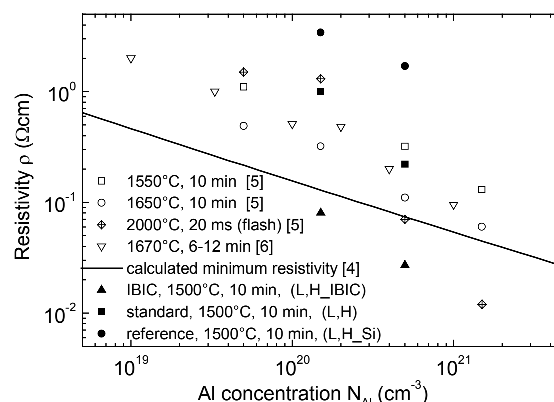

Fig. 1: Resistivity at RT as function of Al concentration. Data from the literature for the standard doping scheme with Al implantation at elevated temperature (open symbols) in comparison with the theoretical limit for noninteracting acceptors (solid line) and results of this study (solid symbols). The annealing conditions are given in the figure.

Because of the problems with the production of low-resistivity, p-type SiC layers in single crystalline substrates we have investigated the electrical behavior of heavily Al doped, nanocrystalline (nc) SiC. It can be supposed that in nc material both the electronic structure and the capability for impurity incorporation are modified. Normally, the resistivity of doped nanocrystalline semiconductors is much higher than that of the

Table I: Sample description.

sample	fluence Al impl., (50-450 keV)	temp. Al impl.	fluence Si impl, (500 keV, 500°C)	layer structure
L	1×10^{16} cm^{-2}	400°C	no	crystalline
L_Si	1×10^{16} cm^{-2}	400°C	5×10^{15} cm^{-2}	crystalline
L_IBIC	1×10^{16} cm^{-2}	- 130°C	5×10^{15} cm^{-2}	nanocrystalline
H	3.3×10^{16} cm^{-2}	400°C	no	crystalline
H_Si	3.3×10^{16} cm^{-2}	400°C	5×10^{15} cm^{-2}	crystalline
H_IBIC	3.3×10^{16} cm^{-2}	- 130°C	5×10^{15} cm^{-2}	nanocrystalline

single crystalline counterpart due to grain boundary effects. However, it could be shown by Lu *et al*. [11] that for Si this difference decreases with increasing doping concentration.

Ion-beam-induced crystallization (IBIC) [12-14] was used in order to transform preamorphized layers of 6H-SiC substrates ((0001)-oriented, Si-face, N-doped, n-type with N_D=2.7×10^{18} N cm^{-3}, ρ=0.052 Ωcm) into the nc structure. This process is compatible with the ion beam doping and allows to control the mean grain size. A multi-energy implantation of Al (50-450 keV), which is equivalent to the doping scheme described in Ref. 5, was carried out in order to form a box-like acceptor profile with a width of about 500 nm. During implantation the target was either heated to 400 °C in order to maintain the crystallinity or cooled by liquid nitrogen in order to form an amorphous layer. It should be noted that the targeted Al concentrations of 1.5×10^{20} cm^{-3} (fluence 1×10^{16} cm^{-2}) and 5×10^{20} cm^{-3} (fluence 3.3×10^{16} cm^{-2}) are in the critical range of the calculated nonmetal-metal transition. A second implantation with 500 keV Si was performed at 500 °C, which stimulates random nucleation of nanocrystals in the preamorphized layer (IBIC process [12-14]). Additionally, reference samples were prepared without Si implantation (standard doping) or Si implantation in the crystalline, Al doped layer. The sample list is given in Table I. After implantation the samples were cut into pieces of about 4.5 × 4.5 mm^2 and annealed in a rf-heated furnace under Ar atmosphere at 1500 °C for 10 min. It should be emphasized that this annealing temperature is lower than typically used for Al activation [4].

The Al profiles were measured with SIMS. The desired box-like Al profiles could be confirmed. The structure of the implanted layers was investigated by XTEM. In the case of IBIC the layer consists of randomly oriented grains with 3C-polytype structure. The mean grain size increases from 3 nm in the as-implanted state to about 37 nm after annealing. The reference samples show the typical structure of implantation damaged 6H-SiC [15]. Details of the Al profile and the layer structure will be published elsewhere. This paper focuses on the electrical properties of the Al doped layers which were determined by sheet resistance (SR) and Hall measurements in van der Pauw configuration [16]. For this purpose Al contacts (0.5 mm diameter, 500 nm thick) were sputter-deposited on the corners of the samples and then annealed at 600 °C for 10 min under Ar flow.

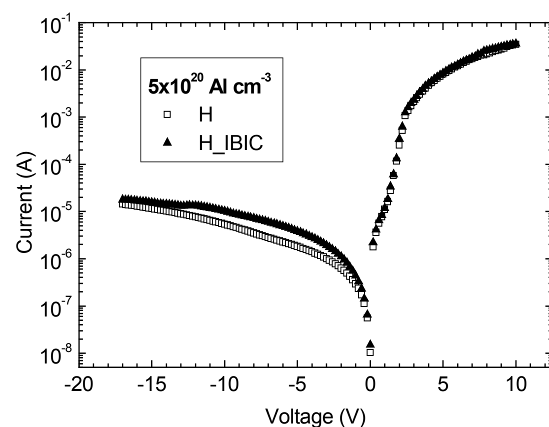

Fig. 2: The current-voltage characteristics of the pn-junction formed by the implanted layer and the substrate in the case of nanocrystalline (H_IBIC) and single crystalline layer structures (H).

It is known that insulation problems between the p-type layer and the n-type substrate can lead to errors in the interpretation of the electrical measurements [17], which can be estimated if the pn-junction resistance is known [18]. Therefore, the diode behavior of the samples was checked by current-voltage measurements across the sample. As an example the current-voltage characteristics of samples H and H_IBIC measured at RT are shown in Fig. 2.

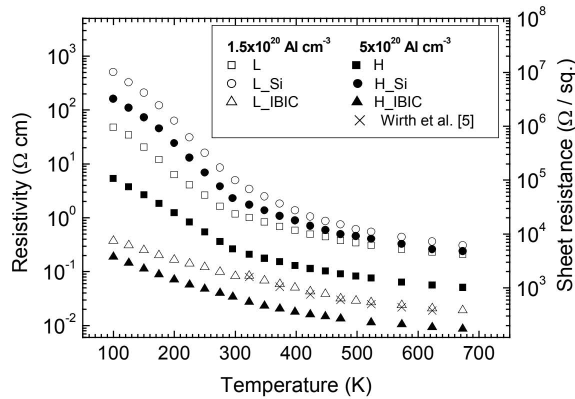

Fig. 3: Resistivity and sheet resistance of the samples after annealing at 1500 °C as function of temperature. The results of Wirth *et al.* [5] for single crystalline samples annealed at 1650 °C are shown for comparison.

According to this investigation the relative errors of the layer resistivity and the hole concentration due to leakage currents are smaller than 10% below 500 K. Moreover, it can be seen that the diode quality between the nc and the single crystalline sample is comparable. The good electrical insulation in the low temperature range is also indicated by the high SR of the Al implanted samples at RT (0.7 - 99 k Ω) which has to be compared with the SR of the substrate (1.4 Ω). At higher temperatures uncertainties up to 50% cannot be excluded. However, no substantial differences were observed between the leakage behavior of the nanocrystalline and the crystalline samples.

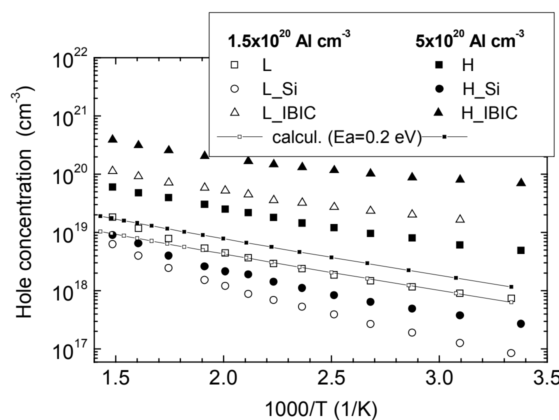

Fig. 4: Hole concentration as function of the inverse temperature. The straight lines are results of calculations for noninteracting acceptors with an ionization energy of 0.2 eV.

The results of the layer resistivity at RT are shown as function of the Al concentration in Fig. 1 (solid symbols) and as function of temperature in Fig. 3. The observed temperature dependence is very similar to recent results [5,6]. However, the nc layers produced by IBIC have much lower resistivities in the whole temperature range than the layers prepared by the standard doping process with annealing at 1500 °C (L, H) and even at 1650 °C [5]. Interestingly, a significantly higher resistivity is observed in the crystalline reference samples (L_Si, H_Si) which were subjected to the Si implantation. This result is in agreement with previous Si coimplantation experiments [19,20] and indicates that the improved conduction in the nc layers is not caused by Si-related defect states.

The p-type character of the Al-implanted layers was proved by Hall measurements. The results of the hole concentration as function of the inverse temperature are shown in Fig. 4. The commonly used ionization model [4] can only fit the experimental results of sample L. According to the theory for ionization of uncompensated, non-interacting acceptors the hole concentration in the freeze-out range should scale with the square root of the acceptor concentration. Instead, an almost linear dependence on concentration has been found for the standard (L, H) and the nc samples (L_IBIC, H_IBIC). Obviously, the hole concentrations of the samples H, L_IBIC and H_IBIC exceed the prediction of the acceptor ionization model. The high values for the nc samples (L_IBIC, H_IBIC) can only be explained by a modified electronic structure and/or the formation of an impurity band, due to a high density of electrically active Al atoms. However, the observed temperature dependence of the hole concentration in the nc layers is not typical for impurity band conduction. In the case of metallic-like conduction a temperature-independent hole concentration equal to the concentration of acceptor atoms is expected. Obviously, the simple theory fails to describe the observed functional dependence of the high hole concentrations and further investigations are necessary in order to understand the complex behavior.

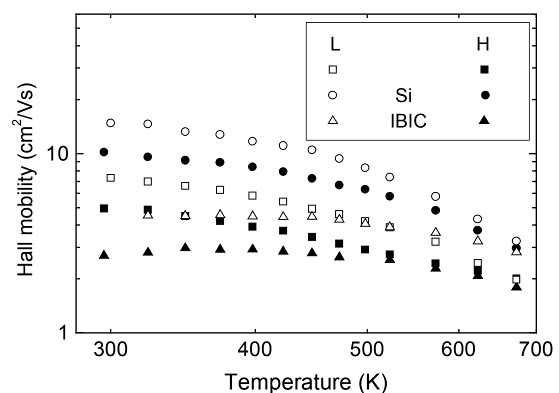

Fig. 5: Hall mobility as function of temperature.

The Hall mobilities (Fig. 5) are in the typical range for heavily Al doped SiC [5,6]. The mobility

decreases with increasing hole concentration which can qualitatively be understood in terms of hole scattering at ionized acceptor atoms. The increasing influence of hole scattering on phonons leads to a decreasing mobility with increasing temperature. However, the temperature dependence is much weaker than predicted by the scattering theory. In the case of the nc samples the mobility is almost temperature independent.

In summary, it has been shown that SiC layers with resistivities below 0.1 Ωcm at RT can be produced by the combination of high dose Al ion beam doping and IBIC. In this process annealing at 1500 °C is sufficient for acceptor activation. In comparison with the standard doping process the hole concentration is enhanced by more than one order of magnitude. The layers have a nanocrystalline structure consisting of randomly oriented grains of mainly 3C-SiC. It can be speculated that the loss of active Al acceptors by precipitation is reduced in the nanocrystalline layers. Therefore, the critical concentration for a collective acceptor activation in an impurity band can be achieved. Such layers could be useful for the formation of Ohmic contacts to moderately doped p-type SiC.

Acknowledgements

The financial support by Deutsche Forschungsgemeinschaft under contract He2604/2-3 is gratefully acknowledged.

Part of this work has been recently published as V. Heera et al., Appl. Phys. Lett. **81** (2002) 70.

References

[1] W.J. Choyke, H. Matsunami, G. Pensl (eds.), Silicon Carbide - A Review of Fundamental Questions and Applications to Current Device Technologies, Vols. I+II, Akademie-Verlag, Berlin, 1997

[2] Y. S. Park (ed.), SiC Materials and Devices, Academic Press, London, 1998

[3] V. Heera, W. Skorupa, Mat. Res. Soc. Symp. Proc. **438** (1997) 241

[4] V. Heera, D. Panknin, W. Skorupa, Appl. Surf. Sci. **184** (2001) 307

[5] H. Wirth, D. Panknin. W. Skorupa, E. Niemann, Appl. Phys. Lett. **74** (1999) 979

[6] J.M. Bluet, J. Pernot, J. Camassel, S. Contreras, J.L. Robert, J.F. Michaud, T. Billon, J. Appl. Phys. **88** (2000) 1971

[7] A. Schöner, N. Nordell, K.Rottner, R. Helbig, G. Pensl, Inst. Phys. Conf. Ser. **142** (1995) 493

[8] C. Persson, U. Lindefelt, B. E. Sernelius, J. Appl. Phys. **86** (1999) 4419

[9] C. Persson, A.Ferreira da Silva, B. Johansson, Phys. Rev. B **63** (2001) 205119

[10] M. K. Linnarsson, M. S. Janson, U. Zimmermann, B. G. Svenson, P. O. A. Persson, L. Hultman, J. Wong-Leung, S. Karlsson, A. Schöner, H. Bleichner, E. Olsson, Appl. Phys. Lett. **79** (2001) 2016

[11] N. C.-C. Lu, L. Gerzberg, C.-Y. Lu, J.D. Meindl, IEEE Trans. Electron. Dev. ED-**30** (1983) 137

[12] V. Heera, J. Stoemenos, R. Kögler, W. Skorupa, J. Appl. Phys. **77** (1995) 2999

[13] A. Höfgen, V. Heera, A. Mücklich, F. Eich horn, W. Skorupa, Nucl. Instr. Meth. B **161-163** (2000) 917

[14] A. Höfgen, V. Heera, A. Mücklich, W. Skorupa, Mat. Sci. For. **338-342** (2000) 897

[15] J. Grisolia, B. de Mauduit, J. Gimbert, Th. Billon, G. Ben Assayag, C. Bourgerette, A. Claverie, Nucl. Instr. Meth. B **147** (1999) 62

[16] P. Blood, J.W. Orton, The Electrical Characterization of Semiconductors, Academic Press, London, 1992

[17] A. Schöner, K. Rottner, N. Nordell, Mat. Res. Soc. Symp. Proc. **423** (1996) 661

[18] R. D. Larrabee, W. R. Thurber, IEEE Trans. Electr. Dev. ED-**27** (1980) 32

[19] M.V. Rao, P. Griffiths, J. Gardner, O.W. Holland, M. Ghezzo, J. Kretchmer, G. Kelner, J.A. Freitas, J. Electr. Mat. **25** (1996) 75

[20] H. Itoh, T. Troffer, G. Pensl, Mat. Sci. For. **264-268** (1998) 685

Synthesis of Nano-Sized SiC Precipitates in Si by Simultaneous Dual Beam Implantation of C^+ and Si^+ Ions

R. Kögler, F. Eichhorn, J.R. Kaschny, A. Mücklich, H. Reuther, W. Skorupa, C. Serre[1] and A. Perez-Rodriguez[1]

[1]Universitat de Barcelona, Dept. Fisica Aplicada i Electronica, Barcelona , Spain

Ion beam synthesis (IBS) of SiC in Si has been investigated for many years because of the outstanding physical material properties of SiC making it applicable for devices working under extreme conditions. The basic processes of the formation and evolution of SiC precipitates during IBS and subsequent thermal treatment, their nucleation, growth and ion induced destruction were widely described in the literature [1,2]. In this study the IBS of nanometer-sized SiC precipitates in Si was performed for the first time by simultaneous implantation using two ion beams, one C^+ ion beam and a second Si^+ ion beam [3]. The effect of the simultaneous dual beam IBS is compared with single beam IBS and with the sequential dual beam IBS of SiC.

The simultaneous implantation of (100) CZ-Si was carried out in the recently constructed Rossendorf Dual Implantation Chamber (DIC) at a temperature of 450 °C with 360 keV C^+ ions and with Si^+ ions either of 500 keV (low energy case, labeled LE) or of 1.5 MeV (high energy case, labeled HE). The projected ion ranges, R_P, were $R_P(C^+)$ = 0.75 µm, $R_P(Si^+_{LE})$ = 0.73 µm and $R_P(Si^+_{HE})$ = 1.55 µm.

Both implantations were performed simultaneously using two ion implanters, a 500 kV implanter and a 3 MV Tandetron implanter. A scheme of the experimental equipment is shown in Fig. 1. Both ion beams are synchronized in phase and amplitude during scanning that the beam spots permanently overlap. In this way a total sample area of A~2.5 cm² is homogeneously and simultaneously implanted by two ion beams. The time averaged ion current densities for C^+, Si^+_{HE} and Si^+_{LE} ions were 7×10^{12} /cm²s, 1.5×10^{12} /cm²s and 0.5×10^{12} /cm²s, respectively, and they were stable in the range of ±15%. The beam spot area of the C^+ ion beam on the sample was A~0.2 cm², and the spot of the Si^+ beam was somewhat smaller, A~0.05 cm². The current densities measured in the center of the beam spot were found to be in all cases about $i = 5\times10^{13}$ /cm²s.

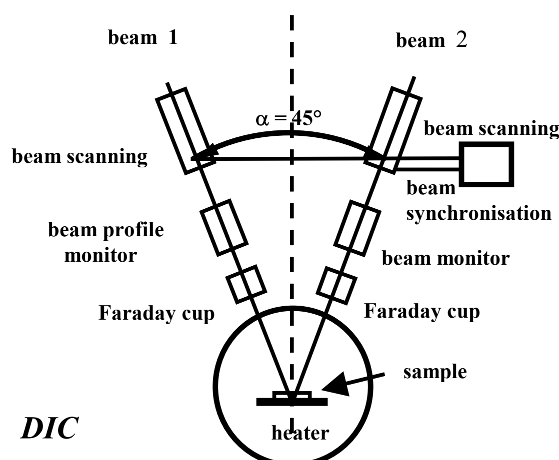

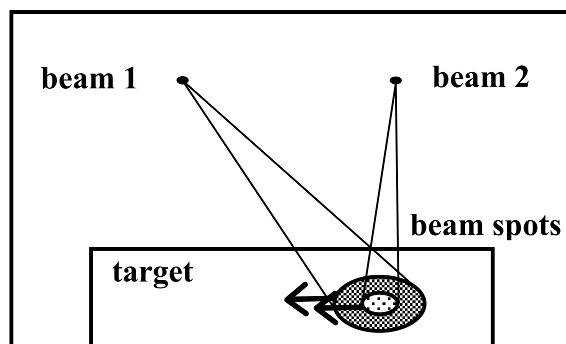

Fig. 1: Scheme of the Rossendorf Dual beam Implantation Chamber (DIC). Beam scanning proceeds in such a way that the two beam spots always overlap during beam scanning.

SiC is synthesized mainly in the depth range at 0.55 < x < 0.85 µm (C range) where the C^+ ions come to rest and the highest C concentration of $c_C \geq 2$ at% is expected according to TRIM calculations. The Si^+ ions come to rest either in much deeper position (for the HE implant) or inside the C range (for the LE implant). The energy deposition into atomic collisions by the Si^+ ions inside the C range amounts to 3.8×10^{20} eV/cm² and 2.8×10^{20}eV/cm² for the HE and LE case, respectively. These values are somewhat smaller than the energy deposition of 1.3×10^{21} eV/cm² calculated for the C^+ ions themselves [3].

The calculated ion range profiles for both cases, HE and LE, are shown in Fig. 2. Note that

the depth scales in both cases are different. The implantation data are given in detail in Table 1.

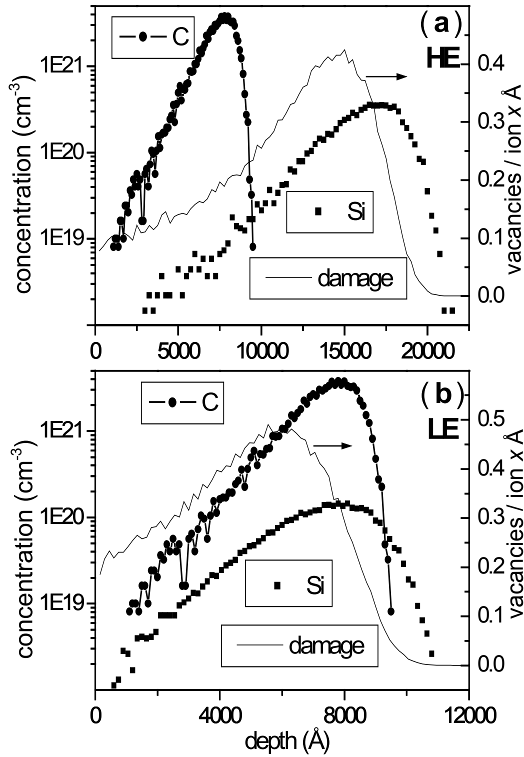

Fig. 2: Range profiles of C and Si (left scale) implanted into Si under 22.5° and the damage created by the Si^+ ion implantation (right scale) calculated by TRIM for the implants used. Results for implantation of 1.5 MeV Si^+ (HE) and for 500 keV Si^+ (LE) are shown in Figs. (a) and (b), respectively.

Sample	*C^+: $\phi/10^{16}$ (cm^{-2})*	*Si^+: $\phi/10^{16}$ (cm^{-2})*	*Si^+: E (MeV)*
SiC_{ref}	8.4	--	--
$C+Si_{HE}$	8.4	2.0	1.5
$SiC+Si_{HE}$	8.4	1.6	1.5
$C+Si_{LE}$	8.4	0.5	0.5
$SiC+Si_{LE}$	8.4	0.6	0.5

Table 1: Implantation data, C+Si denotes the simultaneous double implantation mode, and SiC+Si the sequential mode, for which the C^+ and the Si^+ ion implantations were performed subsequently.

The C range profiles were measured by Auger electron spectroscopy (AES). The quantity of SiC in the samples was analyzed by Fourier transform infrared spectroscopy (FTIR) and X-ray diffraction (XRD), using high resolution XRD of synchrotron radiation with a wavelength of 0.15382 nm at the ROBL beamline at the ESRF Grenoble and with Cu-Kα radiation at a double crystal diffractometer at FZ Rossendorf. The structure of the SiC precipitates was investigated by cross sectional transmission electron microscopy (XTEM) and high resolution transmission electron microscopy (HREM).

The C depth profile of the HE-implanted sample $C+Si_{HE}$ (not shown) is very similar to the reference sample in Fig. 3(a). In contrast. an astonishing result was found for the sequentially HE-implanted sample $SiC+Si_{HE}$. In this case no pronounced C profile could be detected by AES. This implies that the C profile is completely redistributed during the subsequent HE implantation and the maximum concentration of C falls below the AES detection limit of about 0.5 at%. On the other hand, the C profiles for low-energy Si^+ ion implantation (LE case) are significantly different from the reference sample both for simultaneous and sequential implantation, as presented in Fig. 3. The maximum of the C profile is found to shift towards a lower depth position. Also the concentration of C is decreased in comparison to the SiC_{ref} and $SiC+Si_{HE}$ samples.

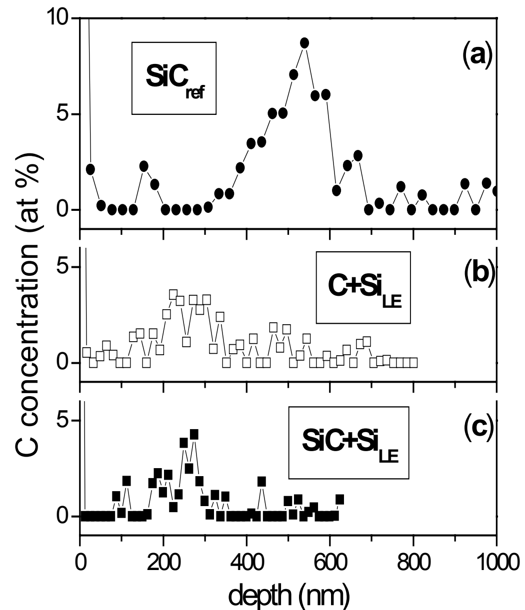

Fig. 3: Depth distributions of C in the reference sample (a) and for the low-energy (LE) silicon implantations (b,c) as measured by AES. The C peak is shifted towards the surface compared to the reference sample.

This result indicates that for both modes of the LE implant the SiC precipitates formed during implantation in the C-range are resolved and newly formed at a shallower depth.

The TEM results of Fig. 4 show dislocations generated by the C^+ implantation at the left side of the image and SiC precipitates (spots) for the simultaneously dual implanted sample $C+Si_{HE}$. The density and size distribution of SiC precipitates is well visible in Fig. 4. The precipitates are

distributed over the whole implanted layer and their density maximum is at a depth of about 800 nm in the C-range. The precipitates show a Moiré pattern in HREM images (insert in Fig. 4). Their shape appears spherical and their diameter is quite homogeneous d = 4-5 nm (monomodal). Nearly the same size and the same depth distribution of the precipitates was observed for the reference sample SiC_{ref}. For the LE-implanted samples the precipitates are harder to be visualized by TEM because of their lower crystal quality. No SiC precipitates were detected in sample $SiC+Si_{HE}$.

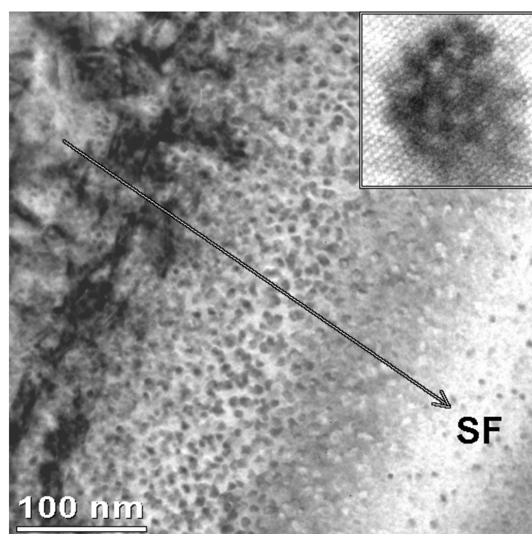

Fig. 4: XTEM micrograph of sample $C+Si_{HE}$ showing the C-range. Dislocations (left) and SiC precipitates (dark or bright spots) are visible. The insert shows a HREM image of a single SiC precipitate with Moiré pattern. The arrow indicates the direction toward the sample surface (SF).

	AES	*IR*	*XRD*
Sample	*C peak area*	*SiC 800 cm^{-1} absorption peak*	*SiC (220) diffraction peak*
SiC_{ref}	100 %	100 %	100 %
$C+Si_{HE}$	128 %	117 %	115 %
$SiC+Si_{HE}$	---	10.9 %	7.3 %
$C+Si_{LE}$	24 %	35 %	10.3 %
$SiC+Si_{LE}$	29 %	26 %	13.5 %

Table 2: Summary of analysis results for the fraction of C measured by AES and of SiC measured by FTIR and XRD in comparison to the singly implanted reference sample. C+Si denotes the simultaneous double implantation mode, and SiC+Si the sequential mode. For the implantation modes, see Table 1.

The total amount of C as well as of SiC determined with the different analysis methods is summarized in Table 2. The values in Table 2 were normalized to the reference sample. It is easily visible that the best conditions for SiC synthesis were found for the simultaneous HE Si^+ ion implantation and the worst case was the subsequent HE Si^+ ion implantation. The LE Si^+ ion implant always results in a lower yield of SiC compared to the reference sample independent of simultaneous or sequential implantation mode.

The results can be explained assuming that the formation of SiC precipitates proceeds as a C concentration of $c_C \cong c_{Si}$ is accumulated in a certain volume which exceeds a threshold size. Moreover, precipitation preferentially proceeds in regions with open volume defects in order to allow the Si interstitial ejection and SiC swelling under the ion beam. The implantation process itself generates such regions with vacancy excess ($x < R_P$) and also regions with interstitial excess ($x \sim R_P$). The forward momentum of the impinging ions results in the spatial separation of the created Frenkel pairs [4,5]. This process can be calculated by binary collision models like TRIM. During thermal treatment vacancy and interstitial defects locally recombine leaving the excess defects. The calculations using our experimental data (Table 1) were performed by TRIM98 and are described in more detail elsewhere [6]. The results are shown in Fig. 5. The vacancy-dominated region (labeled V_{Si}) with (I –V) < 0 and also the interstitial-dominated region (labeled I_{Si}) where (I – V) > 0 are indicated. The implantation conditions in the experiment are not perfectly described by the simulation as diffusion processes are not taken into account. However, the calculated interstitial-rich regions in Fig. 5 agree well with the regions where interstitial-type defects (dislocation loops) are observed in TEM images. The total number of excess vacancies generated per ion (integral over the V_{Si} region) for the simultaneous double implantation is nearly equal for both implants, HE and LE. It is higher by a factor of approximately 2 than the value for the single C^+ implant. However, in the case of the LE implant the depth distribution of the excess vacancies does not fit with the C range. For the samples SiC_{ref} and $C+Si_{HE}$ the C depth distributions which contains SiC, its precursors and dissolved C atoms is found somewhat shallower than the calculated C-range (Fig. 2) and is well inside the V_{Si} region. C atoms appear to diffuse under the ion beam to the V_{Si} region to form there precipitates. For the simultaneously implanted sample $C+Si_{HE}$ the vacancy excess in the V_{Si} region is significantly larger and, therefore, the content of C in precipitates is higher. On the other hand, in sample $SiC+Si_{HE}$ the SiC precipitates are post-irradiated. C atoms released

from the precipitates may be distributed over the whole implanted depth range $0 < x < 3$ µm. Probably the C concentration is decreased by the redistribution over a larger layer thickness leading to a higher amount of C below the threshold density for precipitate formation, $c_C < c_{Si}$. We suggest that only precursors to SiC precipitates are formed.

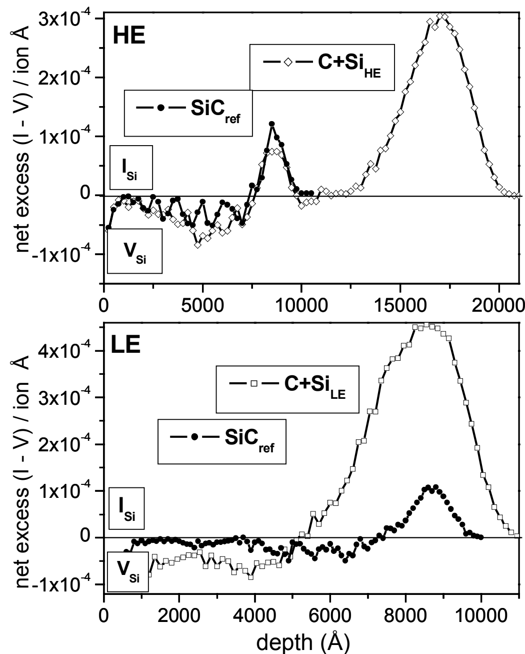

Fig. 5: Depth profiles of the net excess of interstitials or vacancies as calculated by TRIM98 for double implantation of C^+ and Si^+ ions under 22.5° corresponding to the data in Table 1. Results of the dual implantations of C^+ and 1.5 MeV Si^+ ions (HE), and of C^+ and 500 keV Si^+ ions (LE) are reported in comparison to the single C^+ ion implantation. The implanted Si^+ ions (+1 atoms) for the dual implantation were taken into account. Interstitial dominated regions, I_{si}, and vacancy dominated regions, V_{si}, are indicated. Notice the different depth scales for the HE and LE case.

The same process as for the HE implantation works also for the LE implantation. However, there are a few differences: first, the C is implanted in the I_{Si} region (and the interstitial excess is higher (+1) than the vacancy excess), second, the V_{Si} region is located shallower ($x < 0.5$ µm) and does not fit with the C range, and finally, the straggling of the implanted Si^+ profile is only about 1/2 of the HE implant. In both cases, C+Si_{LE} and SiC+Si_{LE}, SiC precipitates do not survive at the C-range. Instead, they are decomposed in the I_{Si} region and newly formed in the V_{Si} region. The resulting amount of C in the precipitates is similar for both cases of the LE implantation and is lower than in the reference sample. Apparently, a high fraction of the C atoms forms precursor defects similar to the SiC+Si_{HE} situation.

Summarizing, the results obtained for simultaneous dual beam ion implantation cannot be explained simply by the energy deposition of the second ion beam. The details of point defect generation in the reaction volume appear to be important. The second Si^+ ion beam significantly changes the conditions for the SiC precipitate formation. The results of IBS were found to depend on the ion energy of the second beam and on the implantation mode, either simultaneous or sequential. For the sequential dual beam implantation it was found that SiC precipitates were predominantly decomposed and the C atoms distributed in the whole implanted region. This process decreased the C concentration especially in the HE implanted case. For the simultaneous dual implantation it was demonstrated that for suitable implantation conditions (HE case) the dual beam IBS can improve the *in-situ* SiC formation in comparison to the single beam IBS. The dual beam IBS can be further optimized and applied for other synthesis processes as well.

Acknowledgements

Valuable discussions with V. Heera, M. Posselt and J.K.N. Lindner (Univ. Augsburg) are gratefully acknowledged.

References

[1] F. Eichhorn, N. Schell, W. Matz, R. Kögler, J. Appl. Phys. **86** (1999) 4184

[2] J.K.N. Lindner, Nucl. Instr. Meth. B **178** (2001) 44

[3] R. Kögler, F. Eichhorn, J.R. Kaschny, A. Mücklich, H. Reuther, W. Skorupa, C. Serre, A. Perez-Rodriguez, Appl. Phys. A (2002) accepted

[4] M. Tamura, T. Ando, K. Ohyu, Nucl. Instr. Meth. B **59/60** (1991) 572

[5] P. Werner, S. Eichler, G. Mariani, R. Kögler, W. Skorupa, Appl. Phys. Lett. **70** (1995) 252

[6] R. Kögler, A. Peeva, J.R. Kaschny, W. Sko rupa, H. Hutter, Nucl. Instr. Meth. B **186** (2002) 298

Size and Location Control of Si Nanocrystals at Ion Beam Synthesis in Thin SiO_2 Films

T. Müller, K.-H. Heinig and W. Möller

Recently, nonvolatile memory concepts based on nanocrystals (NCs) embedded in the gate oxide of MOS transistors have attracted much interest [1]. For that aim, NCs have been synthesized by a variety of techniques like chemical vapor deposition [2], ion implantation [3, 4], and Si aerosol deposition [5]. Ion implantation followed by thermally activated precipitation of the implanted impurity atoms is most compatible with current silicon technology. By low-energy Si^+ ion implantation into thin SiO_2 layers on (001)Si, NCs of Si were formed a few nanometers above the Si/SiO_2 interface [3]. This allows charging of the NCs by direct electron tunneling, which is a prerequisite for high endurance and low operation voltages [6].

Further optimization of location and size of ion beam synthesized NCs for memory application requires a deeper understanding of the mechanisms involved, which determine (i) the build-up of Si supersaturation by high-fluence ion implantation and (ii) NC formation by phase separation. Therefore, process simulations, which have been reported recently [7], were divided into two steps. The Si implantation was studied using the binary collision code TRIDYN [8], which includes dynamic target changes. The phase separation of Si from SiO_2 during subsequent annealing was simulated with a kinetic lattice Monte-Carlo code, which describes the thermally activated processes.

The TRIDYN depth profiles are shown in Fig. 1 for 1 keV Si^+ ion implantation into SiO_2. TRIDYN takes into account dynamic target changes due to ion deposition, ion erosion and ion beam mixing. The input parameters required by the simulation include the displacement and surface binding energies of target atoms. The displacement energies E_d for both, Si and O, were assumed to be 8 eV. This value proved to yield satisfactory agreement between earlier TRIDYN simulations of ion mixing and experiments [9] and is also consistent with the choice of Sigmund and Gras-Marti [10] in their theoretical treatment of ion mixing. For the present problem, simulations with E_d varied by factors of 0.5 and 2 did not show any significant differences of the Si deposition profiles. The surface binding energies of Si and O are assumed to vary linearly with the surface composition in a way that they balance the enthalpies of sublimation and decomposition of Si and SiO_2, respectively [11, 12].

The Si profile broadens by ion beam mixing, sputtering and swelling. For comparison, a Si implantation profile calculated by TRIM [13] has been added to Fig. 1, which is much sharper than the corresponding TRIDYN profile. The Si peak concentration is significantly overestimated by TRIM. Additionally, sputtering has led to a Si enrichment at the target surface.

During subsequent annealing, Si implanted into the thin SiO_2 separates from the oxide phase. In general, the process of phase separation is expected to be a sequence of physical mechanisms like nucleation, growth, and Ostwald ripening of Si precipitates or, at higher Si concentrations, spinodal decomposition and interfacial energy minimization of the Si/SiO_2 mixture, respectively. However, these mechanisms are the result of a variety of elementary events (like bond breaking, diffusional jumps of atoms, chemical reactions etc.) that occur in random sequence. Here, they are studied by a kinetic 3D lattice Monte Carlo (KMC) method which is discussed in detail elsewhere [14].

The kinetics of Si atoms is described in a solid host matrix (SiO_2), which is the background or "system's vacuum". Thereby, an underlying fcc lattice has been assumed, which is the most isotropic lattice. Within this host dissolved Si diffuses and can form precipitates. (The lattice spacing was chosen such that the correct atomic Si density is obtained.) Applying the classical lattice gas model with attractive Si-Si interaction, the energetics is determined by the nearest neighbor Ising model. The Metropolis algorithm [15] is used to describe the kinetics of the system.

Si dissolved in the matrix performs diffusional jumps from one lattice site to another with the probability $1/\tau \cdot \exp\{-E_A / k_B T\}$, where E_A is the activation energy of diffusion, $1/\tau$ is the attempt frequency and $k_B T$ has its usual meaning. Due to a timescale normalization, the internal time unit of the KMC simulation is a Monte Carlo step (MCS) given by $\tau \cdot \exp\{-E_A / k_B T\}$, thus depending on the temperature. Si dimers, trimers and larger agglo-

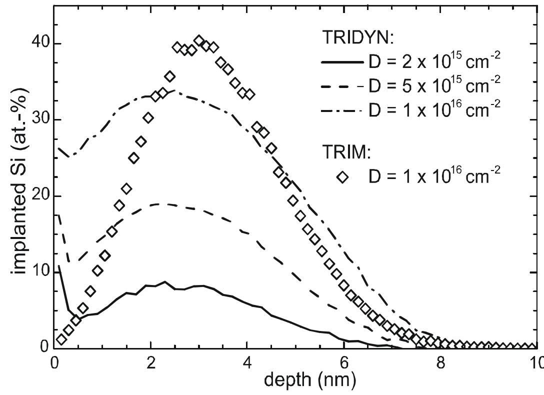

Fig. 1: TRIDYN depth profiles for 1 keV Si^+ implantation into SiO_2. For comparison, a TRIM profile has been added.

merates can form and exhibit a binding energy, which is the product of the Si-Si bond strength E_B by the number of Si-Si bonds. A Si atom having n_i Si neighbors jumps to an empty neighboring site having n_f Si neighbors with a reduced probability

$$P_{if} = \frac{1}{\tau}\exp\left\{-\frac{E_A + \left(n_i - n_f\right)E_B}{k_B T}\right\}$$

if $n_i < n_f$. Otherwise, the diffusional jump probability remains valid.

In principle, the bond strength E_B for the KMC simulation can be determined from the solubility of Si in SiO_2 via the detailed balance of Si attachment/detachment at the Si/SiO_2 interface. (It has to be taken into account that the coordination number in the *fcc* lattice is 12 instead of 4 in the case of the Si lattice.) However, the diffusivity and the solubility of Si in SiO_2 are largely unknown. Thus, a direct relation of simulation and experimental temperatures is difficult, which holds for the time scale too. Nevertheless, the path of system's evolution towards equilibrium and the regimes of phase separation predicted by KMC simulations may improve the process understanding substantially.

In Fig. 2, snapshots of KMC simulations of phase separation are shown for E_B / k_BT = 2.0. Thereby, the TRIDYN profiles of Fig. 1 were used as initial Si distributions. The size of the simulation cell is 56 x 56 x Δz nm^3, where Δz is 8 nm plus swelling due to implantation. Except for the image at the lower right corner, a quarter of the simulation cell is shown only. The simulation cell borders on a fixed (001) layer of the Si substrate to account for the Si/SiO_2 interface. Periodic boundary conditions were applied in the oxide plane, whereas reflecting boundary conditions were assumed at the surface.

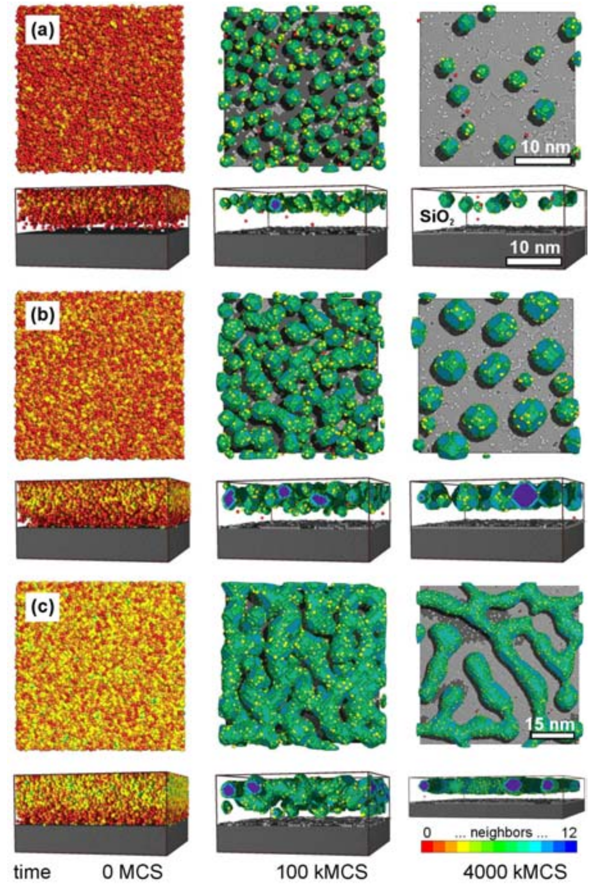

Fig. 2: Snapshots of KMC simulations (top view and cross-section) of phase separation in 8 nm thick SiO_2 on (001) Si during annealing. The simulations start from 1 keV Si^+ TRIDYN profiles for fluences of (a) 2×10^{15} cm^{-2}, (b) 5×10^{15} cm^{-2}, and (c) 1×10^{16} cm^{-2}, respectively. Two regimes were identified, "nucleation and growth" (a) and "spinodal decomposition" (b),(c). Additionally, percolation is observed at the highest fluence (c). Atoms are colored according to their coordination. The 15 nm scale only applies for the lower right corner.

Two regimes of phase separation are predicted by the KMC simulations. A "nucleation and growth" regime is observed for 2×10^{15} Si^+cm^{-2}. Si NCs form by nucleation and grow further at the expense of Si supersaturation (Fig. 2 (a), 100 kMCS). Later on, NCs grow by Ostwald ripening and finally dissolve by Si loss to the SiO_2/Si interface. Above 2×10^{15} Si^+cm^{-2} a "spinodal decomposition" regime is identified, where due to the vanishing nucleation barrier [16] non-spherical, elongated Si structures are formed (Fig. 2 (b), 100 kMCS). At even higher Si concentrations (1×10^{16} Si^+cm^{-2}), above the percolation threshold, the phase separated Si becomes laterally connected (Fig. 2 (c), 100 kMCS). This network of Si does not decay into droplets during longer annealing (Fig. 2 (c), 4000 kMCS). An electrical charge brought to this network can spread over several tens of nanometers, i.e. the phase separated Si behaves like a floating gate in a conventional

metal-oxide-silicon transistor. Below the percolation threshold at 5×10^{15} cm^{-2}, the initially non-spherical Si structures evolve into spherical NCs, which can hardly be distinguished at this late stage from that formed by nucleation and growth (see Fig. 2 (a),(b), 4000 kMCS).

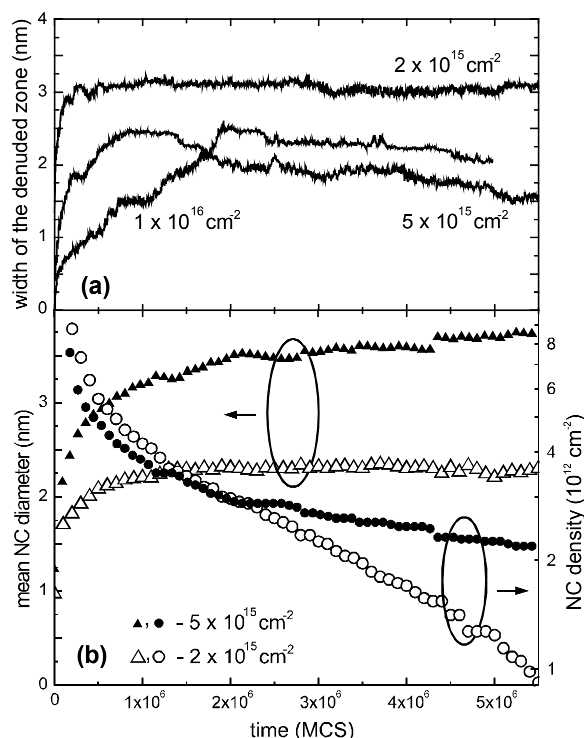

Fig. 3: Evolution of the width of the denuded zone (a) as well as the mean NC diameter and density (b) during annealing for both regimes, nucleation and spinodal decomposition.

The SiO_2/Si interface acts as an effective sink for Si in both regimes, which results in a zone denuded of NCs. However, a more detailed consideration reveals some differences between the nucleation regime and the spinodal decomposition regime. As shown in Fig. 3 (a), for the nucleation regime (2×10^{15} cm^{-2}) the width of the denuded zone is constant over long annealing times. A similar dependence is observed for the NC size (Fig. 3 (b)). The competition between Ostwald ripening and Si loss to the Si/SiO_2 interface keeps the mean NC diameter constant over a long period of annealing. The Si loss manifests itself in a rapid decrease in NC density (Fig. 3 (b)). On the other hand, for the spinodal decomposition regime ($\geq 5\times10^{15}$ cm^{-2}), the interface minimization of the non-spherical Si structures leads to a narrowing of the denuded zone (Fig. 3 (a)). Moreover, Ostwald ripening is more effective than Si loss to the interface and, hence, up to 4000 kMCS the mean NC size is increasing as can be seen in Fig. 3 (b). In contrast to the nucleation regime, the NCs become larger and dissolve slower (Fig. 3 (b)). Of course, a long lasting annealing results also in this regime in a complete dissolution of NCs.

It should be emphasized that NCs form behind a zone completely denuded of NCs (see cross section views of Fig, 2). Additionally, the distance of the NCs from the interface is small enough to allow their charging by direct electron tunneling. This self-alignment of NCs as well as their degradation free charging/decharging is crucial for application in nonvolatile memories [7]. Varying ion implantation energy and annealing temperature gives additional control over the width of the depleted zone and the NC size, which will be described elsewhere [17]. Using Si implantation profiles predicted by TRIM instead of TRIDYN lead to a strong overestimation of the percolation behavior during phase separation, which will be shown there too.

In conclusion, two regimes of Si NC formation by 1 keV Si^+ ion implantation into thin SiO_2 and subsequent annealing have been found by process simulation. Below a Si fluence of 2×10^{15} cm^{-2}, NCs form by nucleation and growth, while at higher fluences spinodal decomposition occurs. At 1×10^{16} cm^{-2}, percolation leads to a spatially connected 2D pattern of Si in SiO_2. The present KMC simulations predict that NC fabrication for non-volatile memory applications should be performed preferably in the nucleation regime. In this regime, the width of the denuded zone does not depend critically on the annealing time and/or temperature. The synthesized NCs are small (2…3 nm diameter) and of high area density (> 10^{12} cm^{-2}).

Acknowledgements

This work was sponsored by the European Community under the auspices of the GROWTH project GRD1-2000-25619.

References

[1] S. Tiwari, F. Rana, H. Hanafi, A. Hartstein, E. F. Crabbe, K. Chan, Appl. Phys. Lett. **68** (1996) 1377

[2] N. Takahashi, H. Ishikuro, T. Hiramoto, Appl. Phys. Lett. **76** (2000) 209

[3] P. Normand, K. Beltios, E. Kapetanakis, D. Tsoukalas, T. Travlos, J. Stoemenos, J. V. D. Berg, S. Zhang, C. Vieu, H. Launois, *et al.*, Nucl. Instr. Meth. B **178** (2001) 74

[4] J. von Borany, R. Groetzschel, K.-H. Heinig, A. Markwitz, B. Schmidt, W. Skorupa, H. Thees, Solid-State Electron. **43** (1999) 1159

[5] M. Ostraat, J.D. Blauwe, M. Green, L. Bell, M. Brongersma, J. Casperson, R. Flagan, H. Atwater, Appl. Phys. Lett. **79** (2001) 433

[6] B. De Salvo, G. Ghibaudo, G. Pananakakis, P. Masson, T. Baron, N. Buffet, A. Fernandes, B. Guillaumot, IEEE Trans. Electron Devices **48** (2001) 1789

[7] T. Müller, K.-H. Heinig, W. Möller, Appl. Phys. Lett. **81** (2002) 3049

[8] W. Möller, W. Eckstein, Nucl. Instr. Meth. B **2** (1984) 814

[9] W. Möller, Nucl. Instr. Meth. B **15** (1986) 688

[10] P. Sigmund, A. Gras-Marti, Nucl. Instr. Meth. B **182/183** (1981) 25

[11] W. Möller, M. Posselt, Wissenschaftlich-Technische Berichte FZR-317, Forschungszentrum Rossendorf, 2001, URL: http://www.fz-rossendorf.de/FWI/FWIT/tridyn.htm

[12] R. Kelly, Surf. Sci. **100** (1980) 85

[13] J.F. Ziegler, J.P. Biersack, U. Littmark, The Stopping and Range of Ions in Solids, Pergamon Press, New York, 1985; URL: http://www.srim.org

[14] M. Strobel, K.-H. Heinig, W. Möller, Phys. Rev. B **64** (2001) 245422

[15] N. Metropolis, A. Rosenbluth, M. Rosenbluth, A. Teller, E. Teller, J. Chem. Phys. **21** (1953) 1087

[16] F.K. LeGoues, Y.W. Lee, H.I. Aaronson, Acta Metall. **32** (1984) 1837

[17] T. Müller, K.-H. Heinig, to be published

Silicon Nanocrystal Memory Devices Prepared by Magnetron Sputtering

J.U. Schmidt and B. Schmidt

In a novel memory device, nanometer-sized silicon quantum dots or nanoclusters (Si NCs) embedded in the gate oxide of a transistor act as discrete charge trapping sites [1]. The transistor threshold voltage is controlled by direct electron/ hole tunneling through a barrier layer into and out off the isolated Si NCs. Alternatively to a direct growth of Si NCs on top of the tunneling oxide [2], the devices can be prepared using the phase separation of metastable silicon rich oxide (SRO, i.e. SiO_x with x<2) into SiO_2 and Si during a high temperature anneal, yielding Si NCs embedded in SiO_2 for sufficiently low Si excess [3]. To form memory devices, in the present work magnetron sputtering of SiO_x and SiO_2 (for use as Si NC precursor and a capping oxide layer, respectively) is investigated as an alternative method to low-energy Si ion implantation into SiO_2 [4]. This process enables the deposition of SiO_x layers with an arbitrary silicon excess profile onto an arbitrary tunneling barrier without causing significant damage. It also allows the preparation of ultrathin (<4 nm) SiO_x layers, sandwiched between the tunnel barrier and the capping oxide film. Annealing of such a stack leads to growth of separated Si NCs constrained to a single Si NC layer at a well-defined distance to the Si substrate, while the mean Si NC size corresponds to the initial SiO_x layer thickness [5].

SiO_x films were deposited by simultaneous magnetron sputtering from two targets: a poly-silicon target (DC powered, 4N purity) and a SiO_2 target (RF powered at 13.6 MHz, 5N purity) in argon atmosphere. The Si substrates, mounted on a rotating table, passed the two targets sequentially at a rotation speed of 30 min^{-1} for a constant deposition time of 270 s. Different compositions x were adjusted by changing the power at the Si target (P_{Si}), while fixing the power at the SiO_2 target at 1 kW. A reference SiO_2 film was sputtered from the SiO_2 target in an $Ar:O_2$=7:1 mixture. In both cases the substrate temperature was 20 °C, the target to substrate separation 5.5 cm and the pressure during deposition 0.6 Pa. The composition of the as-deposited films was determined by elastic recoil detection analysis (ERD) using 35 MeV Cl^- ions. The samples were then cut and left as deposited or exposed to a 30 s rapid thermal anneal (RTA) at 800 °C, 950 °C or 1050 °C in an $Ar:N_2$=1:1 mixture. The composition and film thickness after annealing were investigated by variable angle spectral ellipsometry (VASE), treating SiO_x as a Bruggemann-type mixed medium [6] made up from thermal SiO_2 and crystalline Si. Samples annealed at 1050 °C were analyzed by cross-section electron microscopy (X-TEM). Phase separation and Si-NC formation was monitored by infrared spectroscopy in transmission mode at normal incidence and by photoluminescence (PL) excited at 532 nm. Finally, MOS memory capacitors were prepared by annealing (2 min at 1100 °C) a 20 nm SiO_2/20 nm $SiO_{1.9}$ stack, sputter deposited on a roughly 3 nm thermal oxide on n-type float zone Si. After sputter deposition of Al contacts the devices were annealed for 30 min at 400 °C in forming gas.

The composition analysis of sputter deposited SiO_x films is summarized in Fig. 1. The ellipsometric results of sample composition correlate well with the ERD values and do not differ significantly between different RTA treatments, thus oxidation effects during RTA are considered to be negligible. After the anneal at 1050 °C, crystalline Si NCs were found by X-TEM only for samples with a composition x<1.3 (Fig. 2). In contrast, Si NC-related photoluminescence (PL) is observed for all annealed SiO_x samples (see below). One reason may be the low scattering contrast for small Si crystallites in SiO_2. Also the presence of Si NC related PL does not exclude that the NCs are amorphous [10] for samples with a low Si excess.

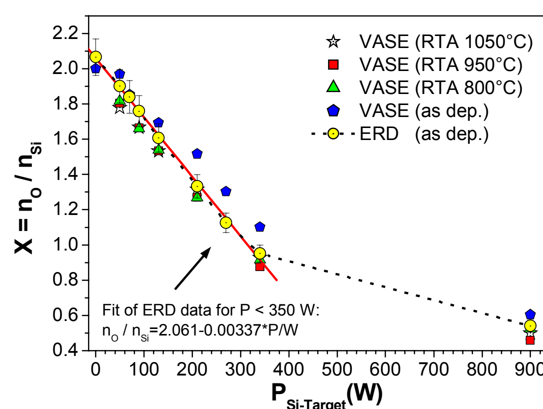

Fig. 1: SiO_x composition measured by ERD and VASE before and after annealing.

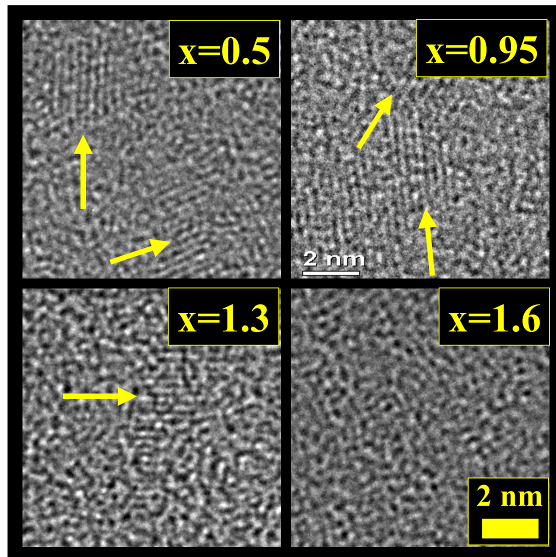

Fig. 2: Cross-section TEM image of annealed SiO_x films with different composition *x*.

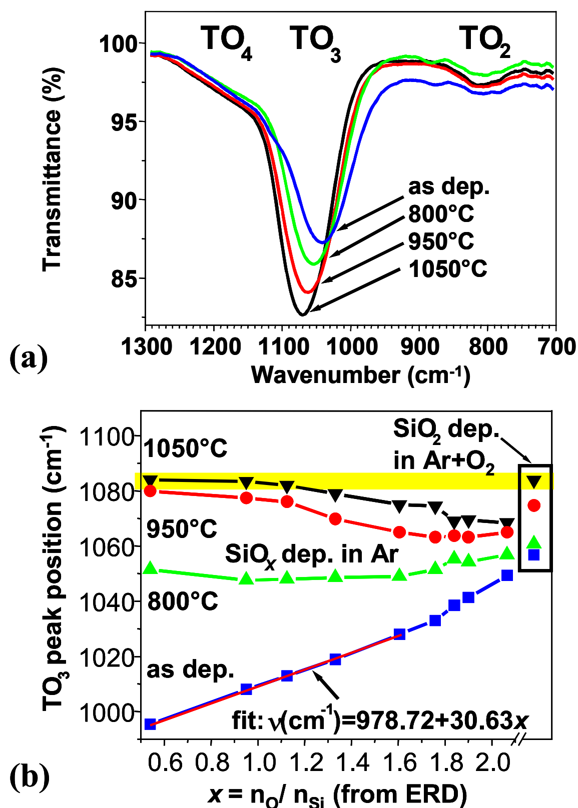

Fig. 3: (a) Infrared absorption of 50 nm $SiO_{1.9}$ film as deposited and after a 30 s anneal at 800 °C, 950 °C and 1050 °C in N_2. Acquired spectra were corrected for substrate absorption. (b) Energy of oxygen stretch vibration of SiO_x deposited in pure Ar as function of composition *x* and annealing temperature *T*. Right: Data from reference SiO_2 film deposited in Ar/O_2 mixture.

Features of the SiO_2 IR transmission spectrum at normal incidence are the TO_1 or Si-O rocking mode at 460 cm^{-1}, the TO_2 Si-O bending mode at 805 cm^{-1}, the TO_3 asymmetric Si-O-Si stretch mode with adjacent O atoms in phase at 1050 cm^{-1} to 1085 cm^{-1} and the TO_4 asymmetric Si-O-Si stretch mode with adjacent O atoms out of phase at 1150 cm^{-1} to 1200 cm^{-1}. The TO_3 band is made up from sub-bands with a relative weight depending on the local bonding configuration [7]. In case of SiO_2 it consists of two sub-bands. One at about 1054 cm^{-1} is typical for compacted films with a high density. The other at about 1090 cm^{-1} dominates in films with a lower density and relaxed structure, like thermally grown and high temperature annealed silicon oxides. For SiO_x the TO_3 band is made up from four sub-bands (1000 cm^{-1}, 1038 cm^{-1}, 1066 cm^{-1}, 1090 cm^{-1}) according to the several ($Si\text{-}O_{4-k}\text{-}Si_k$) ($0 \leq k \leq 4$) bonding tetrahedra to which the two Si next neighbors of the vibrating O atom may belong [8,9]. The phase separation of SiO_x leads to a decrease of excess silicon in the oxide matrix and an increase of Si-O-Si configurations in which the two Si next neighbors of the vibrating O atom are part of Si-(O_4) tetrahedra, as in SiO_2. Consequently the relative weight of the 1092 cm^{-1} sub-band increases during the anneal of SiO_x, giving a rough measure of the progress of phase separation achieved with a particular annealing regime. As shown in Fig. 3(a), the effective TO_3 center frequency of the sputtered $SiO_{1.9}$ sample changes from 1041 cm^{-1} to 1070 cm^{-1} at increasing annealing temperature. Fig. 3(b) shows the energy of the TO_3 mode for as-deposited and annealed samples with different compositions *x* (derived by ERD). Data points on a vertical line correspond to identically prepared samples, but different anneals. On the right, the corresponding data for the SiO_2 reference sample, sputtered in Ar+O_2, are shown. This sample yields an increase in TO_3 energy from 1049 cm^{-1} to 1084 cm^{-1} with increasing annealing temperature, indicating a structural relaxation. Before annealing of SiO_x films deposited at P_{Si}<350 W, the TO_3 band shifts linearly with silicon excess, according to $\nu(cm^{-1})=978.72+30.63x$. Obviously the effect of RTA anneals depends strongly on the initial SiO_x composition *x*. The progress in phase separation (i.e. the gradual shift of the TO_3 center frequency towards the limit of 1090 cm^{-1}) is more pronounced for SiO_x samples with a higher silicon excess (smaller *x*). Even at 1050 °C samples with an oxygen/silicon ratio *x*>1 do not complete the phase separation during the 30 s anneal. The reason for this behaviour can be derived from classical nucleation theory [11]. In order to form a silicon precipitate, a nucleation energy barrier must be overcome. This barrier rises with decreasing silicon excess due to a higher probability of Si

atoms to detach from the precipitate and to diffuse into the oxide matrix. Consequently, for a given annealing temperature, the initial precipitate density is always higher in films with higher silicon excess. The mean distance between a Si impurity atom and a precipitate is smaller and therefore growth and ripening processes governed by diffusion proceed faster, compared to samples with a lower precipitate density. For very high precipitate densities, an additional contribution of Si monomer transport by surface diffusion is expected to accelerate the growth and ripening processes.

The mechanism of the Si NC related PL is still under debate. Apparently oxygen related interface states at Si NCs are involved in the PL mechanism with a short (µs) decay time for which optical gain from Si NCs was demonstrated [12]. On the other hand, many features of the slow (ms) PL (red-shift of PL emission with increased annealing time or temperature) can be explained assuming a quantum confinement model, in which both phonon-assisted transitions (PAT) and no-phonon transitions (NPT) within the Si NC contribute to the emission with a relative weight depending on the Si NC diameter L. The oscillator strength of PAT scales as $(1/L)^3$, the probability of the NPT as $(1/L)^6$ [13], i.e. the emission intensity decreases rapidly with increasing cluster size. The emission energy is expected to rise with decreasing NC diameter due to quantum confinement, although for oxygen passivated clusters the effect is weaker since silicon-oxygen bonds introduce new states in the energy gap of the Si NC [14,15]. From this model one expects that, during annealing, the PL intensity initially increases rapidly with the number of formed precipitates. Due to the mentioned size effects, the PL intensity would then saturate and even decrease when the nucleation rate is too small to compensate for the decrease in intensity due to cluster growth and ripening. This would allow to experimentally distinguish nucleation and growth/ripening phases by monitoring the maximum of the intensity of the NC-related PL in a series of isochronal anneals at different temperatures. For this purpose, SiO_x films of various compositions were annealed at 800 °C, 950 °C or 1050 °C. Similar to the IR measurements, differences are found between films with low and high Si excess, due to a different progress in phase separation (Fig. 4) achieved with a fixed thermal budget. The top of Fig. 4 shows a sample with low Si excess, for which phase separation is slow and not completed after annealing at 1050 °C, as known from the IR spectra (see Fig. 3(b)). The PL rises with annealing temperature while the energy of the PL maximum is constant (about 1.6 eV). This indicates the predominant nucleation of Si NCs. This behaviour observed for x=1.9 changes continuously with decreasing x to the one shown for x=1.6 in Fig. 4 (bottom). As known from Fig. 3(b), for this film with a high Si excess the phase separation proceeds faster than for the other one.

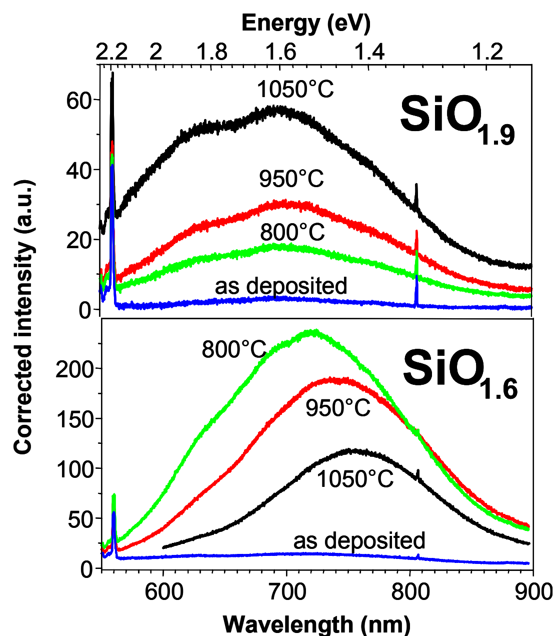

Fig. 4: Change of Si NC related PL with rising annealing temperature. Top: Low Si excess ($SiO_{1.9}$). The growth of PL intensity with temperature is attributed to dominant nucleation. Bottom: High Si excess ($SiO_{1.6}$). The red-shift and a decreasing PL intensity for increased annealing temperature indicate the dominance of growth and ripening.

Consequently the PL maximum is found already at the lowest annealing temperature. A redshift and decrease of PL intensity occurs for higher annealing temperatures. This indicates that nucleation of Si NCs is largely completed at 800 °C, and higher annealing temperatures are already sufficient to initiate cluster growth and ripening. Hence, the annealing temperature required to achieve the final state of Si NC nucleation and to start growth and ripening (indicated by the PL maximum) decreases with rising silicon excess.

MOS capacitors with Si NCs embedded in the gate oxide have been investigated by current-voltage and capacitance-voltage measurements as well as by write/erase and retention tests. The current-voltage behaviour of sputtered and annealed SiO_2 resembles that of thermal SiO_2, except for a minor contribution of trap-assisted tunneling in the mid-field region. The traps originate most likely from residual defects in the oxide network due to low temperature deposition and are essentially removed by thermal annealing. Fig. 5 shows that large memory windows (>1 V) are achieved when charging/discharging the Si NCs by applying short

and rather low voltage pulses (write: 1 ms, 6 MV/cm; erase: 5 ms, 6 MV/cm). The charge retention time at room temperature, determined using the constant capacity method, exceeds 2 days (Fig. 6). In contrast reference capacitors using sputtered SiO_2 without Si NCs show only slight hole charging after high field stressing at positive gate potential, accompanied by the generation or de-passivation of interface traps.

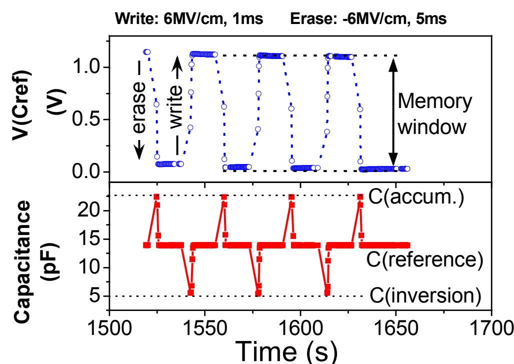

Fig. 5: Write/erase test using a MOS capacitor prepared from a 20 nm SiO_2 / 20 nm $SiO_{1.9}$ stack, sputtered onto a 3 nm thermal oxide on Si (constant capacity method).

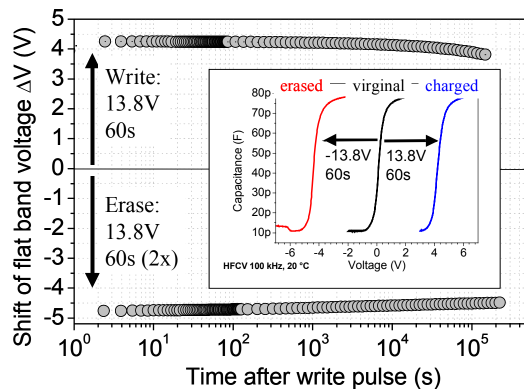

Fig. 6: Room temperature charge retention test on the same device. The Si substrate is close to flat band condition.

In summary photoluminescence and infrared spectroscopy were used to study the formation of Si NCs in SiO_x films. The full functionality of Si NC memory devices prepared by sputter deposition and annealing of SiO_x has been demonstrated.

Acknowledgements

We acknowledge the help by A. Mücklich and U. Kreissig with XTEM and ERD, and thank the German research foundation (DFG) for grant number SCHM 1490 1-1.

References

[1] S. Tiwari, F. Rana, K. Chan, L. Shi, H. Hanafi, Appl. Phys. Lett. **69** (1996) 1232

[2] T. Baron, F. Martin, P. Mur, C. Wyon, M. Dupuy, C. Busseret, A. Souifi, G. Guillot, Appl. Surf. Sci. **164** (2000) 29

[3] L.A. Nesbit, Appl. Phys. Lett. **46** (1985) 38

[4] P. Normand, D. Tsoukalas, E. Kapetanakis, J.A. van den Berg, D.G. Armour, J. Stoemenos, Microel. Eng. **36** (1997) 79

[5] M. Zacharias, J. Heitmann, R. Scholz, U. Kahler, M. Schmidt, J. Bläsing, Appl. Phys. Lett. **80** (2002) 66

[6] D.A.G. Bruggemann, Annalen der Physik (1900) **22** (1935) 636

[7] A. Lehmann, L. Schuhmann, K. Huebner, phys. stat. sol. (B) **117** (1983) 689; phys. stat. sol. (B) **121** (1984) 505

[8] I.P. Lisovskii, V.G. Litvichenko, V.G. Lozinskii, G.I. Steblovskii, Thin Solid Films **213** (1992) 164

[9] I.P. Lisovskii, V.G. Litovchenko, V.B. Lozinskii, S. I. Frolov, H. Flietner, W. Fussel, E. G. Schmidt, J. Non-Cryst. Solids **187** (1995) 91

[10] H. Rinnert, M. Vergnat, A. Burneau, J. Appl. Phys. **89** (2001) 237

[11] M. Volmer, A. Weber, Z. Phys. Chem. **119** (1926) 277

[12] L. Pavesi, L. Dal Negro, C. Mazzoleni, G. Franzo, F. Priolo, Nature **408** (2000) 440

[13] D. Kovalev, H. Heckler, G. Polisski, F. Koch, phys. stat. solidi (B) **215** (1999) 871

[14] I. Vasiliev, J.R. Chelikowsky, R.M. Martin, Phys. Rev. B **65** (2002) 121302

[15] A. Puzder, A.J. Williamson, J.C. Grossman, G. Galli, Phys. Rev. Lett. **88** (2002) 97401(4)

Charge Trapping in Ge-Implanted Light Emitting SiO_2 Layers

T. Gebel, L. Rebohle, W. Skorupa, A.N. Nazarov[1], I.N. Osiyuk[1] and V.S. Lysenko[1]

[1]*Institute of Semiconductors Physics, National Academy of Sciences, Kyiv, Ukraine*

Metal-oxide-silicon (MOS) devices implanted with Ge^+ ions are very promising for room temperature silicon-based electro-luminescence (EL) devices [1-5]. However, because these devices are operated at high-electric fields (7–8 MV/cm), stability and charge accumulation in the oxide are the main problems for their application [3]. In this work for the first time negative and positive charge trapping phenomena in the Ge^+ ion implanted oxides that occurs during EL device operation in the constant current regime are reported.

Thermally grown 80 nm thick SiO_2 films on (100) n-type Si wafers were implanted with Ge^+ ions at an energy of 50 keV to fluences of 6.5×10^{15} cm^{-2}. As measured by Rutherford backscattering (RBS), the Ge profile shows a maximum concentration of about 3 at% at about 30 nm below the oxide surface. The as-implanted devices were divided into 3 sets and rapid thermal annealing (RTA) at 1000 °C was performed for 6, 30 and 150 s. MOS capacitors for electrical measurements were fabricated using sputtered layers of Al for both, the gate electrode (area 1×10^{-3} cm^2) and the back contact.

High-field electron injection from the silicon substrate into the oxide was performed at constant current ($J_{inj}=2\times10^{-5}$ A/cm^2) at room temperature with a Keithley 237 source measurement unit. Charge trapping was studied by combined measurements of the change of the voltage which was applied to the MOS structures at constant current regime (ΔV_{CC}) [6,7], and the shift of the flat-band voltage (ΔV_{FB}) of high-frequency (1 MHz) capacitance-voltage (C-V) characteristics performed at definite intervals [6]. The C-V characteristics were measured with a Keithley 590 CV meter. The use of the flat-band voltage shift was motivated by the minimum concentration of electron surface states generated during the high-field electron injection in this band gap depth at the SiO_2-Si interface compared to the mid-gap condition.

The change of the voltage applied to the MOS structure at constant current operation under high-field electron injection from the silicon substrate as a function of the injected charge (Q_{inj}) is depicted in Fig. 1. The increase in the voltage during the high-field electron injection suggests negative charge trapping in the oxide volume at a distance from the injecting SiO_2-Si interface larger than the tunneling length [8]. It is worth noting that the measurement characteristics show only negative charge trapping in the oxide during the measurement cycle (increase of ΔV_{CC}).

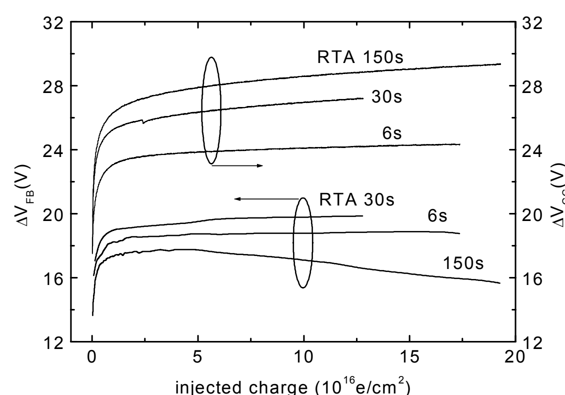

Fig. 1: Flat band voltage shift (left scale) and change of the voltage, applied to the MOS structure at constant current (right scale), as a function of electron fluence for different times of the RTA treatment at 1000° C.

At the same time the ΔV_{FB} shift (C-V method) shows a negative charge trapping followed by positive charge trapping in the oxide as visible in Fig. 1 by the increasing and later decreasing voltage shift. This effect is especially pronounced for samples annealed for 150 s. Since this method allows one to measure a total net charge in the oxide and gives the maximum sensitivity to the charge located at the oxide-semiconductor interface, it is obvious that the trapped positive charge is located at the SiO_2-Si interface.

Since in our case the ΔV_{CC} vs. Q_{inj} method is only sensitive to the trapped negative charge, but the ΔV_{FB} vs. Q_{inj} method takes into account both, negative and positive trapped charge, the parameters of the trapped negative charge can be estimated directly from the first characteristic and the positive charge by subtraction of the first from the second one. In Fig. 2 these results are plotted vs. the injected electron charge.

Assuming first-order trapping kinetics, the trapped charge (both, the negative and positive one) versus the injected charge can be described by the expression [9]

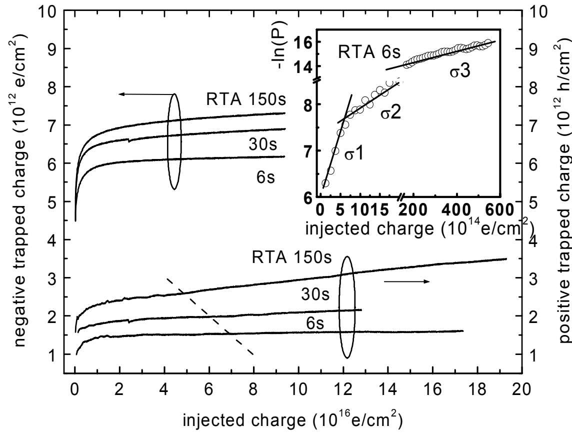

Fig. 2: Negative trapped charge (left scale) and positive trapped charge (right scale) as a function of electron fluence for different times of RTA treatment at 1000° C. The inset shows the trapping efficiency as a function of electron fluence for 6 s RTA treatment at 1000° C.

$$Q_t = Q_t^{\max}[1 - \exp(-\sigma_i Q_{inj})], \qquad (1)$$

where Q_t is the trapped charge, Q_t^{max} is the maximum trapped charge and σ_i is the effective capture cross-section of the trap.

If the trapping efficiency P is defined as the first derivation of the injection charge in Eq. (1), then we obtain [10]

$$P = \frac{dQ_t}{dQ_{inj}} = \sigma_i Q_t^{\max} \exp\left(-\sigma_i Q_{inj}\right) . \qquad (2)$$

From Eq. (2) it is easily understood that for each trap the plot of ln(P) vs. Q_{inj} will consist of a linear part with the slope corresponding to σ_i. The extrapolation to Q_{inj}=0 for such a plot provides $\sigma_i Q_t^{max}$. Thus, using this method [10], the number and the main parameters of the traps can be estimated. Our calculations demonstrate (see inset in Fig. 2) that three types of electron traps with average values of the capture cross-section of σ_1=2.6×10^{-15} cm^2, σ_2=6.3×10^{-16} cm^2 and σ_3=3.0×10^{-18} cm^2, and maximum concentrations (for 6 s RTA) of Q_{t1}^{max}=1.0×10^{12} cm^{-2}, Q_{t2}^{max}=1.0×10^{12} cm^{-2} and Q_{t3}^{max}=6.5×10^{12} cm^{-2} can be found in this manner.

In the case of high-field electron injection from the silicon substrate the capture of the positive charge near the SiO_2-Si interface, as evaluated from the C-V measurements, can be explained by the band-to-band impact ionization (BTB) [11] and the anode hole injection mechanism [6]. In both mechanisms the charge trapping can be described by Eq. (1), where the effective capture cross-section (σ_i^+) includes the probability of positive charge generation and the recombination cross-section for electrons in positively charged traps [12]. For both mechanisms the maximum equilibrium positive charge (Q_{pos}^{max}) can be estimated from the saturation value of the accumulated positive charge. Since the initial slope of the Q_t – Q_{inj} characteristics provides $\sigma_i^+ Q_{pos}^{max}$ (see Eq. (1)), the effective capture cross-section can be easily calculated.

In our case, using the saturation value of the accumulated positive charge on the level determined by the dashed line in Fig. 2, that is Q_{pos1}^{max}=1.5×10^{12} cm^{-2}, Q_{pos2}^{max}=1.8×10^{12} cm^{-2} and Q_{pos3}^{max}=2.5×10^{12} cm^{-2}, the average value of the effective capture cross-section σ_i^+=1.5×10^{-17} cm^2 was obtained. It should be noted that the increase in the injected charge above the marked level leads to the accumulation of additional positive charge that, possibly, is related to an additional trap generation.

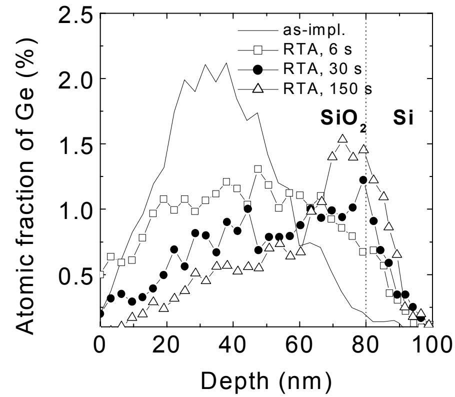

Fig. 3: Distribution of the implanted Ge (50 keV, 6.3x10^{15} cm^{-2}) in the SiO_2 layer, measured by RBS. The initially implanted Ge diffuses towards the SiO_2 / Si interface and forms an additional peak. After 150 s RTA already 30% of the implanted Ge diffused out through the surface.

It should be emphasized that both positive and negative charge trapping increase with the annealing time of the Ge^+ ion implanted MOS devices. The enhancement of positive charge trapping at the SiO_2-Si interface is associated with the diffusion of Ge atoms and their embedding at the interface region during the high-temperature annealing. This behavior was experimentally confirmed by RBS measurements. Fig. 3 shows the distribution of the implanted Ge as a function of the RTA time. The initial Ge peak shows a strong broadening during annealing and a second Ge peak is formed near the SiO_2-Si interface, as known from similar systems with Ge implanted oxide layers [13]. Additionally, out-diffusion of the Ge through the surface of the SiO_2 layer was observed. Within a 150 s RTA treatment about 30% of the initially implanted Ge diffused out. The increase in negative charge trapping in the bulk of

the oxide with increase in RTA time might be related to the generation of defects during the diffusion of the implanted Ge atoms through the oxide. Furthermore the effect of cluster evolution due to Ostwald ripening has also to be taken into account.

In conclusion, we have demonstrated that Ge^+ implanted and subsequently RTA treated SiO_2 layers contain a sufficient high concentration of electron traps (of the order of 10^{12} cm^{-2}) with different capture cross-sections $\sigma_1^- = 2.6\times10^{-15}$ cm^2, $\sigma_2^- = 6.3\times10^{-16}$ cm^2 and $\sigma_3^- = 3.0\times10^{-18}$ cm^2, which effectively capture negative charge during the operation of EL devices. Additionally, in the case of high-field electron injection from the silicon substrate into the silicon dioxide positive charge generation at the SiO_2-Si interface is observed.

Acknowledgements

We thank the German Bundesministerium für Bildung und Forschung (BMBF) for financial support (contract WTR UKR 01/054).

Part of this work has been recently published as T. Gebel et al., Appl. Phys. Lett. **81** (2002) 2575.

References

[1] J.Y. Zhang, X.L. Wu, X.M. Bao, Appl. Phys. Lett. **71** (1997) 2505

[2] L. Rebohle, J. von Borany, R.A. Yankov, W. Skorupa, I.E. Tyschenko, H. Fröb, K. Leo, Appl. Phys. Lett. **71** (1997) 2809

[3] L. Rebohle, J. von Borany, H. Fröb, W. Skorupa, Appl. Phys. B **71** (2000) 13

[4] L. Rebohle, J. von Borany, D. Borchert, H. Fröb, T. Gebel, M. Helm, W. Möller, W. Skorupa, Electrochem. Sol. State Lett. **4** (2001) G57

[5] T. Gebel, L. Rebohle, J. Zhao, D. Borchert, H. Fröb, J. von Borany, W. Skorupa, Mat. Res. Soc. Symp. Proc. **638** (2001) F18.1.1

[6] M.V. Fischetti, J. Appl. Phys. **57** (1985) 2860

[7] P. Samanta, C.K. Sarkur, Solid State Electronics **41** (1997) 459

[8] D.A. Buchanan, A.D. Marwick, D.J. DiMaria, L. Dori, J. Appl. Phys. **76** (1994) 3595

[9] V.V. Afanas'ev, V.K. Adamchuk, Progress in Surface Science **47** (1994) 301

[10] T.N. Ning, H.N. Yu, J. Appl. Phys. **45** (1974) 5373

[11] D.J. DiMaria, Solid-State Electron. **41** (1997) 957

[12] D. Arnold, E. Cartier, D.J. DiMaria, Phys. Rev. B **49** (1994) 10278

[13] J. von Borany, K.-H. Heinig, R. Grötzschel, M. Klimenkov, M. Strobel, K.-H. Stegemann, Microelectronic Engineering **48** (1999) 231

Current Bistability in an Efficient Silicon Light-Emitting Diode

J. M. Sun, T. Dekorsy, W. Skorupa, B. Schmidt and M. Helm

In recent years there has been significant effort for the development of active optoelectronic components based on silicon, which can be fabricated with mainstream CMOS technology. The main pathways for the development of electroluminescent light emitters are based on porous silicon [1], Erbium doping of silicon [2], Si nanoclusters in SiO_2 [3], and silicon pn diodes under forward bias [4]. We followed the route of the latter approach by employing high dose B implantation into silicon for the formation of planar pn diodes. Here, we report on the optical and electrical characterization of these diodes at low temperatures, which reveals a current bistability of the diodes which is closely related to the exciton dynamics in the structures. The investigation of the coupled dynamics of excitons and free carriers contributes to the understanding of the performance of the diodes and will help in their future optimization.

The bistable current-voltage (I-V) characterristics of a semiconductor device usually manifest in a hysteretic switching between a high-impedance, low-current (off) state and a low-impedance, high-current (on) state [5]. This nonlinear transport phenomenon is the basis of a family of static random access memories (SRAM) [6], logic circuits [7,8] as well as high-frequency oscillators [9,10]. Although the conditions or origins leading to the bistability might differ for various device structures, it is commonly assumed that the charge accumulation at or the release from the potential wells in the structures cause a change of the band bending of the potential barriers, and subsequently, the electrostatic feedback leads to the bistability in the I-V characteristics [5]. Exciton-induced *optical* bistability is well known in III-V semiconductors. However, there have been very few studies on the exciton-induced current bistability in heterostructures [11]. The reason is probably that excitons cannot cause a band bending and redistribution of charge profiles due to their intrinsically neutral-charged states. In this report, we present the observation of a novel S-type differential resistance in the I-V characteristics of a silicon pn diode produced by boron ion implantation. Similar devices have recently attracted large interest as efficient silicon based light-emitting diodes (LED) [4]. The current bistability in our device is based on the formation and ionization of excitons bound to the shallow traps introduced by boron ion implantation and subsequent high-temperature annealing, as determined by the simultaneous measurement of the bistable current and the excitonic electroluminescence (EL) as a function of the applied voltage. A new model gives a complete description of the origin of the S-type negative differential resistance.

The silicon pn diode was prepared by boron implantation into (100) oriented n-type (0.1 Ω·cm) silicon substrates with a dose of 4×10^{15} cm^{-2} at an energy of 25 keV through a 50 nm thermally grown SiO_2 layer. The sample was subsequently annealed at 1050 °C for 20 minutes and processed into 1 mm diameter diodes (A = 0.00785 cm^2). The diode was mounted on the cold finger of a closed-cycle cryostat by silver paste for low temperature EL studies. I-V characteristics were measured with a sourcemeter (Keithley 2410) in a current- or voltage-controlled mode. EL spectra were measured with a monochromator and a liquid nitrogen cooled InGaAs detector. The EL peak intensity was recorded simultaneously with the I-V characteristics.

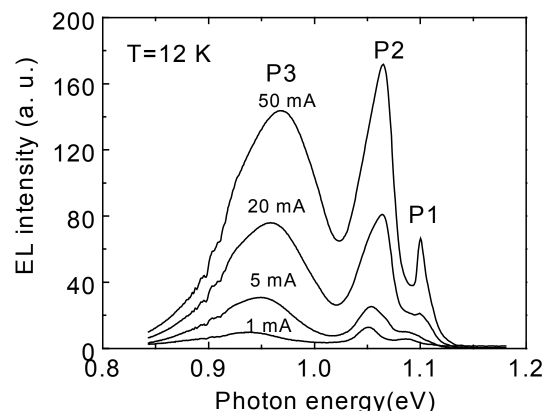

Fig. 1: EL spectra of a silicon pn diode at a temperature of 12 K with different injection currents as given in the figure.

The diode shows efficient room temperature EL from band-edge electron-hole recombination of silicon with an external quantum efficiency up to 0.1%. EL spectra are measured at 12 K for different injection currents, as shown in Fig. 1. The EL spectra show three bands, marked as P1, P2 and P3. The band P1 (1.1 eV) is due to transverse opti-

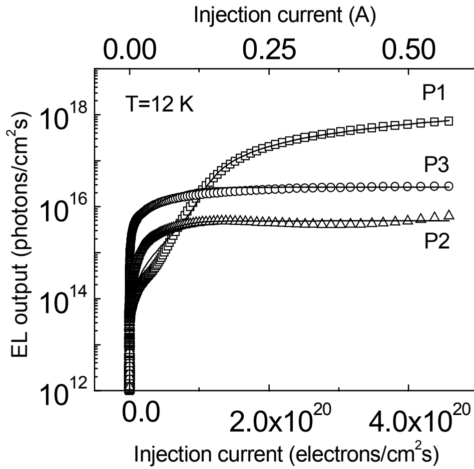

Fig. 2: Dependence of EL output photons as a function of the injection current for different emission peaks P1 (open squares), P2 (open triangles), and P3 (open circles) measured at 12 K. The scattered plots are experimental data, and the solid lines represent a fit using the rate equation model.

cal (TO) phonon-assisted recombination of free excitons in silicon. The spectral shape and the peak energy of P2 are similar to the photoluminescence (PL) band from a boron doped p^+ silicon wafer with a hole concentration of 3×10^{18} cm^{-3} [12]. It is therefore assigned to TO phonon-assisted recombination of the bound excitons in the p^+ region close to the pn junction. The broad band P3 at 0.9-1.0 eV is probably related to the strain-induced reduction of the band gap in combination with the confinement of carriers by localized electric fields due to high boron concentrations around the dislocations [13]. The dependences of the integrated EL intensity as a function of injection current for the three peaks are shown in Fig. 2. Initially, only the trap bands P2 and P3 are observed in the EL spectra at low current injection. Then, the EL intensities of P2 and P3 saturate with increasing current. Finally, after saturation of the shallower trap band P2, the free exciton peak P1 emerges and its intensity grows linearly with increasing current.

The I-V characteristics of the diode show a novel S-type negative resistance characteristic in a current-controlled sweeping mode at temperatures ranging from 12 to 30 K, as shown in Fig. 3. The negative resistance region starts from a low-current stable state at the emergence of P2 and ends at a high-current stable state where the EL of the shallower trap band P2 saturates. The typical current contrast between the two stable branches is of the order of 10^4. The high and the low current states can be well fitted by simply setting a small and a large value to the series resistance, R_s, in the equation of a pn junction diode,

$$J = J_0[\exp(V_j - J\cdot R_s)/(nkT) - 1],$$

where V_j, J, and T are the applied voltage, current, and the temperature, respectively. J_0, n and k are constants. At 50 K, the S-type negative resistance should be thermally quenched through a decrease of the series resistance R_s of the lower current state due to increasing free carrier emission from the shallow traps. Since no obvious overall shift of the I-V characteristics of the pn junction is observed with increasing current, the shallow traps, which contribute to the negative resistance at low temperatures, must be neutral-charged traps such as excitonic traps, neutral donors and acceptors.

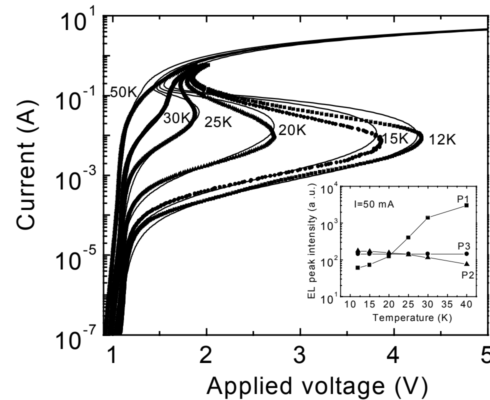

Fig. 3: Current-controlled I-V characteristics of the silicon pn junction diode at different temperatures. The scattered plots are experimental data and the solid lines represent calculations. Note that the high-current branch can only be measured up to 600 mA due to the high dissipated power. The insert shows the temperature dependence of the EL intensity at different peaks.

In order to determine which trap band contributes to the negative resistance, the temperature dependence of the peak intensities of P1, P2 and P3 is measured at a fixed current of 50 mA, as shown in the insert of Fig. 3. The thermal emission of the free carriers from the shallower excitonic traps is confirmed by an increase of P1 and the simultaneous decrease of P2 with increasing temperature. The EL intensity of P3 is constant in this temperature range due to insufficient thermal energy for ionization of deeper traps. The above results indicate that the shallower bound excitons at least partially contribute to the negative differential resistance of the pn diode.

The above interpretation of the observed correlation between carrier transport and EL can be fully accounted for by a simplified system containing free and bound excitons [14]. Assuming that the minority free-carrier concentration is proportional to the free-exciton concentration with a thermal equilibrium constant γ, the relationships between the EL intensity of the free (bound) excitons and the injection current can be simulated

by solving the steady state solutions of three rate equations for the number of free excitons, the shallower bound excitons P2, and traps P3, taking into account all the ionization, capture and recombination processes. The solutions are shown in Fig. 2. The series resistance R_s of the diode can be expressed as a function of the mean filling factor f_t of bound exciton P2 and trap P3,

$$R_s \approx R_c + \frac{1-f_t}{e\cdot(\mu_e+\mu_h)\left[(\gamma\alpha - n_{0b})\cdot f_t + n_{0b}\right]} \quad (1),$$

where R_c is a constant small resistance related to the ohmic contact of the electrode; μ_e (μ_h) and e are the mobilities of free electrons (holes) and electron charge, respectively; n_{0b} is the background free carrier concentration at zero current; α is a parameter determined by $\alpha = N_t(e_t+W_t)/c_t$, where N_t, e_t, W_t, and c_t are the sum of the trap densities, the average thermal emission, recombination, and capture rate, respectively, of bound exciton P2 and trap P3. Eq. (1) shows that α and n_{0b} are key parameters for the observation of the negative resistance, i.e., the second term of the right side of Eq. (1) would decrease dramatically with the increasing filling factor f_t of the trap states at a low temperature when $n_{0b} << \gamma\alpha$. The series resistance R_s is reduced from a high stable value $\sim 1/ e \cdot (\mu_e + \mu_h) \cdot n_{0b}$ to a low stable value close to R_c as f_t varies from 0 to 1 with increasing the injection current; this is the origin of the negative resistance at low temperature. As the temperature increases, the thermal ionization of the shallower excitonic traps and of the neutral acceptors (donors) causes a strong increase of n_{0b} in the diode. Finally, the series resistance is reduced to a single value $\sim R_c + 1/ e \cdot (\mu_e + \mu_h) \cdot n_{0b}$ for $n_{0b} << \gamma\alpha$, where the capture and emission of free carriers by traps has a weak influence on the series resistance of the diode. Therefore, thermal quenching of the negative resistance can be observed at high temperature, as shown in Fig. 3. The S-type I-V curves are also calculated at different temperatures in Fig. 3 by this model. The theoretical calculations fully reproduce the experimental results.

In summary, bound exciton-induced current and EL bistabilities with an S-type I-V characteristic are observed in a silicon pn-junction diode at temperatures below 30 K. The two stable states in the current and the EL intensity from bound excitons and free excitons observed for a given voltage are correlated to the empty and occupied bound exciton states in the silicon pn diode. The consistency between the theoretical and experimental results indicates that bound excitons, despite their neutral-charged states, contribute to the S-type differential resistance in silicon pn-junction diode.

Acknowledgements

The authors would like to thank I. Beatus, I. Winkler, S. Sinning, T. Gebel and U. Lucchesi for assistance in the sample preparation and EL experiments, and U. Hornauer for fruitful discussions.

References

[1] B. Gelloz, N. Koshida, J. Appl. Phys. **88** (2000) 4319; N. Koshida, H. Koyama, Appl. Phys. Lett. 60 (1992) 347

[2] G. Franzo, F. Priolo, S. Coffa, A. Polman, A. Carnera, Appl. Phys. Lett. 64 (1994) 2235; M. Markmann, A. Sticht, F. Bobe, G. Zandler, K. Brunner, G. Abstreiter, E. Müller, J. Appl. Phys. **91** (2002) 9764

[3] D. J. DiMaria, J. R. Kirtley, E. J. Pakulis, D.W. Dong, T. S. Kuan, F. L. Pesavento, T.N. Theis, J. A. Cutro, S. D. Brorson, J. Appl. Phys. **56** (1984) 401

[4] W. L. Ng, M. A. Lourenco, R. M. Gwillia, S. Ledain, G. Shao, K.P. Homewood, Nature **410** (2001) 192

[5] A. Wacker, E. Schöll, J. Appl. Phys. **78** (1995) 7352

[6] T. K.Carns, X. Zheng, K.L. Wang, IEEE Electron. Device Lett. **16** (1995) 256

[7] W. C. Liu, J. H. Tsai, E. S. Lour, L.W. Laih, S.Y. Cheng, K. B.Thei, C. Z. Wu, IEEE Trans. Electron. Devices **44** (1997) 520

[8] A.A. Lakhani, R. C. Potter, Appl. Phys. Lett. **52** (1988) 1684

[9] A. Krotkus, A. Reklaitis, A. Geizutis, J. Appl. Phys. 84 (1998) 3980

[10] E. R. Brown, J. R. Söderström, C.D. Parker, L.J. Mahoney, K.M. Molvar, T. C. Mc Gill, Appl. Phys. Lett. **58** (1991) 2291

[11] P. A. Parlangeli, P. C. M. Christianen, J. C. Maan, M. Henini, Phys. Rev. B **63** (2001) 115307

[12] J.-P. Noël, N. L. Rowell, J. E. Greene, J. Appl. Phys. **77** (1995) 4623

[13] H. Weman, B. Monemar, G. S. Oehrlein, S.J. Jeng, Phys. Rev. B **42** (1990) 3109

[14] X.Y. Zhang, K. Dou, Q. Hong, M. Balkanski, Phys. Rev. B **41** (1990) 1376

Femtosecond Electron and Phonon Dynamics in High-Temperature Superconductors: New Insight into the Pseudogap Regime

T. Dekorsy, N. Georgiev, M. Helm and O.V. Misochko[1]

[1] *Institute of Solid State Physics, Russian Academy of Sciences, Chernogolovka,Russia*

The time-resolved investigation of elementary properties of matter has led to a deep insight into the underlying physics of solid state. Especially optical methods employing femtosecond (fs) laser pulses allow us to disentangle the most important processes in semiconductors and superconductors like energy relaxation of electrons, electron-phonon inter-action, plasmon-phonon dynamics etc. The understanding of these processes on a sub-picosecond time scale is of prime importance for the development of future THz electronic and optoelectronic devices. Despite more than a decade of research since their discovery, the physics of high temperature superconductivity in copper oxides - especially the relevant pairing mechanism of Cooper pairs - is still unresolved. Time-resolved methods may shine more light on this hot topic of solid-state physics, since concurring phenomena on equal energetic scales may be discriminated by their different temporal dynamics.

The present picture of the different phases of high-temperature superconductors is shown in Fig. 1, where the occurring phases are plotted versus the hole concentration for p-doped $YBa_2Cu_3O_{7-x}$ [1]. In a certain range of doping concentration the material is superconducting with a maximum transition temperature of 90 K for the optimally doped case, at low doping concentrations the system is an antiferromagnet. In the normal conducting phase a doping dependent transition temperature T^* has been found, which is characterized by the fact that below this temperature certain evidence for the existence of superconducting properties above the transition temperature T_c was found. The origin of this so-called pseudogap regime, which is associated with several anomalies, is presently discussed very controversially. There are two basic scenarios for explaining the pseudogap anomalies. The first one is based on preformed electron pairs with the subsequent establishment of their phase coherence below T_c. The second scenario suggests that the pseudogap state emerges due to short-range order fluctuations of dielectric type (antiferromagnetic order, charge-density-waves, phase separation on a microscopical scale etc.). Most theoretical models consider the pseudogap regime as uniform, whose width [T^*-T_c] in the phase diagram depends on the doping level. This width is maximal for underdoped compositions, shrinking to zero at a doping level slightly higher than optimal. However, a few theoretical studies suggest that there is a crossover within the pseudogap state making the state non-uniform and split into two regimes characterized by distinct dynamical and relaxational properties [2-4]. Though in recent years an enormous progress in clarifying the properties of the pseudogap state including its symmetry was made, many problems remain open yet [1]. This is related in part to the fact that the energy scales characteristic of superconducting and pseudogap states are very close, which, coupled to the fact that the symmetry of the two gaps seems to be the same, makes it extremely difficult to distinguish them. Although not yet employed as extensively as well established spectroscopic methods, time-domain spectroscopy can potentially delineate which electronic states are responsible for the superconductivity and what is the connection, if any, of the pseudogap above T_c with the superconducting gap below T_c. This distinction could be achieved through the study of non-equilibrium relaxation dynamics that may be quite different even for excitations with almost equal energies.

Previous time-domain studies of the lattice and carrier dynamics in $YBa_2Cu_3O_{7-x}$ have already revealed changes on a subpicosecond scale close to T_c. In the superconducting state, the coherent amplitude of the Ba phonon mode starts to grow [5,6] and a strong increase in the relaxation time is observed [7-9]. Both anomalies were linked to the breaking of Cooper pairs, even though described within different theoretical approaches - the displacive excitation of coherent phonons [10] and changes of the Drude tail, modification of matrix elements, and a two-fluid model for the non-oscillatory part of the ultrafast response [7-9,11]. Moreover, a few studies performed on underdoped samples showed that the characteristics of the pseudogap can be observed in the time-domain [12-14].

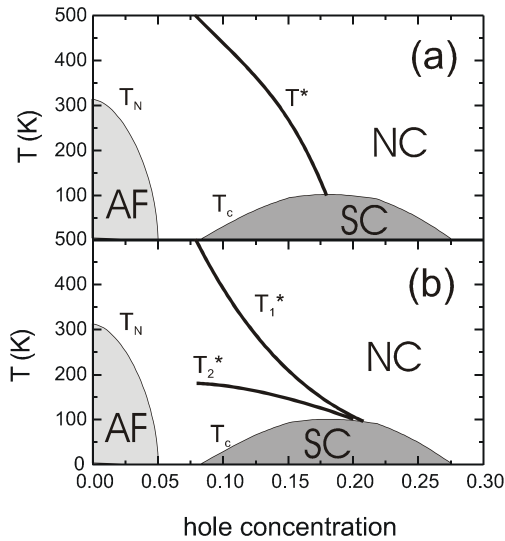

Fig. 1: Schematic sketch of the phase diagram of $YBa_2Cu_3O_{7-x}$ with the superconducting (SC), anti-ferromagnetic (AF) and normal conducting (NC) phase. Below the temperature T* a pseudogap exists. (a) depicts a model with a homogenous pseudogap regime below T*, (b) shows a model with inhomogeneities in the pseudogap regime characterized by two transition temperatures T_1* and T_2*.

Guided by these experimental and theoretical developments, we have undertaken a thorough time-domain study to elucidate the uniformity of the pseudogap state. In this paper we report (i) the existence of two crossover temperatures above T_c, which are identified through an abrupt modify-cation of both the lattice and carrier dynamics on a subpicosecond scale, and (ii) a hysteresis-like behavior for these crossovers, indicative of competing ground states.

As sample we used a c-axis-oriented film of $YBa_2Cu_3O_{7-x}$ grown by off-axis laser deposition on <100> MgO. The film is 350 nm thick and has a superconducting transition at T_c=88 K. In Raman spectroscopy the sample exhibits a softening of the 340 cm^{-1} mode (by 4 cm^{-1}), which proves that the doping is close to the optimum [15].

The film was mounted on the cold finger of an optical cryostat and the excitation and detection of reflectivity transients were carried out with a degenerate pump-probe setup. In the pump-probe experiment the pump beam excites the carriers and the delayed probe pulse beam monitors the reflectivity change $\Delta R(t)$ as a function of the delay time between the two beams. We employed a Ti:sapphire mode-locked laser operating at 780 nm and delivering a 78 MHz train of 50 fs pulses. These pulses were divided into high-intensity pump and low-intensity probe pulses polarized perpendicular to each other. The average power ratio of the pulses was 30:1, with the probe power not exceeding 3 mW.

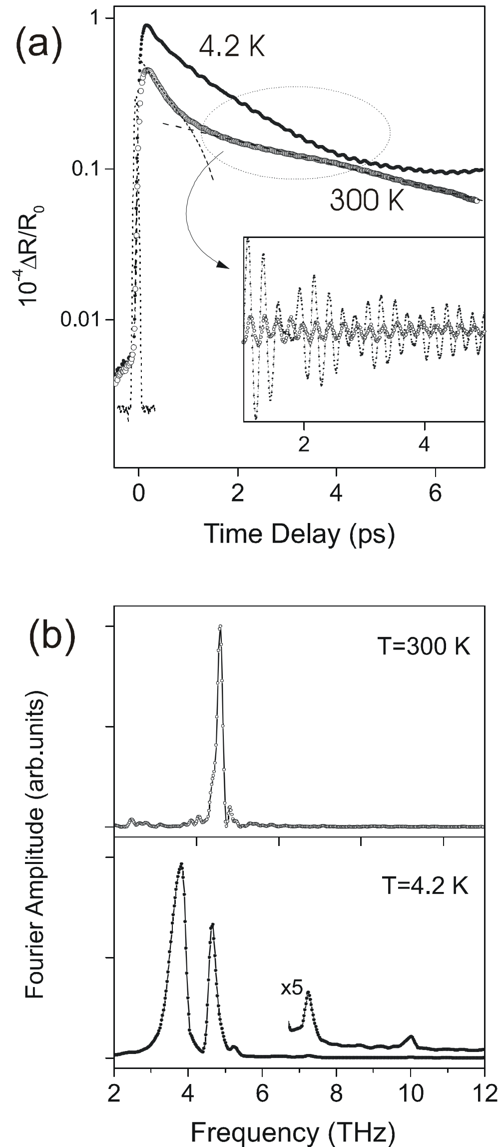

Fig. 2: (a) Transient differential reflectivity $\Delta R(t)/R_0$ versus time delay at 300 K (open circles) and 4 K (closed circles) on a logarithmic scale to emphasize the fast and slow components of the transients, both indicated by dashed lines for the room temperature transient. The laser auto-correlation signal is shown by a dotted line. The inset depicts enlarged the oscillatory components. (b) FT spectra of the oscillatory component.

Typical transient reflectivity changes for $YBa_2Cu_3O_{7-x}$ are shown in Fig. 2 (a). There is a pulse-limited increase of the reflectivity on the order of $10^{-4}\times\Delta R/R_0$ at t=0 and a subsequent relaxation back to equilibrium. The transient at positive time delay consists of two contributions: an oscillating signal, due to the excitation of coherent phonons, superimposed on a non-exponentially decaying signal due to electronic excitation. At room temperature the non-oscillatory decay consists of a fast and a slow component as can be seen from the plots in logarithmic scale shown in Fig. 2 (a). For low lattice temperatures the decay is

not biexponential with a long relaxation time which becomes increasingly longer for larger time delays. This decay appears, for certain temperatures, at negative time delays, stemming from incomplete signal decay between successive laser pulses. Given the laser repetition rate of 78 MHz, the slow signal decays on a nanosecond scale.

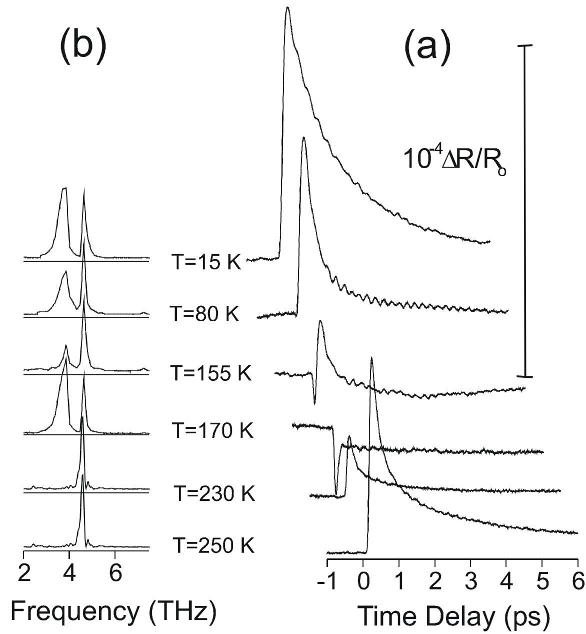

Fig. 3: (a) The transient differential reflectivities $\Delta R(t)/R_0$ (offset horizontally and vertically for clarity) and (b) normalized FT spectra of the oscillating parts of $\Delta R(t)/R_0$, obtained for different temperatures on the way from the superconducting to the normal state.

As far as temperatures well below and far above T_c are concerned we observe a behavior similar to previous time domain experiments. At room temperature the short relaxation time of the overall signal is close to 0.5 ps and the tiny oscillations, superimposed on the decaying signal, correspond to the coherent A_g phonon (4.6 THz) generated by the Cu displacement. At helium temperature, the relaxation time is modified and the oscillations are dominated by the A_g phonon (3.7 THz) generated by the Ba displacement. In addition to the two A_g phonons observed earlier [5,6], for helium temperature we observe for the first time the coherent excitation of the B_{1g}-like mode centered at 10 THz and the Raman-forbidden mode at 7.2 THz, see Fig. 2 (b). However, in this study we are primarily interested in the ultrafast response above T_c and we will use the superconducting behavior as a reference for the comparison to the normal state behavior. The series of transients in Fig. 3 (a) illustrate the temperature dependence of the ultrafast optical response. Below T_c, the relaxational dynamics is dominated by the slow relaxation within 3-5 ps. With increasing temperature, $(\Delta R/R_0)_{max}$ decreases [7,8,11,12], however the temperature dependence of $(\Delta R/R_0)_{max}$ in the superconducting state follows neither the BCS nor the two-fluid model behavior. The amplitude ratio of the Ba/Cu phonons in the Fourier transformed (FT) spectra also decreases as the temperature approaches T_c, see Fig. 3 (b). Above T_c, this ratio is reduced almost to zero. There exist two distinguished temperatures, T_1* and T_2*, *above* T_c which are associated with a drastic change of the carrier and lattice dynamics: At around 160 K (T_2*) the initial differential reflectivity changes $\Delta R/R_0$ reverse sign, and the ratio of Ba/Cu amplitudes jumps to its helium temperature value. The main difference from the superconducting state is that the differential reflectivity, reduced to a spike, has opposite sign. These features, both of the lattice and carrier dynamics, continue approximately up to 220 K (T_1*) and then again, the sign of $\Delta R/R_0$ is changed, and the Ba mode vanishes from the transients. Close to the temperatures T_1* and T_2* the signals are of mixed type, whereas within the T_1*-T_2* range the signal consists of a time-resolution limited spike and an electronic component not decaying on a ps time scale.

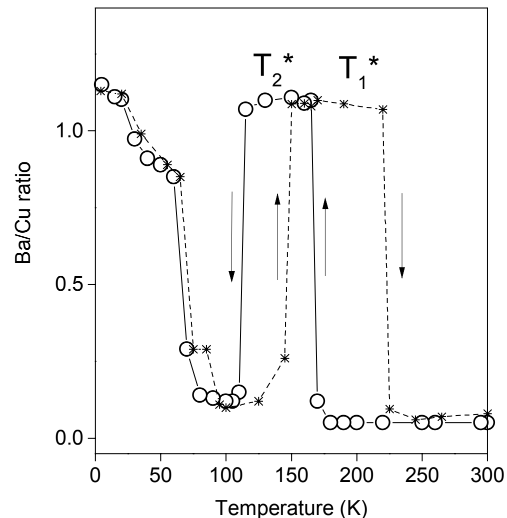

Fig. 4: Temperature dependence of the intensity ratio of the Ba/Cu phonons from the FT spectra. Arrows indicate the direction of temperature change. Open circles - decreasing temperature, stars - increasing temperature. The transitions temperatures T_1* and T_2* above T_c exhibit a large hysteresis.

It is most remarkable that the temperatures T_1* and T_2*, which border the regime with slow carrier dynamics and altered lattice dynamics in the metallic state, exhibit a hysteretic behavior. When approaching the superconducting transition

from above, their values (T_1*~175 K, T_2*~115 K) are different from those attained for crossing T_c from below (T_1*~220 K, T_2*~160 K). For the lattice contribution this memory effect is illustrated by the amplitude ratio of the Ba/Cu phonons as a function of temperature, shown in Fig. 4. One can see that there is no hysteresis for the superconducting state: the ratios are the same for increasing and decreasing temperatures.

We are not able at present to provide a full description of the non-equilibrium dynamics of the lattice and carriers, nevertheless we will try to summarize the most important facts that may help in doing this. The ultrafast relaxation dynamics in $YBa_2Cu_3O_{7-x}$ have been explained within the model for displacive excitation of coherent phonons [10]. Two experimental facts question this description: (i) The phase of coherent phonons observed in femtosecond experiments does not obey a cosine dependence [5,6], and (ii) the excitation of B_{2g} (B_{3g}) off-diagonal coherent phonons in $YBa_2Cu_3O_{7-x}$ crystals, which are not expected to be excited by the displacive mechanism [16]. These two observations may point to a Raman-like mechanism for the coherent phonon excitation. Obviously, the identification of the mechanism for coherent phonon generation is a prerequisite for the interpretation of the peculiar dependence observed in our pump-probe study. In this respect we would like to mention the hysteretic behavior observed in spontaneous Raman scattering for optimally doped crystals $YBa_2Cu_3O_{7-x}$ [17]. The connection between the hysteresis observed in Raman and the memory effect in the time domain experiments is not clear. If such a relation exists, the origin of the hysteresis can be linked to CuO chains.

The non-uniform pseudogap regime has been theoretically considered as coming from (i) local pairing and itinerant behavior of the electron pairs [3], (ii) weak and strong pseudogap regimes for a nearly antiferromagnetic Fermi liquid [2], or (iii) the formation of charge inhomogeneities (stripe fluctuations) and the onset of superconductivity on individual stripes [4]. Our present results do not strongly favor any of these interpretations. Some features of the observed temperature behavior can readily be explained within a particular model, whereas others cannot be accounted for. For example, the existence of the slowly decaying component (indicative of a localized nature of the excitation) in the temperature range T_1*-T_2* may be taken as an evidence for the onset of local pair formation, whereas its disappearance suggest that the local pairs become itinerant. The coherent phonon spectra in the T_1*-T_2* range being similar to those in the superconducting spectra support such explanation. However, in the T_2*-T_c range, where the pairs are presumably itinerant, the coherent phonon spectra are quite similar to those observed for temperatures above the upper crossover temperature T_1*. Why the itinerant but non-coherent pairs are decoupled from the lattice remains unclear. Still, the similarity of coherent lattice dynamics in the superconducting and pseudogap states encourages us to suggest that electron-phonon coupling is necessary to explain the data. Alternatively, the upper crossover temperature can be ascribed to the onset of a weak pseudogap regime where hot spots in the Fermi surface start to appear, whereas the low crossover temperature can be taken as the beginning of a strong pseudogap regime where the Fermi surface starts losing its pieces. However, there is no place for the lattice in this near antiferromagnetic Fermi-liquid picture since the coupling of hot quasi-particles to the lattice is presumably weak [2].

In summary, we have reported the existence of three distinct crossover temperatures in nearly optimally doped $YBa_2Cu_3O_{7-x}$. One is the superconducting transition temperature T_c, and two other temperatures, T_1* and T_2*, are found at $T>T_c$. At these temperatures both the carrier and lattice dynamics are radically altered. These facts point to a non-uniform pseudogap regime of the phase diagram [18]. This interpretation, based on the changes of the phonon dynamics as a function of temperature, is corroborated by the analysis of the relaxation dynamics [19]. Our data pose a new challenge to the theories attempting to describe the pseudogap. The most striking finding of our experiments is the observation that the crossovers in the pseudogap regime exhibit a hysteresis-like behavior. Hopefully, this feature will allow singling out a correct theoretical model for the pseudogap state.

Acknowledgements

This work was supported by the Alexander-von-Humboldt Foundation and the Russian Foundation for Basic Research.

References

[1] For a review, see T. Timusk, B. Statt, Rep. Prog. Phys. **62** (1999) 61

[2] J. Schmalian, D. Pines, B. Stojkovic, Phys. Rev. B **60** (1999) 667

[3] P. Devillard, J. Ranninger, Phys. Rev. Lett. **84** (2000) 5200

[4] V.J. Emery, S. A. Kivelson, O. Zachar, Phys. Rev. B **56** (1997) 6120

[5] W. Albrecht, T. Kruse, H. Kurz, Phys. Rev. Lett. **69** (1992) 1451

[6] O.V. Misochko, K. Kisoda, K. Sakai, S. Nakashima, Phys. Rev. B **61** (2000) 4305

[7] S.G. Han, Z. V. Vardeny, K. S. Wong, O. G. Symko, G. Koren, Phys. Rev. Lett. **65** (1990) 2708

[8] G.L Eeasley, J. Heremans, M. S. Meyer, G. L. Doll, S. H. Liou, Phys. Rev. Lett. **65** (1990) 3445

[9] D.H. Reitze, A. M. Weiner, A. Inam, S. Etemad, Phys. Rev B **46** (1992) 14309

[10] I. Mazin, A. I. Liechtenstein, O. Jepsen, O. K. Andersen, C. O. Rodriguez, Phys. Rev. B **49** (1994) 9210

[11] C.J. Stevens, D. Smith, C. Chen, J. F. Ryan, B. Podobnik, D. Mihailovic, G. A. Wagner, J. E. Evetts, Phys. Rev. Lett. **78** (1997) 2212

[12] J. Demsar, B. Podobnik, V. V. Kabanov, T. Wolf, D. Mihailovic, Phys. Rev. Lett. **82** (1999) 4918

[13] R.D. Averitt, G. Rodriguez, A. I. Lobad, J. L. W. Siders, S. A. Trugman, A. J. Taylor, Phys. Rev. B **63** (2001) 140502

[14] R.A. Kaindl, M. Woerner, T. Elsaesser, D. C. Smith, J. F. Ryan, G. Farnan, M. McCurry, G. Walmsley, Science **287** (2000) 470

[15] E. Altendorf, X. K. Chen, J. C. Irwin, R. Liang, W. N. Hardy, Phys. Rev. B **47** (1993) 8140

[16] O.V. Misochko, Zh. Exp. Teor. Fiz. **119** (2001) 285 [JETP **92** (2001) 246].

[17] D.R. Wake, F. Slakey, M. V. Klein, J. P. Rice, D. M. Ginsberg, Phys. Rev. Lett. **67** (1991) 3728

[18] O.V. Misochko, N. Georgiev, T. Dekorsy, M. Helm, Phys. Rev. Lett. **89** (2002) 067002

[19] O.V. Misochko, N. Georgiev, T. Dekorsy, M. Helm, JETP Letters **75** (2002) 642

Ion-Solid Interaction

D. Kost
H. Tyrroff
G. Zschornack[1]
W. Möller

Potential energy retention of highly charged argon ions in silicon

A UHV device with a base pressure of < 10^{-9} mbar was constructed and connected to the ECR ion source for improved calorimetric measurements of the retention of the potential energy of highly charged ions. The chemical state of the target surface is controlled by AES using LEED optics. With a clean silicon surface prepared by sputtering using Ar^{1+} ions, the retained energy of Ar^{q+} (q = 1…9) ions was determined at kinetic energies between 60 eV·q and 200 eV·q. By extrapolation to zero kinetic energy, the retained fraction of the potential energy is obtained, which is related to the full potential energy given by the ionization potentials. The potential energy retention coefficient results as (0.8 …0.9) ± 0.2 and decreases weakly with increasing charge state. This is about three times larger than earlier results with contaminated copper surfaces.

Collaboration: [1]Technical University of Dresden

M. Posselt
L. Bischoff
J. Teichert
A. Ster[1]

Influence of dynamic annealing on the shape of channeling implantation profiles in Si and SiC

The influence of dose rate and temperature on the dose dependence of the shape of Ge depth profiles obtained by channeling implantation into Si and SiC was investigated. A focused ion beam system was employed which enables the application of two widely different dose rates (10^{11} and 10^{18} cm^{-2} s^{-1}). Implantations into Si were performed at room temperature (RT) and 250°C. SiC was implanted at RT, 225, 450, and 580°C. The Ge depth distributions were measured by secondary ion mass spectrometry. The shape of the channeling implantation profiles is affected by the formation and evolution of complex defects formed during ion bombardment, since these defects cause significant dechanneling of the implanted particles. The competing influence of dose rate and temperature on the shape of Ge depth profiles is explained in terms of intracascade defect relaxation. The time scale for the reduction of complex defects was estimated. At RT, in Si some defect relaxation occurs within the first 100 s after an ion impact. At temperatures of 225 and 250°C, in SiC and Si, a considerable defect reduction is found within the first 10 µs as well as between 10 µs and 100 s after an ion impact. The complex defects in Si vanish entirely between 10 µs and 100 s, whereas in SiC some of them survive. At 450 and 580°C, defects in SiC relax mainly within the first 10 µs after an ion impact. The defect reduction increases with increasing implantation temperature. A phenomenological model was developed in order to treat the dose rate and temperature dependence of the defect-induced dechanneling within the framework of atomistic computer simulations of ion implantation. The simulated Ge depth profiles agree very well with the measured data.

Collaboration: [1]Research Institute for Technical Physics and Materials Science, Budapest, Hungary

M. Kokkoris[1]
S. Kossionides[1]
R. Vlastou[2]
R. Grötzschel

Proton channelling parameters in SiC polytypes determined in backscattering geometry

Direct stopping power measurements of channelled ions in transmission geometry are often impossible because thin monocrystalline membranes are not available like in the case of SiC.

To study the channelling of protons along the (0001) axis of 4H, 6H, 15R, 21R SiC crystals in the energy region E_p=1.7–2.5 MeV, energy spectra were taken in backscattering geometry and analysed with a phenomenological model. Computer simulations, based on the assumption that the dechannelling of protons follows an exponential law, are in very good agreement with the measured spectra. Two crucial channeling parameters, the mean channelling distance and

the ratio of the stopping powers for aligned and random trajectories, were compared for the various polytypes. The data analysis does not show a significant energy dependence of these parameters. However, there is a clear indication that the stopping power ratio depends on the polytype.

Supported by EU

Collaboration: [1]NCSR `Demokritos', Athens, Greece; [2]National Technical University of Athens, Greece

P. Pathak[1]
F. Eichhorn
R. Grötzschel
N. Schell

Strain in multi quantum well semiconductor structures after high-enery ion irradiation

RBS/Channeling and HRXRD was employed to study the strain induced by swift heavy ion irradiation in multi quantum wells of lattice mismatched $In_xGa_{1-x}As$/GaAs with varying thickness and with varying composition of Indium, and in lattice matched samples of $In_{0.53}Ga_{0.47}As$/InP. The pristine layers were compared with samples after irradiation with varying fluences of energetic (order of 100 MeV) Ag ions in the range $10^{12} – 10^{13}$ ions/cm^2. The irradiation results in diffusion of Indium across the interfaces of the layers and results in variation of the strain. The strain values obtained using RBS/C and HRXRD techniques compare well and the strains induced after irradiation, due to diffusion of Indium, tend to decrease with increase of the irradiation fluence.

Collaboration: [1]School of Physics, University of Hyderabad, India

C. Neelmeijer
H.P. Neuheuser[1]

Inks on parchments – characterisation using external PIXE analysis

Interesting notations accompanied by characteristic initials were found on the rear sides of ancient documents[1]. 4 MeV external proton beam PIXE was used for the identification of different mixtures of ferro-gallic ink, in particular from the Fe/Cu and Fe/Zn X-ray intensity ratios. With one exception the inks of the master texts were proven to differ significantly from those of the comments and the initials on the reverses of the parchments. Three documents, characterised by the visually identical initials “TV”, have been of special interest. Here, identical Fe/Cu and Fe/Zn X-ray intensity ratios were obtained from all the “T” and “V” letters. However, Hg as a striking element in the PIXE spectrum was observed only in two cases. As known from the literature, preparation of the inner walls of the inkpots with a mercury sublimate is of advantage in order to prevent the ink from moulding. Supposing mercury to be concentrated in the bottom of the barrel, Hg containing ink of the initials can be interpreted as resulting from deep dunking of the writing utensil into the inkpot. This assumption is corroborated by high absolute Fe and Cu X-ray intensities arising from the viscous ink consistency at the bottom of the inkpot.

Collaboration: [1]Rheinisches Archiv- und Museumsamt, Abtei Brauweiler, Pulheim, Germany

S. Dankert[1]
U. Schwarz-Schampera[1]
D. Grambole
F. Herrmann

Micro PIXE analysis of trace elements in sulfide ore minerals

Trace element distributions in principal ore-forming minerals play an increasingly important role in exploration of mineral deposits. The incorporation of trace elements into mineral assemblage occurs at the time of formation and preserves the physical and chemical properties of the mineralizing fluids. In this study sulfide mineral samples of the porphyry-epithermal environment were investigated to identify mineral hosts and mineralogical sitings of the trace elements Bi, Se, Te, Ag, In and Sn. In polished thin sections of representative sulfide minerals the major element composition of expected mineral host were identified by EDX whereas the trace elements were detected by micro PIXE at the Rossendorf nuclear microprobe. The trace element concentrations were calculated by the Guelph PIXE software package fitting the trace elements in a matrix known from previous electron microprobe studies for pyrite, chalcopyrite, sphalerite, galena, bornite, digenite, enargite and luzonite.

Collaboration: [1]TU Bergakademie Freiberg, Lagerstättenlehre

R. Bugoi[1]
B. Constantinescu[1]
V. Cojocaru[1]
D. Grambole
F. Herrmann

Micro PIXE studies on archaeological gold objects

The study of trace elements in archaeological metallic objects can provide important clues about the metal provenance and the involved manufacturing procedures. Therefore several small fragments of ancient gold objects coming from an Eneolithical treasury (IVth Millenium B.C.) found on Danube border in Romania and from Pietroasa 'Golden Brood Hen with its Chicken' Visigoth treasury were studied together with some nuggets from Transylvanian mines using micro PIXE at the Rossendorf nuclear microprobe. The Eneolithical samples have more than 90 wt.% gold. Si, Ca and Fe inclusions, proceeded probably from quartz and feldspar, hint at alluvial gold used for manufacturing. The parts of the Pietroasa treasury belong to Germanic, Roman and Persian stylistic groups. The Germanic style fibulae exhibited Ta, Nb and Cr inclusions. This lead to the conclusion that Ural Mountains gold was employed to manufacture the Germanic style objects.

Supported by EU

Collaboration: [1]National Institute for Physics and Nuclear Engineering 'Horia Hulubei', Bucharest, Romania

A. Macková[1]
P. Nekvindová[2]
R. Grötzschel

Erbium lattice site location in APE modified lithium niobate

The incorporation of Er in $LiNbO_3$ waveguides produced by an annealed proton exchange process (APE) at 213°C for 3 h was investigated. The waveguides were single mode for 1.5 µm and the proton profile reaches to a depth of about 10 µm into the bulk material. RBS/C analysis with 1.8 MeV He ions was used for the Er lattice site location.

The angular yield curves of axial channelling were analysed. Samples of three different crystal cuts were used, for which the <1120>, <0110>, and the <0001> axis, respecticely, are about perpendicular to the surface. From the nearly identical <1000> angular scans of Nb and Er an Er position off the z-axis can be disregarded and it can be concluded that the Er atoms are located in one of three possible positions, the Nb site, the Li site or at a structural octahedral site. From the missing maximum in the RBS yield from Er in the scan along <1120> axis it is possible to exclude the latter case. The shape of the <0110> and <1120> scans indicate that Er occupies a position shifted a small amount of about 0.1 nm from the Li site along the z- direction.

Collaboration: [1]Nuclear Physics Institute of ASCR, Rez, Czech Republic; [2]VSCHT, Prague, Czech Republic

Ch. Akhmadaliev
L. Bischoff

Elastic waveforms in solids generated by a short pulse high energy ion beam

The interaction of a pulsed ion beam with a solid leads to a small temperature variation in the near subsurface region. Due to the local heating of the target and the momentum transfer elastic waves are generated. The measurement of these waves gives new information about the internal structure and properties of the sample. Experiments were carried out using a pulsed beam of high energy ions provided by the 3 MeV-Tandetron accelerator. In order to form short pulses of the ion beam a high voltage switch based on a RS685 power tube was designed. The obtained shortest pulse duration was about 500 ns with a switching time of about 180-250 ns for O^+, O^{2+}, O^{3+}, O^{4+}, Si^{2+}, Si^{3+}, Si^{4+}, Au^{2+}, Au^{3+} ions. The energy was varied in the range from 1.5 to 12 MeV. The acoustic signal was detected on the rear side of the sample using piezoelectric transducers based on lead zirconium titanium (PZT) ceramic and polyvinylidene fluoride (PVDF) polymer films. The amplitude and shape of the elastic wave signal, measured in aluminum, iron, copper and silicon <100> and <111> samples, were investigated in dependence on the duration, energy and spot size of the ion beam pulse. The wave directivity diagrams were determined. The observed linear dependence of the amplitude on the ion energy underlines that the main mechanism of the elastic wave generation in solids is

the thermal acoustic component. No dependence on the ion species or charge state was found. The contribution of the momentum transfer from the projectile ions to the target atoms is negligible in this energy range.

M. Friedrich
W. Pilz
N. Bekris[1]
M. Glugla[1]
R. Hellborg[2]
M. Kiisk[2]
R. Vesanen[2]
V. Liechtenstein[3]

Tritium detection by AMS

The compact AMS-facility based on a SF_6-insulated 100 kV tandem accelerator was applied for high-dose tritium depth profiling at samples from JET Culham/UK and TFTR Princeton/USA. Depth profiles of deuterium and other light elements can be measured simultaneously using a Faraday cup at the entrance of the accelerator (SIMS-mode of the facility) or in case of very low concentrations or disturbing isobar molecules after acceleration using a Si detector (AMS-mode).

The preparation of test samples for low-dose tritium detection at the 3 MV Tandetron was successfully finished. The reason for former problems at TiH_2 sample preparation was the high sensitivity of the preparation process to vacuum leaks.

Collaboration: [1]Forschungszentrum Karlsruhe; [2]University of Lund, Sweden; [3]RRC Kurchatov Institute, Moscow, Russia

Thin Films

H.U. Jäger
A. Belov

Time-resolved dynamics of ta-C formation: Insight from atomistic simulation

Atomistic computer simulations enable to specify the times scales for the tetrahedral amorphous carbon (ta-C) film formation process and to explain its critical dependence on substrate temperature T_s. Using a time-resolved analysis of atomic trajectories generated by molecular-dynamics simulations of ion beam deposition, the film formation process can be characterized by four stages instead of the three ones used in the phenomenological subplantation model (collision, thermalization, long-term relaxation). The new classification scheme includes a short-term temperature-dependent relaxation stage (t~70-1000 fs), where the film formation is considerably influenced by T_s. During this stage, depending on T_s, the carbon atoms occupying metastable four- or fivefold coordinated sites relax into either three- or fourfold coordinated positions. In agreement with experiment the simulations predict a sharp transition from ta-C to graphitic carbon as T_s exceeds a critical temperature T_c. The calculated value for T_c (~100°C for E_{ion} = 40 eV) is lower than experimental data.

Supported by DFG

A. Belov
H.U. Jäger

Effect of deposition temperature on grown-in stress in ta-C films

Atomistic computer simulations were employed to study the effect of the substrate temperature, T_s, on the grown-in stress in a-C films deposited from low-energy ions (E_{ion} = 10-80 eV). The depth profiles of the stresses were computed at T = 0 K, using a hydrocarbon Brenner potential and the film structural models from molecular dynamics deposition simulations for substrate temperatures below (100 K and 20°C) and above (200°C) the sp^3/sp^2 transition temperature, T_c. In agreement with experiment, in tetrahedral a-C films ($E_{ion} \geq$ 40 eV) the stress decreases only slightly as T_s increases from 100 K to 20°C. Above T_c, the stress reduces more strongly. In the deposition simulation with E_{ion} = 40 eV, the average film stress at T_s = 20 and 200°C is 10.0 and 8.2 GPa, respectively, whereas the measured stress reduction is about 50 %. However, like in experiment, the simulated stress reduction exactly follows the density reduction.

Supported by DFG

A. Belov

Modeling relaxation phenomena in amorphous carbon films: Stress relief

Depending on temperature, thermodynamically favored structural relaxations in deposited tetrahedral amorphous carbon (ta-C) films can either essentially retain the sp^3 content or result in a transition to a graphitic phase with dominating sp^2 bonding. The structural relaxation occurs at low temperatures (less than T_1 ~ 600°C) and is accompanied by reduction of the grown-in film stress. Molecular dynamics with a modified potential of Brenner for hydrocarbons are employed for ion-beam deposition simulation, resulting in an amorphous network with density of 3.2 g/cm^3 and grown-in compressive stress of ~10 GPa, and subsequent low-temperature annealing. During annealing, energy and stress of the as-deposited ta-C are released with only minor changes in the short-range order characterized by the pair correlation function. The corresponding rearrangements in the amorphous networks consist both in conversions from sp^3 to sp^2 and vice versa. A nearly complete stress relief was simulated at ~1000 K, which is in agreement with the experimental data for T_1. The structural changes in ta-C indicate that as a result of the annealing the sp^3-bonded atoms have lower volumes than upon pure elastic expansion of ta-C to the stress-free state, with the volume difference accounting for the high grown-in stresses in ta-C films.

R. Gago
U. Kreissig
A. Mücklich
A. Kolitsch

CN_x fullerene like compounds deposited by low energy IBAD

In order to deliver ion energies being sufficiently low for the formation of fullerene like structures, a gridless end-Hall ion source was installed in an IBAD chamber, enabling operation in the energy range from 40 to 150 eV. First deposited CN_x films using this configuration show features, which are in agreement with previously reported data on highly fullerene-like CN_x. IR spectroscopy confirms the formation of C-N bonds and, therefore, the effective incorporation of nitrogen on the growing film. A strong re-sputtering effect has also been observed, probably due to the formation of C-N volatile species. The nitrogen content saturates at ~15 at. % (as measured with ERDA) and the film structure becomes more graphitic with increasing nitrogen incorporation (as derived from Raman spectroscopy). The first HRTEM analyses of the microstructure reveal that the samples are not completely amorphous, presenting some fullerene-like structures.

Supported by EU

Collaboration: University of Stockholm, Sweden; University of Linköping, Sweden; University of Newcastle, UK; University Paris-Sud, France; ICMCB-CNRS Bordeaux, France; Hungarian Academy of Sciences Budapest, Hungary

R. Gago
B. Abendroth
M. Vinnichenko
A. Kolitsch

Phase control of IBAD cubic boron nitride films by simultaneous 35 keV N^+ ion implantation

Stress relief in cubic boron nitride (c-BN) thin films by simultaneous 35 keV nitrogen bombardment during deposition by ion assisted evaporation (IAE), has been extended to ion assisted sputtering (IAS) for enhanced process stability. The resulting bonding structure, thickness and layered structure of the samples were determined by the combination of FTIR and spectroscopic ellipsometry. The stress release was confirmed by the enhancement of the mechanical stability of the samples, as compared to non-irradiated samples with equivalent cubic content. The stress relaxation is achieved in detriment of a decreasing cubic content and depends on the interplay between dose and growth rate. In this way, stable films with high cubic content (>50%) and thickness up to 0.5 µm were successfully grown.

Supported by DFG

Collaboration: Zweites Physikalisches Institut, Universität Göttingen; Institut für Technische Physik, Universität-GH Kassel; Hochschule Mittweida; Institut für Plasmaforschung, Universität Stuttgart

T. Fitz
C.E. Foerster[1]
U. Kreissig
E. Richter

Carburizing and carbonitriding of Al by PIII

Carburizing and carbonitriding of Al were performed by PIII from a pure CH_4 plasma or different mixtures of N_2 and CH_4. The samples were biased by negative voltage pulses of 40 kV with a pulse length of 5 µs and a repetition rate of 800 Hz. During implantation a substrate temperature of about 350°C ± 20°C was established. The elemental depth distributions measured by ERDA show that the carbon profile obtained after PIII in pure CH_4 corresponds well to the maximum implantation range estimated by SRIM (about 100 nm). N_2/CH_4 plasma treatment results in significantly deeper carbon and nitrogen profiles, extending to about 600 nm, indicating that diffusion is significantly influenced by the presence of nitrogen. Moreover, after carburizing an over-stoichiometric concentration of carbon is detected, while after carbonitriding the carbon concentration does not exceed the stoichiometric level of Al_4C_3. An increase of the nitrogen content in the process gas from 10% to 40% has no significant influence on the maximum concentration and depth distribution of carbon and nitrogen atoms.

Collaboration: [1]Departamento de Física, Universidade Estadual de Ponta Grossa, Brazil

C.E. Foerster[1]
T. Fitz
E. Richter

Aluminium carbide produced by carbon ion implantation into aluminium at different doses and temperatures

A systematic study was performed on the influence of implantation fluence, ion

F. Prokert
U. Kreissig
A. Mücklich
T. Dekorsy

flux, and substrate temperature on the production of aluminium carbide (Al_4C_3) precipitates during ion beam synthesis. At temperatures between 100°C and 600°C, carbon ions were implanted at an energy of 25 keV, fluences from $1x10^{17}$ to $2x10^{18}$ C/cm^2, and current densities between 1.5 and 6 µA/cm^2. Near surface analysis was performed by ERDA, XRD, TEM and Raman spectroscopy. At room temperature and low carbon fluence, the precipitates exhibit an average grain size of 4 nm independent on the ion flux. By increasing the carbon fluence, an irradiation dissolution process occurs due to the continuous implantation, resulting in an amorphous layer of aluminium carbide plus a high concentration of carbon clusters. By increasing the implantation temperature above 300°C, the precipitates start to grow reaching an average size of 40 nm at 600°C. It is suggested that the growth of aluminium carbide precipitates occurs at the expense of a reduction of the carbon clusters. Whereas carbon diffusion into the bulk was not observed at temperatures lower than 500°C, it is promoted at higher temperature and sufficiently low ion flux.

Collaboration: [1]Departamento de Física, Universidade Estadual de Ponta Grossa, Brazil

U. Hornauer
E. Wieser
E. Richter
A. Donchev[1]
M. Schütze[1]

Improvement of the high-temperature oxidation behavior of TiAl alloys by implantation of halogens

Cl implantation into the alloys Ti41,5Al10Nb und γ-Met [Ti 46,5Al 4(Cr, Nb, Ta, B)] was carried out by PIII in an Ar-Cl plasma, at an RF power between 350 and 1000 W, corresponding to a plasma density between 2 and $4x10^{10}$cm^{-3}. Cl ions were implanted using 30 kV pulses of 5 µs duration at a repetition frequency between 100 and 250 Hz. Both the repetition frequency and the RF power determine the sample temperature (350 – 600°C). The Cl profile decreases from the surface into the depth indicating strong plasma-surface interaction besides the implantation. A good oxidation resistance at 900°C (Al_2O_3-like oxidation kinetics) was obtained for both alloys in a relatively broad range of implantation parameters. Comparable good results were obtained by low energy F implantation (15 keV, $1x10^{17}$ cm^{-2}). Alternatively, an Ar-CH_2Cl_2 mixture was successfully tested to simplify the gas handling. The possibility to implant large work pieces was demonstrated on turbine blade models (200 x 65 mm^2).

Supported by AiF
Collaboration: [1]Karl-Winnacker-Institut, DECHEMA e.V., Frankfurt

S. Mukherjee[1]
H. Reuther
F. Prokert
E. Richter
W. Möller

Substrate bias effects in PIIIAD from a TiAl cathodic arc

$Ti_{1-x}Al_x$ thin films were deposited on stainless steel substrates using plasma immersion implantation and deposition (PIIIAD). A cathodic arc was employed as a source of metallic ions from TiAl cathode, and the arc plasma was guided by a curved magnetic field filter. The resultant thin films were analyzed using AES and XRD. Dynamic profile simulations using TRIDYN were applied to understand the Ti and Al profiles in the deposited thin films. The results indicate that the film composition and phase formation depend on the applied bias, duty cycle and off time energy of the bombarding ions. The results also indicate that in PIIIAD conditions, the assumption of time averaged d.c. bias is improper to describe pulsed biasing, with deposition, resputtering and ion implantation all occuring simultaneously.

Supported by AvH Foundation
Collaboration: [1] Institute for Plasma Research, Gandhinagar, India

E. Richter
J. Piekoszewski[1]
E. Wieser
F. Prokert
J. Stanislawski[1]
L. Walis[2]

Modification of titanium surface by its alloying with silicon using intense pulsed plasma beams

Surface alloying of Ti with Si has been performed with the use of high intense pulsed plasma beams. In this technique, short intense (1 µs, 3-4 J/cm²) plasma pulses serve as a source of heat to melt the near surface layer (up to 2 µm) of the Ti substrate together with Si film (30-70 µg/cm²) pre-deposited on it. In the

H. Reuther

molten state, lasting a couple of microseconds, rapid diffusion of Si into Ti occurs leading to formation of new phases during rapid solidification of the molten surface layer. Ti_5Si_3, i.e. the silicide with the highest melting point (2130°C) of all stable phases in the Ti-Si system, is formed by the transient heat treatment. During subsequent annealing for 1h at 800°C a fraction (14-43%) of Ti_5Si_3 transforms into TiSi. The presence of silicide precipitates in the near surface layer increases the wear resistance significantly.

Collaboration: [1]Andrzej Soltan Institute for Nuclear Studies, Otwock, Poland; [2]Institute of Nuclear Chemistry and Technology, Warsaw, Poland

M. Ružicka[1]
T. Fitz
E. Richter

A new way to increase the nitriding efficiency during nitriding of Al

The role of Mg as an alloying element on the nitriding efficiency of Al was studied. Four different Al-Mg alloys and pure Al were nitrided by PIII at a negative pulse voltage of 10 kV. The experiments were performed at substrate temperatures of 480°C, 570°C and 600°C for nitriding times of 15 min and 3 h. Elemental depth profiles were measured by GDOS. The results demonstrate that Mg is efficient in decreasing the stationary thickness of the surface oxide layer, thus increasing the nitriding rate. This is attributed to the higher sputtering yield of MgO compared to Al_2O_3, in connection with the preferential formation of MgO due to the higher chemical affinity of Mg to oxygen, as compared to Al. Another way to decrease the thickness of the surface oxide layer during nitriding of Al is to use hydrogen in the process gas. Experiments at 70% N_2 and 30% H_2 were performed. Compared to treatment in a pure nitrogen plasma, the thickness of the of the surface oxide layer thickness is reduced due to chemical reaction with hydrogen.

Supported by EU (Marie Curie grant)

Collaboration: [1]University of West Bohemia Plzen, Czech Republic

A.I. Rogozin
M.V. Vinnichenko
A. Kolitsch

Correlations between plasma parameters and thin film properties at MF pulsed dual magnetron sputtering of ITO films

Thin indium tin oxide (ITO) films were grown on insulating substrates by means of pulsed reactive dual magnetron sputtering at different magnetron pulse duration and Ar/O_2 ratio. The plasma parameters were monitored during deposition by a Langmuir probe and optical emission spectroscopy (OES). To characterize the layers after deposition, spectroscopic ellipsometry (SE) was applied in combination with optical transmittance and resistivity measurements. The film deposition rate depends significantly on the magnetron pulse duration. An O/In ratio close to 1.5 corresponds to the lowest film resistivity. Decreasing the magnetron pulse-on time from 100 µs to 50 µs increases the grain size of the films, as determined by AFM, by a factor of five, associated by a strong increase of the resistivity.

Supported by BMBF

Collaboration: Institut für Physik, TU Chemnitz; Fraunhofer Institut für Elektronenstrahl- und Plasmatechnik Dresden

R. Gago
M. Vinnichenko
R. Grötzschel
R.J. Martín-Palma[1]
P. Fernández[2]
J.M. Martínez-Duart[1]

Characterization of SiO_x/TiO_x multilayers for antireflective coating applications

With the purpose to improve the overall performance of polymer ophthalmic lenses, a 5-layer stack of alternating SiO_x and TiO_x layers (supplied by INDO S.A.) was investigated. The thicknesses of the stack (~ 400 nm) and of each individual layer have been adjusted theoretically in order to optimize the optical response. To verify the resulting structure of the stack, single SiO_x and TiO_x layers as well as truncated and complete multilayers have been characterized by RBS and spectroscopic ellipsometry. The composition analysis indicates the formation of stoichiometric oxides (SiO_2 and TiO_2). The real thicknesses of the individual layers have been determined, rendering it possible to resolve a very thin TiO_2 layer of a few nanometers only. The simulations of the experimental data show no indication of interdiffusion. Further, the optical constants of each

layer have also been determined.
Collaboration: [1]Universidad Autónoma de Madrid, Madrid, Spain; [2]INDO S.A., L'Hospitalet de Llobregat, Barcelona, Spain

R.Gago
M. Vinnichenko
U. Kreissig
R.J. Martín-Palma[1]
P. Fernández[2]
J.M. Martínez-Duart[1]

Characterization of SiCO:H films for protective coatings on polymeric lenses

SiCO:H films were studied to be applied as protective coatings on polymeric ophthalmic lenses. The coatings were produced by Plasma Assisted CVD (PACVD) methods from liquid precursors (HMDSO) and oxygen. The thickness, composition, density and optical properties were determined by a combination of ERDA and spectroscopic ellipsometry. The hard coatings based on SiCO:H show high abrasion resistance and optical constants in the visible range quite close to that of SiO_2. The deposition parameters and film properties have been correlated in order to improve the performance of the coatings.
Collaboration: [1]Universidad Autónoma de Madrid, Madrid, Spain; [2]INDO S.A., L'Hospitalet de Llobregat, Barcelona, Spain

M. Kokkoris[1]
R. Vlastou[2]
B. Nsouli[3]
R. Grötzschel

RBS and HIRBS studies of nanostructured $AgSiO_2$ sol–gel thin coatings

Composite $AgSiO_2$ thin coatings were prepared on glass substrates by the sol–gel route and thermally treated in oxidative and reductive conditions up to 500°C for metal nanoparticle formation. The coating structure and the nanoparticle formation were studied using AFM and standard RBS with 1.4 MeV $^4He^+$ ions. Selected samples were investigated with heavy ion RBS (HIRBS) using low energy ^{16}O and ^{12}C ions, in order to improve sensitivity and depth resolution for the profiling of the metal component. The antibacterial activity against *Escherichia coli* was examined by an antibacterial drop test and correlated to the RBS results. The coatings exhibit a high antibacterial activity, which is enhanced with the increase of the metal concentration, and is reduced with the increase of the size of the metal nanoparticles. Further, the antibacterial activity appears to be correlated to the layer interdiffusion after the thermal treatment

Supported by EU
Collaboration: [1]NCSR Demokritos, Institute of Nuclear Physics, Athens, Greece; [2]National Technical University of Athens, Athens, Greece; [3]NCSR Beirut, Lebanon

M. Peikert
R. Bhandari
E. Wieser
C. Wenzel[1]
D. Lipp[1]
H. Reuter
A. Mücklich

The effect of silicon ion implantation on tantalum-silicon contacts

The effect of ion beam mixing on the formation of tantalum–silicon contacts was studied. Si^+ ion implantation into 50 nm Ta layers on n^+-Si (100) was carried out at temperatures from 150 to 500°C and doses between $1x10^{15}$ and $1x10^{17}$ Si/cm². Implantation at low temperature (~150°C) leads to the formation of an amorphous Ta(Si) interface layer and substrate amorphization up to a depth of 200 nm. By implantation at ≥ 300°C substrate amorphization is avoided. The Ta layer is transformed into a $TaSi_2$ layer at the interface followed by an amorphous Ta(Si) sheet with residual polycrystalline Ta on top. The thickness of the silicide layer grows with increasing Si dose. The Ta:Si ratio of 1:1 in the amorphous region indicates the formation of an x-ray amorphous monosilicide. Substrate amorphisation results in an increase of the contact resistance. An improved contact resistance of 50 nm Ta on n^+ poly-Si, measured using the four-point Kelvin method, was achieved by implantation with $5x10^{16}$ Si/cm² at 400°C.

Supported by SMWA
Collaboration: [1]TU Dresden, Institut für Halbleiter- und Mikrosystemtechnik

B. Brijs[1]
U. Kreissig

Carbon as an efficient seal of porous low-*k* dielectric Ta(N) films

The sealing of porous low-*k* dielectric layers by the deposition of thin PVD Ta(N) films was investigated, among other techniques, by means of ERDA using 35 MeV Cl^{7+} ions. Such metallic barriers are used to prevent Cu diffusion from interconnecting wires into the dielectrics. The investigated porous dielectric layers have comparable values of porosity, but differ in pore size and

composition. The carbon concentration varied between 18 and 40 at%. A strong correlation between the carbon concentration of the dielectric and the sealing performance of the PVD Ta(N) films was found. Higher carbon concentrations lead to faster sealing of the pores at similar porosities. These findings contribute to a model of the mechanism which assumes that a transition layer at the Ta(N)/ dielectric interface is formed in which Ta atoms break C-H_x bonds. The resulting Ta-C and C-C bonds lead to an improved crosslinking of the top layers of the matrix.

Supported by EU
Collaboration: [1]IMEC, Leuven (Belgium)

B. Pantchev[1]
P. Danesh[1]
D. Grambole
B. Schmidt

Study of molecular hydrogen in a-Si:H films

Hydrogenated amorphous silicon (a-Si:H) films were prepared by PECVD using hydrogen diluted silane. NRA and infrared spectroscopy were used to evaluate the total amount and bonded fraction of hydrogen in such films, respectively. The comparison provides information about the concentration of molecular hydrogen. In films prepared at 150 and 270°C, the total concentration of hydrogen was determined to about 18.4 and 15.5 at.%, respectively, and the concentration of bonded hydrogen was determined to 18.3 and 15.8 at.%, respectively, from the integrated absorbance of the wagging-rocking mode at 640 cm^{-1}. Thus, the amount of the molecular hydrogen is below or of the order of the experimental error, i.e. 1-2 at.% or at most 10% of the hydrogen content.

Supported by EU
Collaboration: [1]Institute of Solid State Physics, Bulgarian Academy of Sciences, Sofia, Bulgaria

M.T. Pham
K. Ram Mohan Rao[1]
E. Richter
H. Reuther
F. Eichhorn

Optimising corrosion resistive coatings on stainless steel by PIII

Corrosion resistive coatings on austenitic stainless steel (19 w.% Cr, 11 w.% Ni) were optimised by PIII of N. The PIII process parameters under study were ion energy, ion dose, and substrate temperature. The corrosion behavior in 1 w.% NaCl solution was examined by cyclic voltammetry and potentiodynamic polarization. In the energy range 1–10 keV, the corrosion behaviour is independent on the ion energy. Varying the ion dose results in a remarkable alteration of the corrosion behavior. The corrosion current density decreases up to 3 orders of magnitude at an ion dose around 10^{15} ions/cm². An additional lowering of the corrosion was obtained by PIII at a substrate temperature of 380°C. The pitting potential was shown to be less sensitive to the process parameters, but tends to decrease at elevated substrate temperature.

Collaboration: [1]Metallurgical and Materials Engineering Department, Indian Institute of Technology, Kharagpur, West-Bengal, India

E. Wieser
H. Reuther
F. Prokert
L. Bischoff
A.Gorbunov[1]
A. Tselev[1]
M. Mertig[1]
W. Pompe[1]
A.A. Levin[2]
D.C. Meyer[2]
P. Paufler[2]

Structural and magnetic phase transformation in metastable Fe-Cr alloys induced by ion irradiation

Unusual metastable paramagnetic phases have been observed in Fe-Cr thin films (~ 40 nm) fabricated by pulsed laser deposition. Structural and magnetic phase transformations in these alloys induced by ion irradiation have been observed. The critical dose for the transformation to the more stable b.c.c. structure depends on the initial phase of the film and the ion mass. The body-centered tetragonal phase which forms at low Cr content (~30 at.%) can be completely transformed to the b.c.c. phase by a dose of $5x10^{15}$ Cr/cm^2 whereas the primitive orthorhombic phase of roughly equiatomic Fe-Cr alloys is about 4 times more resistant against ion bombardment. A five times higher Ne-ion dose is required to induce the same transformation as by the Cr bombardment. The formed Fe-rich b.c.c. phase is ferromagnetic. A ferromagnetic pattern, written by a fine-focused Cr-ion beam in a paramagnetic alloy (face-centered orthorhombic, 37 at.% Cr) using an alloy liquid metal ion source ($Er_{70}Fe_{22}Ni_5Cr_3$), could be detected by magnetic force microscopy.

Supported by DFG
Collaboration: [1]TU Dresden, Institut für Werkstoffwissenschaft; [2]TU Dresden, Institut

für Kristallographie und Festkörperphysik

F. Prokert
J. Noetzel
E. Wieser
N. Schell
A. Gorbunov[1]

Effect of annealing on the interface structure of cross-beam pulsed laser deposited Co/Cu multilayers

Co/Cu multilayers were prepared by cross-beam pulsed laser deposition and characterised by large-angle X-ray diffraction as well as specular and off-specular reflection before and after annealing (500°C, 2h). Using synchrotron radiation at the K-edge energy of Co and Cu to enhance the scattering contrast, it is shown that annealing does not enlarge the interface roughness, σ_{rms}, but strongly influences the interface morphology. In the fractal model of self-affine structures the latter is expressed by the drastic reduction of the lateral roughness correlation length parameter, ξ, from about 4 µm in the as-deposited state to about 20 nm after annealing, which is attributed to grain coarsening due to growth of crystallites and grain boundaries. Thermal treatment enhances the separation of Co and Cu at the interface, i.e. the initially very jagged (roughness exponent, h, between 0.15 and 0.3) structure is smoothed (h between 0.6 and 0.7).

Supported by DFG

Collaboration: [1]TU Dresden, Institut für Werkstoffwissenschaften

N. Schell
T. Jensen[1]
J.H. Petersen[1]
K.P. Andreasen[1]
M. Skov Jensen[1]
J. Bøttiger[1]
J. Chevallier[1]

The nanostructure evolution during and after magnetron deposition of Au films measured by *in-situ* synchrotron x-ray scattering

The nanostructure of gold films deposited by magnetron sputtering has been investigated by *in-situ* synchrotron XRD and XRR during growth and after subsequent annealing. Grains with (111) planes parallel to the film surface, and with (111) or (200) planes perpendicular to film surface have been identified. The microstrain decreases strongly during initial growth and at the beginning of the annealing period, while continued grain growth was observed both during film deposition and during annealing. A surprisingly small activation energy of grain growth of 0.25 ± 0.02 eV was found. During the first few minutes of growth, the compressive film stress is strongly reduced due to a tensile contribution arising from the coalescence of the initially formed islands. During annealing, stress relaxation was also observed. The orientation distribution of grains with a (111) plane forming a small angle with the film surface narrows both during the early times of growth and during subsequent annealing. The activation energy for texture changes is found to be 0.68 ± 0.08 eV.

Supported by EU

Collaboration: [1]University of Aarhus, Department of Physics and Astronomy, Aarhus, Denmark

J. Cizek[1]
R. Kirchheim[2]
A. Pundt[2]
W. Anwand
G. Brauer

SPIS as a tool for the investigation of hydrogen loaded Nb films

Hydrogen loaded Nb films exhibit optical properties switchable from reflecting to optical transparent due to lattice changes. However, the absorption of hydrogen is accompanied by an extraordinary out-of-plane lattice expansion and in-plane stresses due to the constraint of the film being fixed on a substrate, like Si. The hydrogen solubility in the α-phase was found to strongly depend on the grain size of the films but is independent of film thickness. A substantially extended hydrogen solubility of the α-phase (x_H = 0.2), compared to bulk Nb (x_H = 0.06), is attributed to the hydrogen filling of defects in grain boundaries. SPIS shows no indication that new defects are introduced by the hydrogen loading in the α-phase, which excludes any plastic deformation which was suggested for the interpretation of XRD studies. Further, the onset of β-phase precipitation, being associated with the formation of dislocation loops, is clearly identified by SPIS.

Supported by AvH Foundation

Collaboration: [1]Humboldt Fellow, Universität Göttingen/FZR; [2]Universität Göttingen

Biotechnological Materials

M.F. Maitz
S. Mukherjee[1]

Growth of bone precursor cells on hard $Ti_{1-x}Al_xN$ coatings

Hard Ti based coatings are under consideration as biocompatible coatings for bone integrated implants. Previously it had been shown that mesenchymal stem cells from rat bone marrow adhere and spread better on $Ti_{1-x}Al_xN$ films prepared at 0 V biased substrates. This is an effect of direct cell-surface interaction, because after adsorption with serum proteins, the cell adhesion is independent from the preparation properties of the films. For the following investigation gradient coatings were produced with a well adherent –2 kV biased interphase and a well biocompatible unbiased top layer. Osteoprogenitor cells were grown for two weeks in medium which supports osteoblastic differentiation on these surfaces, then the amount of alkaline phosphates as a key enzyme of osteoblasts was determined and the metabolic activity was rated by the metabolism of a chromogenic substrate. There is no difference between TiAlN and pure Ti coatings for these parameters. This indicates that TiAlN is biocompatible for bone integrated implants.

Supported by AvH-Foundation

Collaboration: [1] Institute for Plasma Research, Gandhinagar, India

M.T. Pham
M.F. Maitz

Characterization of SAOS-cell derived extracellular matrix coatings on Ti surfaces

Native extracellular matrix (ECM) coatings on Ti surfaces have been shown to trigger the cell responses more effectively than specific ECM proteins or peptide sequences. The coatings were produced by growing the osteoblast-like SAOS-2 cells on the Ti surface, thus producing a native ECM, and then removing the cells by treatment with NH_4OH. The effects of the NH_4OH treatment to introduce contaminants from cell lysing into the ECM-Ti surface were examined. The ECM-Ti with its corresponding NH_4OH lysate, and washing solution included in the processing step were analysed for their lactate dehydrogenase (LDH), alkaline phosphatase (ALP), and nucleic acids (DNA). The cellular components were shown to remain in the ECM to different levels. The LDH activity was reduced to a negligible level after 3 washing steps. A significant amount of ALP (~ 25 %) was retained by the ECM. The residual DNA content was < 10 %. The contribution of these cellular contaminants to mediating the cell response is likely not negligible and remains to be determined.

E. Pecheva[1]
L. Pramatarova[1]
M.T. Pham
M.F. Maitz

Hydroxyapatite precipitation on model surfaces to investigate biomineralisation

The present study addresses basic mechanisms of hydroxyapatite (HA) precipitation as it occurs in many biological systems. Na or of Ca and P ions have been implanted at doses in the 10^{17} cm^{-2} range into AISI 316 stainless steel, silicon and quartz glass representing a metal, a semiconductor, and an insulator, respectively. Alternatively, extracellular matrix (ECM) of a bone forming cell line has been deposited. Subsequently, the samples were exposed to simulated body fluid (SBF) for some days. As a result, precipitates are formed consisting of a mixture of HA and other calcium phosphate phases, such as dicalcium phosphate dihydrate and octacalcium phosphate, which are often present as intermediates in the precipitation of HA. The composition was found to be independent of the substrate type and the species of the implanted ions or precipitation mode. However, the precipitation rate depends on the ion species, being highest on stainless steel implanted with Ca + P. On all substrates calcium phosphate precipitated most homogeneous on the ECM, indicating that a complete simulation of the biological system is not possible.

Supported by EU (Marie Curie grant)

Collaboration: [1]Institute of Solid State Physics, BAS, Sofia, Bulgaria

M.T. Pham
M.F. Maitz
H. Reuther
A. Mücklich
F. Prokert
E. Richter

Electrochemical study of NiTi surface alloys generated by ion implantation

To suppress background signals and material corrosion, the NiTi alloy (50:50), rather than pure Ni, is commonly employed as catalyst for the electro-oxidation of carbohydrates. Surface layers of NiTi with thicknesses below 100 nm and a Ni content of 1 – 60 at.% were generated by Ni ions implanted into Ti. Electrochemical properties in 0.1 N NaOH were studied by cyclic voltammetry and potentiodynamic polarization. The electrocatalytic activity was examined by the oxidation of glucose. The material was characterised by XRD, XPS, and TEM. Ni was shown to be electroactive on all surface compositions. The redox reaction Ni(II) ↔ Ni(III) occurs more efficiently on ion beam generated surfaces than on the reference NiTi alloy. The oxidation of glucose is promoted, and its oxidation potential shifts anodically with reduced surface Ni content. The material is electrochemically stable in NaOH exhibiting a corrosion resistance improved by up to 2 orders of magnitude. The material consists of amorphous Ni and Ni oxide embedded in a Ti oxide matrix.

X. Wang
F. Prokert
H. Reuther
M.F. Maitz

IBAD synthesized surfaces as scaffold for vascular endothelial cells

TiO_2, Ti-AgO, DLC and SiC films have been produced by IBAD as candidate coatings for blood contacting implants. The performance of the bovine aortic endothelial cell line GM7373 on the surfaces has been investigated. All surfaces showed minimal toxicity to the cells. After four hours the adhesion and spreading of the cells on all surfaces is good, but as a slight trend the cells form more adhesion points on SiC, TiO_2 and stainless steel 316 than on DLC and Ti-Ag-O. Among the Ti-Ag-O coatings the spreading is better on films prepared at low oxygen flow rate than on those prepared at high oxygen flow rate. At the end of the exponential phase of the cell growth there is a statistically not significant trend that cells have a higher density on SiC and DLC than on TiO_2 and the ternary Ti-Ag-O system, where the cell density is negatively correlated with the Ag content of the film.

M.F. Maitz
E. Richter

Hafnium coating for improved radiopacity and biocompatibility

Hafnium is chemically similar to the highly biocompatible metals titanium and zirconium, but exhibits a higher X-ray absorption, which makes it interesting as a radiopaque and hemocompatible coating on vascular stents. Hafnium films on coupons showed a lower activation of the clotting cascade, and according to morphology the activation of blood platelets on hafnium was lower than on AISI 314 stainless steel, confirming the low thrombogenity. A thick film of Hf both on the outer and inner surfaces of vascular stents has been produced by plasma immersion ion implantation and deposition, up to a thickness of approx. 7 µm. This significantly increases the X-ray contrast of the stent. However, the coating does not withstand the severe deformation of the stent which is exerted during insertion.

Collaboration: Boston Scientific SCIMED

J.-C. Cigal[1]
E. Wagenaars[1]
L. Baede[1]
C. Maurice[1]
L. van Ijzendoorn[1]
G. Kroesen[1]
R. Grötzschel
W. Möller

Interaction of a plasma with bone tissue

With the long-term goal of investigating the perspectives of plasma-based medical treatment, an inductively coupled plasma has been used to treat bone surfaces. The modified bone surface has been characterised with spectroscopic infrared ellipsometry, RBS and ERDA. The hardness and elasticity modulus have been determined with nano-indentation. The experimental data show that the penetration depth of the plasma treatment is a few hundred nanometers. The organic compounds (such as collagen) are most strongly affected. A good correlation between the infrared signatures and the elemental analysis techniques has been found.

Collaboration: [1]Eindhoven University of Technology, The Netherlands

D. Grambole
T. Wang[1]
D. Scharnweber[2]

Influence of the polishing procedure on the hydrogen content of Ti and Ti alloy surfaces

During the mechanical polishing of Ti and Ti alloys a so-called Beilby layer is generated, which may contain an increased concentration of H. Being detrimental for medical implant applications, the presence of H is associated with a degradation of the mechanical properties due to H embrittlement as well as increased bacterial growth. In order to investigate the influence of the polishing procedure on the H content of Beilby layers, the H depth distribution was analysed in mechanically polished samples of c.p.-Ti, Ti6Al7Nb, Ti6Al4V, and Ti15Mo (grinded by wet SiC paper and polished by SiO_2 colloid) from three different laboratories using the $^{1}H(^{15}N, \alpha\gamma)^{12}C$ nuclear reaction. Strongly different H concentrations (2 – 60 at.%) in layers from about 5 to 400 nm were observed, being attributed to different procedures of polishing.

Supported by MPG
Collaboration: [1]Institute of Modern Physics, Chinese Academy of Sciences, Lanzhou, China; [2] TU Dresden, Institut für Werkstoffwissenschaft

Nanostructures

K.-H. Heinig
T. Müller
B. Schmidt
W. Möller

Interfaces under ion irradiation: Growth and taming of nanostructures
The synthesis of nanostructures as well as the control of their size and location has been investigated by means of ion beams. The phase separation and interface kinetics under ion irradiation give new possibilities to control the growth of nanostructures. Additionally, the contribution of collision-assisted chemical decomposition of the host matrix to self-organization of nanostructures has been studied, especially at interfaces. It has been demonstrated how collisional mixing during ion implantation affects nanocrystal (NC) synthesis and how ion irradiation through NCs modifies their size and size distribution. An analytical expression for solute concentration around an ion-irradiated NC was found which may be written like the well-known Gibbs-Thomson relation. However, parameters have modified meanings which has a significant impact on the evolution of NC ensembles. The theoretical prediction has been confirmed experimentally for Au NCs in SiO_2 and by computer experiments, i.e. by kinetic lattice Monte-Carlo simulations. At interfaces, this ion-irradiation induced mechanism may contribute to self-organization of NCs in a thin δ -layer. The self-alignment of the δ -layer with the SiO_2/Si interface renders the structure being applicable for non-volatile memory structures.

Supported by EU

A. Wellner[1]
V. Paillard[1]
C. Bonafos[2]
M. Carrada[2]
A. Claverie[2]
B. Schmidt
K.-H. Heinig

The origin of stress in Ge nanoparticles embedded in silicon oxide films
The origin of stress in Ge nanocrystals being embedded in silicon oxide was explored using Raman spectroscopy. The samples were produced by Ge^+ implantation into a thermally grown 500 nm thick SiO_2 layer on top of a silicon (001) substrate and subsequent annealing at various temperatures. The size of the nanocrystals was measured by TEM. It was demonstrated that the increase in the phonon peak line width can be understood within the phonon confinement model. The shift of the peak position is due to compressive stress which originates from the Ge volume change at liquid-solid phase transition. The samples were annealed above the Ge melting temperature, and the significant volume increase of Ge nanoclusters at solidification produces stress which cannot relax during the short cooling down period.

Supported by EU
Collaboration: [1]Université Paul Sabatier, Toulouse, France; [2]CEMES/ CNRS, Toulouse, France

J. Heitmann[1]
J. von Borany
F. Eichhorn
D. Kovalev[2]
M. Schmidt[1]
L.X. Yi[1]
R. Scholz[1]
M. Zacharias[1]

Size-control of Si nanocrystals synthesized from SiO/SiO_2 superlattices
The SiO/SiO_2 superlattices were prepared by alternative evaporation of SiO powder in either vacuum or oxygen atmosphere. The thickness of the SiO layers varied between 1 and 6 nm, whereas the SiO_2 layers had a fixed thickness of about 3 nm. The subsequent thermally induced phase separation of the SiO at 1100°C leads to the formation of Si nanocrystals (NC) within these layers. The superlattice arrangement was derived from XRR studies (ROBL) and the NC size was determined from XRD (laboratory source) spectra using the Scherrer formula. The NC diameter corresponds to the initial SiO layer thickness with only a small variation of about 0.5 nm depending on the interface roughness. Therefore, this technique enables the formation of NC with well-controlled size und narrow size distribution. The room-temperature photoluminescence (PL) of the superlattice shows a significant blueshift of the PL signal from 950 to 750 nm with decreasing nanocrystal size. Several size dependent features of the PL, such as decreasing radiative lifetime and increasing no-phonon transition strength with decreasing crystal size, are in good agreement with the quantum confinement model.

Collaboration: [1]MPI für Mikrostrukturphysik, Halle; [2]TU München, Physik Department E16

V. Beyer
J. von Borany
R. Grötzschel
D. Henke[1]
K. Knobloch[1]
A. Mücklich

Comparison of ion beam synthesized Si and Ge nanocluster properties in thin gate oxides

Si or Ge nanoclusters (NCs) in 20 nm SiO_2 films were prepared by ion beam synthesis combining low energy ion implantation and subsequent rapid thermal processsing (950/1050°C). The implantation (Si or Ge, 6-18 keV, $5x10^{15}$-$2x10^{16}cm^{-2}$) was performed in such a way that with identical impurity concentrations (7 or 20 at.%) the peaks of the profiles were located in a distance of 3 or 7 nm from the Si/SiO_2 interface. Significant differences in the microstructural and electrical properties have been obtained for the two implanted species. For the near-interface Ge implant (δx = 3 nm) ion beam mixing of the interface occurs which results in an interface roughness of about 2-3 nm (rms) after annealing. In addition, the considerable amount of Ge in the substrate leads to the formation of a thin SiGe layer and single isolated Ge island at the interface. Using a lower implantation energy (suitable for δx = 7 nm) the interface quality considerably improves and the formation of a near-interface Ge nanocluster band have been obtained. For Si implantation no significant interface mixing effects have been obtained, but the evidence of Si nanocrystals succeed only for some individual crystals. CV, IU and pulsed-Ct or -It measurements carried out at MOS structures can be summarized as follows: Gate oxides with Ge NCs near the Si/SiO_2 interface are characterized by a fast charging / decharging process and a flatband voltage shift (ΔU_{FB}) of several volts. In contrast, Si implanted oxides exhibit a smaller ΔU_{FB}, but considerably improved data retention. For both cases programming is possible with an electrical field strength of 4-6 MV/cm. Based on these investigation a first run for non-volatile nanocrystal memory fabrication using 8 and 25 nm gate oxides have been started by Infineon Technologies Dresden.

Collaboration: [1]Infineon Technologies Dresden

F. Eichhorn
V. Beyer
T. Müller

Ion beam synthesized epitaxial Au nanolenses at the Si(001)/SiO_2 interface

70 keV Au ions with a fluence of $4x10^{15}$ cm^{-2} were implanted into 30 nm thick amorphous SiO_2 on Si(001). Two different types of Au nanostructures are found after annealing (1000°C, 5-60 min), namely spherical nanocrystals (4-5 nm diameter) in the SiO_2 and Au nanolenses at the Si/SiO_2 interface, as proved by XRD and TEM. The lenses are arranged parallel to the interface and have a diameter of approx. 20 nm with an aspect ratio of 2.5. During annealing the substrate is successively enriched with gold from SiO_2 leading to a local Si/Au melt. During cooling the melt separates into a gold and a silicon phase forming Au lenses. The crystal lattice of these Au lenses is oriented to the Si lattice as studied with XRD pole figures: Au<210> directions are parallel to the interface normal Si<001>, and within the interface Au<100> coincides with Si<110>. Au<210> is a one-fold crystal axis whereas Si<001> is a four-fold one. Therefore, four groups of Au lenses are formed at the interface with 90° differences in the azimuthal angle. The small differences (of the order of 5 percent) between the atomic distances of the Au and Si lattice in the directions mentioned above may favour this epitaxial growth.

V. Beyer
T. Müller
J. von Borany
K.-H. Heinig

Charge storage capability of ion-beam synthesized Au nanocrystals

Semiconductor nanocrystals (NCs) in the MOS gate oxide have received much interest due to their application in non-volatile memory devices. However, the detailed charge storage mechanism is still under discussion. Defect-based charge trapping at NC surfaces is hard to distinguish from confinement-based storage in the conduction band of NC. For metal NCs in SiO_2 the situation is different, as charge trapping at the Au/SiO_2 interface can be neglected at first sight. Au NCs were synthesized in a 30 nm SiO_2 film by low-energy ion implantation followed by annealing (1000°C). XTEM studies confirm the formation of well-separated NCs (4-5 nm diameter) at a distance of < 4 nm from the

Si/SiO_2 interface. Thus, the formed NC-layer enables the charging by direct electron tunneling. The charge storage in Au NCs was successfully demonstrated by capacitance-voltage measurements in MOS capacitors.

J. von Borany
V. Beyer
F. Eichhorn
A. Mücklich
N. Schell

Comparative GIXRD and XTEM studies of ion beam synthesized nanoclusters in thin SiO_2 films

Ion beam synthesized Au, Ge, and Si nanoclusters (NCs) embedded in SiO_2 films of 30 or 100 nm thickness were investigated by XTEM and GIXRD (ROBL). Au NCs can be easily detected both by GIXRD and XTEM even in thin SiO_2 films of 30 nm. Depending on the Au content (7-20 at.%) and the annealing temperature (800-1100°C) the NC sizes vary between 1.5 and 5 nm. As derived from the existence of different XRD reflexes [(111), (200), (220), (311)] the Au NCs are nanocrystals with a random crystalline orientation, which is confirmed by XTEM. Au nanocrystals were found even for the as-implanted state due to the high mobility of Au atoms during ion implantation. Ge NCs with cluster sizes between 2-4 nm could be identified with GIXRD only for the highest impurity content of 20 at%, whereas XTEM enables the detection of (amorphous and crystalline) clusters down to an impurity content of about 5 at.%. Both methods failed in the detection of small Si nanocrystals (< 3 nm). A main drawback of GIXRD with synchrotron radiation is the small beam divergence, which restricts the diffraction condition to a small number of nanocrystals.

B. Schmidt
L. Bischoff
B. Köhler[1]
J. Renger[2]
S. Grafström[2]
L. Eng[2]

Aperture SNOM levers fabricated by FIB patterning and wet chemical etching

To produce cantilevers with an integrated optical tip, focused ion beam (FIB) 3D-patterning was used to define both the tip and cantilever as a monolithic structure in the silicon substrate. By varying the dose of implanted gallium ions, levers with various force constants were fabricated at small cantilever lengths of < 20 µm. A point-like FIB irradiation of Si, leading to hole erosion by sputtering, allows to produce hollow tips with a truncated Gaussian shape of high aspect ratio and less than 100 nm diameter. Various forms are possible, including open and closed tips. The cantilever and tip structure predefined by Ga^+ FIB implantation and sputtering is subsequently etched in KOH:H_2O solutions to remove the surrounding silicon, which is not irradiated by the FIB. Micromechanical cantilever structures with lateral dimensions of a few microns and a thickness of only some tens of nanometers were tested interferometrically. From this, their lowest mechanical resonance frequency was determined to be in the range of 0.5 to 5 MHz, depending on their lateral dimensions and the cross-sectional shape. The corresponding spring constants are in range of 0.01 to 1 N/m.

Collaboration: [1]FhG, EADQ Dresden, [2]TU Dresden, Institut für Angewandte Photophysik

J. Grenzer[1]
U. Pietsch[1]
L. Bischoff

Depth resolved strain analysis at lateral nanostructures defined by FIB implantation

We report on the strain analysis of Si wafers which were laterally patterned by focused ion-beam (FIB) implantation using 70 keV ions of either Au (dose: $2\cdot10^{14}$ cm^{-2}) or Ge (dose: $9\cdot10^{14}$ cm^{-2}) from an $Au_{77}Ge_{14}Si_9$ alloy source in the IMSA-100 FIB instrument. A lateral grating with a period of 550 nm along the [100] direction was composed from stripes with a width of almost 300 nm. The strain distribution and the vertical damage profile induced during ion implantation were studied by means of X-ray grazing-incidence diffraction (GID). At different incidence angles, two symmetry equivalent in-plane reflections, the strain sensitive (400) and the strain insensitive (0 -4 0) reflection, were observed. The results reflect the periodic structure consisting of implanted stripes,

whereas the strain induced during implantation shows a non-periodic behavior, which can be explained by an overlap of the strain fields created in each individual implanted stripe.
Collaboration: [1]Universität Potsdam, Institut für Physik

T. Dekorsy
S. Facsko[1]
T. Bobek[1]
H. Kurz[1]
S. Kyrsta[2]
R. Cremer[2]

Generation of regular quantum dots by low-energy ion sputtering of amorphous semiconductor layers

The large potential of nanoelectronics has stimulated many efforts to find new methods for the parallel processing of nanostructures. Promising techniques, like Stranski–Krastanov growth of semiconductor heterostructures and self-assembly of semiconductor nanocrystals by colloid chemistry have been exploited. Recently, a self-organizing mechanism has been discovered which is based on the erosion of semiconductor surfaces by low-energy ion beams. This mechanism leads to regular dot patterns with periods of some tens of nanometers. We could show for the first time that the formation mechanism does not work only on crystalline surfaces but also on amorphous semiconductor layers by investigating the surface morphology of amorphous GaSb layers during ion erosion. This observation opens the potential for a cost-effective patterning of semiconductor surfaces and provides insight into the important role of an amorphous surface layer for the formation process of the dot patterns.

Supported through the Bennigsen-Förder Award, NRW

Collaboration: [1]Institut für Halbleitertechnik, RWTH Aachen; [2]Institut für Theoretische Hüttenkunde, RWTH Aachen

H. Bernas[1]
D. Halley[2]
K.-H. Heinig
J.-Ph. Attané[2]
D. Ravelosona[3]
A. Marty[2]
P. Auric[2]
C. Chappert[3]
Y. Samson[2]

Ordering intermetallic alloys by ion irradiation: A way to tailor magnetic media

Combining He ion irradiation and thermal mobility below 600 K, the transformation from chemical disorder to order in thin films of an intermetallic ferromagnet (FePd) is both triggered and controlled. Kinetic Monte Carlo simulations show how a week initial directional short-range order results in long-range order evolution. Magnetic ordering perpendicular to the film plane was achieved, promoting the initially weak magnetic anisotropy to the highest values known for FePd films. This post-growth treatment is expected to find applications in ultrahigh density magnetic recording.
Collaboration: [1]CSNSM, CNRS, Orsay, France; [2]CEA, DRFMC, Grenoble, France; [3]Inst. d'Electronique Fdtale, CNRS, Orsay, France

Doping and Defects in Semiconductors

B.N. Guo[1]
N. Variam[1]
U. Jeong[1]
S. Mehta[1]
M. Posselt
A. Lebedev

Experimental and simulation studies of the channeling phenomena in high energy implantation

As feature sizes of devices shrink, there is an increasing trend for high energy CMOS well implants to migrate to small incidence angles (near zero degree), and therefore to avoid the well spacing limitations caused by shadowing of the ion beam by the photoresist mask. However, this transition results in the replacement of traditional de-channeling profiles by channeled dopant profiles. The stronger dependence of the channeled profiles on implantation parameters such as incidence angle, dopant species, energy and dose, requires detailed investigations of dopant distributions obtained by such well implants. Boron ions were implanted at 540 and 1500 keV at a dose of $5x10^{13}$ cm^{-2}. Phosphorus implantations were performed at 800 keV, at doses between $5x10^{12}$ and $5x10^{13}$ cm^{-2}. Both in B and P implants, the tilt angle between the direction of the ion beam and the surface normal of the silicon wafer was varied between 0° and 1.5°. The depth profiles of B and P were measured by SIMS. As expected, a significant influence of the incidence angle is found. In order to achieve a high uniformity of the channeled dopant profiles across the wafer, this angle must be tightly controlled. From a device engineering perspective, accurate modeling of channeled well implants becomes therefore very important. This was achieved by Crystal-TRIM simulations which reproduce the experimental depth profiles well.

Collaboration: [1]Varian Semiconductor Equipment Associates, Gloucester, MA, USA

A. Lebedev

Integration of the Crystal-TRIM module into the process simulator FLOOPS as a part of the ISE TCAD package

Due to limitations of the present ISE (Integrated Systems Engineering AG Zürich) process simulator DIOS (Diffusion Implantation Oxidation Simulator), its replacement by the new, more flexible and extendable process simulation tool FLOOPS (University of Florida Process Simulator) is in progress. Crystal-TRIM has been successfully used as “Monte Carlo (MC) implantation engine” in DIOS and is supposed to be the primary MC implantation tool in FLOOPS. Being a fully integrated part of a process simulator, Crystal-TRIM requires in each case a different implementation of the program interface to communicate with the main program unit. This new implementation was successfully done in collaboration with the ISE development group. Almost all features existing in the old tool have been re-implemented and some of them extended, e.g. the transition from two- to three-dimensional process simulations is realized. The interface unit was made to be easily extendable to include new physical models and target materials in the future.

Collaboration: Integrated Systems Engineering (ISE) AG, Zürich, Schweiz

M. Voelskow
W. Skorupa
D. Panknin
M. Smith[1]
N. Morrison[1]
R. McMahon[1]
J. Stoemenos[2]

Determination of the Si melting depth in flash lamp irradiated SiC/Si heterostructures

The goal of FLASiC as a European GROWTH project is the reduction of high defect densities in epitaxially grown SiC/Si heterostructures by intense flash lamp pulses in the ms regime. To clarify the mechanism, especially, whether solid phase annealing or liquid phase epitaxy takes place near to the SiC/Si interface, antimony atoms as a marker element were implanted through the SiC film (27 nm thick) into the silicon substrate beneath the interface. The diffusion coefficient of Sb in silicon, even in close vicinity to the silicon melting point, is rather low, about $2x10^{-12}cm^{-2}$, so that in the case of a 20 ms solid-phase annealing step, no redistribution of Sb should be visible. On the other hand, due to the high diffusion coefficient of impurities in liquid Si (of the order of

10^{-4} cm^{-2}), a significant change of the implanted profile should be visible in the case of melting. Furthermore, due to the impurity segregation coefficient of Sb (< 0.1), even if the solidification velocity is high, there should be a significant change in the profile, whether the silicon melts or not and whether the solidification process starts from the deeper (liquid silicon- solid silicon) or from the upper (liquid silicon – SiC) interface. In the course of first experiments it could be shown by RBS that up to a certain flash energy no redistribution of Sb occurs, whereas at higher energies a distinct segregation peak near the SiC/Si interface arises. This demonstrates that (i) the silicon was molten, and (ii) the solidification process starts from the deeper liquid/solid interface towards the Si / SiC interface.

Supported by EU GROWTH Program
Collaboration: [1]University of Cambridge, UK; [2]University of Thessaloniki, Greece

H. Weishart
V. Heera
F. Eichhorn
W. Skorupa
B. Pécz[1]
A. Barna[1]

High-fluence Si-implanted diamond: sheet resistance and formation of SiC nanocrystals

Fabrication of p-type diamond and n-type SiC heterostructures may be achieved by high-fluence Si implantation into diamond. In order to retain the diamond structure, however, implantation was performed at 900°C. XRD, IR absorption spectrometry and high-resolution XTEM confirmed the formation of a buried layer inside the implanted diamond, which contains perfectly epitaxially aligned 3C-SiC nanocrystals. A first characterisation of the implanted and annealed samples by four-point probe measurements in van der Pauw geometry indicates a highly conductive layer. However, the conductivity is dominated by defects when the Si implantation fluence exceeded $5.3x10^{17}$ cm^{-2}. Since additionally Hall measurements will be employed to determine the carrier concentration, the new Hall measurement system has been tested and calibrated for use from LN_2-temperature up to 600°C.

Supported by DFG
Collaboration: [1]Research Institute for Technical Physics and Materials Science, Budapest, Hungary

H. Weishart
V. Heera
W. Skorupa
B. Pécz[1]
A. Barna[1]

High-fluence C-implanted 3C-SiC: effects of dose rate

The possible fabrication of p-type diamond and n-type SiC heterostructures by high-fluence C implantation into 3C-SiC is investigated. Implantation was performed at elevated temperatures (900°C) in order to retain the crystallinity of SiC. It is well known that the flux of implanted ions also may play a crucial role in phase formation. Therefore, the dose rate of C-ions is kept constant during each implantation run and varied in different experiments. High-resolution XTEM revealed the formation of a buried layer inside the implanted SiC, which contains either graphite or diamond precipitates. Diamond, which is always epitaxial to the SiC, is found only in samples implanted at low dose rate. Increasing the dose rate leads to formation of graphite in a textured form instead of diamond.

Supported by DFG
Collaboration: [1]Research Institute for Technical Physics and Materials Science, Budapest, Hungary

W. Anwand
G. Brauer
W. Skorupa

Vacancy-type damage in ion implanted SiC characterized by PAS

Slow positron implantation spectroscopy (SPIS) investigations were carried out on 6H-SiC implanted with Al^+, B^+, and N^+ in the range of $10^{13} – 10^{16}$ ions/cm^2 at different substrate temperatures. It is found that with increasing fluences both the size of the vacancy-type defects and the depth of the damage increase. A long tail of Si-C divacancies and monovacancies is proved up to a depth of ~ 1000 nm which is not predicted by TRIM. The optimal substrate temperature could be found to be 190°C, where amorphization is avoided and vacancy clusters of only two Si-C divacancies are the dominating defects.

The vacancy-type damage formed in Al^+ and B^+ implanted samples may be completely annealed due to a heat treatment at 1650°C for 10 min in Ar atmos-

phere. However, in Al^+ implanted samples the resulting structure is found to be not identical to the virgin structure, whereas in B^+ implanted samples B precipitates are formed. In contrast, in N^+ implanted samples very large vacancy agglomerates are formed as a result of nitrogen diffusion during the heat treatment which leads to bubble formation.

Supported by DFG

H. Weishart
V. Heera
W. Skorupa
T. Dekorsy

Graphitization of Si-implanted diamond: fluence dependence

Since the Raman cross-section of phonon bands for visible excitation wavelengths in graphite is much larger than in diamond, Raman spectroscopy is a very useful tool to detect smallest amounts of graphite within diamond. Therefore, emerging graphitic phases in high-fluence Si-implanted diamond are investigated using Raman spectroscopy. The spectra demonstrate a rather rapid evolution of non-diamond carbon phases with increasing Si fluence due to increasing damage. A very weak graphitic G peak appears in the Raman spectrum of diamond implanted with Si^+ to a fluence of $5.3x10^{17}$ cm^{-2}. Therefore, we conclude that the diamond was not significantly converted to graphitic carbon during implantation of this sample. Graphitic D (1360 cm^{-1}) and G (1600 cm^{-1}) peaks in the spectra become more and more pronounced with increasing the Si fluence to $5.7x10^{17}$ cm^{-2}. Concurrently, the diamond signal decreases. The amount of graphitic parts within the diamond top layer, as estimated from the intensities of the graphitic G and the diamond peak, are 0.7% graphite in the sample implanted to $5.3x10^{17}$ Si^+cm^2 and 44% for the sample implanted to $5.7x10^{17}$ Si^+cm^{-2}. A shift of the G band towards 1600 cm^{-1} together with the clearly visible D peak indicates the formation of nanocrystalline graphite. Using the Tuinstra-Koening-relation the size of the nanocrystals is calculated to 3 nm and 12 nm for the samples implanted to fluences of $5.5x10^{17}$ cm^{-2} and $5.7x10^{17}$ cm^{-2} respectively.

Supported by DFG

A. Peeva
R. Kögler
W. Skorupa

Visualization of vacancy type defects in the $R_P/2$ region of ion implanted and annealed silicon

The existence of small defects in the $R_P/2$ region of ion implanted and annealed silicon has been proven mainly by indirect methods such as metal decoration. So far, the $R_P/2$ defects have been considered to be too small to be visible by TEM. In this study, a direct TEM observation of vacancy-type defects in the $R_P/2$ region of ion implanted Si was achieved. Small cavities (diameter ~ 2÷4 nm) were observed for MeV Si^+ and also for keV He^+-ion-implanted and annealed Si. The crucial point for visualization of the vacancy type defects at $R_P/2$ by TEM is the specimen preparation technique. The very widely used conventional ion milling technique for TEM specimen preparation introduces damage on the surface of the XTEM specimen, which blurs the original defect structure at $R_P/2$ and obscures it from visualization. Minimum damage production caused during the preparation of the TEM specimen by the use of cleaving allows the imaging of the cavities at $R_P/2$. The experimental observation of cavities at $R_P/2$ can be taken as a direct proof for the existence of the theoretically predicted excess vacancies in the $R_P/2$ region of ion implanted Si substrates.

G. Brauer
W. Anwand
W. Skorupa
A.G. Revesz[1]
J. Kuriplach[2]

Low-quartz structure at the SiO_2/Si interface

Positron annihilation spectroscopy (PAS), mainly in the form of slow-positron implantation spectroscopy (SPIS), was used to study the SiO_2/Si system. An annihilation state is revealed in the thermally grown and etched, as well as a native oxide which must resemble low quartz in its structure. A lower limit of about 2.2 nm of the thickness of this layer at the interface was evaluated. Additionally, a variety of state-of-the-art theoretical calculations were done to aid the experimental findings. Moreover, these SPIS results corroborate the model of quasi-epitaxial oxide growth and pseudo-polymorphic relaxation of

the grown oxide.

Collaboration: [1]Revesz Associates, Bethesda, MD, USA; [2]Charles University, Prague, Czech Republic

B. Pécz[1]
V. Heera
S. Sinning
T. Dekorsy
W. Skorupa

High-dose N^+ ion implantation into GaAs at elevated temperatures

The ion beam synthesis of electrically or optically active nanoclusters inside insulating or semiconducting substrates is of current interest. A promising nanocluster/substrate combination is GaN/GaAs. 200 keV nitrogen ions were implanted into (100) GaAs with doses of $2x10^{17}cm^{-2}$ and $6x10^{17}cm^{-2}$. Under these implantation conditions maximum nitrogen concentrations of about 15 at.% and 35 at.%, respectively, can be predicted in a depth of about 370 nm if matrix changes are neglected. The implantations were carried out at temperatures of 400°C and 600°C in order to reduce the radiation damage and to stimulate phase formation. The as-implanted layers were investigated by XTEM and selected area diffraction (SAD). There is clear evidence for GaN nanocluster formation after implantation at 600°C. Epitaxially aligned, hexagonal GaN precipitates with sizes in the range between 5 nm and 10 nm were detected. In the case of implantation with the higher dose at 400°C the XTEM investigation revealed the formation of nitrogen bubbles and amorphous pockets in a band located between 400 nm and 500 nm depth.

Collaboration: [1]Research Institute for Technical Physics and Materials Science, Budapest, Hungary

Materials for Optoelectronics

T. Dekorsy
V.A. Yakovlev[1]
F. Keilmann[2]
W. Seidel[3]
M. Helm

Determination of the dispersion of the second order susceptibility of GaAs in the THz range

Nonlinear optics in the THz regime remains to a great extent unexplored due to the lack of high-power laser sources. However, nonlinear optical experiments in this frequency range would give important insight into higher order terms of the lattice potential. We performed second harmonic generation experiments of thin GaAs crystals below the optical phonon frequency of 8.8 THz in GaAs at the free-electron laser facility FELIX, Netherlands. This laser generates optical pulses of picosecond duration and µJ pulse energies tunable in the THz frequency range. In agreement with theoretical calculations we observed for the first time a resonance of the second order nonlinear susceptibility at half the phonon frequency. In addition, a sign reversal associated with a zero-crossing of the nonlinear susceptibility is observed at higher frequencies, but below the phonon resonance. The determination of this zero-crossing frequency allows the first experimental determination of absolute values for higher order terms of the lattice potential.

Supported by EU (LSF – FELIX, NL)

Collaboration: [1]Institute of Spectroscopy, Russian Academy of Sciences, Troitsk, Russia; [2]Max-Planck Institut für Biochemie, Martinsried; [3]Institute for Nuclear and Hadron Physics, FZR

S. Winnerl
A. Dreyhaupt
T. Dekorsy
M. Helm

Generation and detection of single cycle THz radiation pulses

In recent years there has been a tremendous effort to close the so-called THz gap, i.e. the lack of inexpensive sources for THz radiation. Spectroscopy in the THz frequency range is of interest in many material systems ranging from superconductors and semiconductor heterostructures to biomolecules and biological tissue. We have built a system to generate and detect THz radiation pulses. The pulses are emitted from the surface of III-V semiconductor crystals irradiated with pulsed radiation (wavelength 800 nm, pulse duration 50 fs) from a Ti:sapphire laser. The carriers created by the optical pulses are accelerated in the surface field of the semiconductor and thereby emit THz radiation. Amplitude and phase of the THz radiation are detected by electro-optical sampling, making use of the ultrafast Pockels effect in a (110) ZnTe crystal. Typical THz field strengths are of the order of 10 V/cm. The setup can be used for THz time-domain spectroscopy (TDS) experiments to study the reflection or transmission of materials in the frequency range from 0.5 to 3.5 THz. Besides spectroscopic experiments the setup can also be used to study the carrier dynamics in the emitter crystals on ultrashort timescales. First experiments have been carried out with nitrogen implanted GaAs. Different implantation and annealing conditions yield different THz traces, reflecting the difference in the carrier dynamics.

S. Sinning
T. Dekorsy
M. Helm
G. Mußler[1]

Time resolved investigations of nitrogen implanted GaAs

III-V-semiconductors with incorporation of a small fraction of nitrogen are of current interest due to the associated strong decrease of the bandgap energy with increasing nitrogen content. We investigated optical properties of nitrogen implanted GaAs and their dependence on implantation and annealing conditions. (100) oriented GaAs was implanted with $^{14}N^{+}$ to create a 600 nm thick surface layer with homogenous N-distribution (c_N = 0.5% - 4%). Subsequent RTA annealing was carried out to maximize both nitrogen incorporation into the lattice and lattice quality. The bandgap shift is determined from photoreflectance measurements. A maximum bandgap reduction of 63 meV for 1 % nitrogen implantation is observed. The crystal quality of the samples is inferred from TEM and Raman scattering investigations. The influence of the modified

band structure on the carrier relaxation dynamics is investigated by femtosecond pump-probe experiments.
Collaboration: [1]Paul-Drude-Institut für Festkörperelektronik, Berlin, Germany

T. Dekorsy
M. Först[1]
H. Kurz[1]
R.V. Leavitt[2]

Coupling of Bloch oscillations to coherent phonons in InGaAs/InAlAs superlattices

Bloch oscillations in semiconductor superlattices are a fundamental and intriguing problem of solid-state physics. They describe the oscillatory motion of an electronic wavepacket under the combined influence of a static periodic potential and a constant electric field. While over the last years all investigations of Bloch oscillations were performed on $GaAs/Al_xGa_{1-x}As$ superlattices, we performed first experiments on $In_{0.53}Ga_{0.47}As/ In_{0.52}Al_{0.48}As$ superlattices. The superlattice exhibits a first electronic miniband width of 60 meV, which is larger than the optical phonon energies of the system. In addition, the miniband is only weakly confined (approx. 10 meV) below the barriers. These peculiarities allow us to tune the Bloch frequency via an applied electric field across the optical phonon resonances of the ternary barrier and well material. However, at higher electric fields a rapid dephasing due to tunneling into continuum states sets in. When the Bloch frequency approaches the phonon frequencies we observe the coherent excitation of the different phonons. The rapid tunneling into continuum states provides a further excitation mechanism for coherent optical phonons at higher fields. These experiments provide new insight into electron-phonon interaction in semiconductor nanostructures.
Collaboration: [1]Institut für Halbleitertechnik, RWTH Aachen; [2]US Army Research Laboratories, Adelphi, Maryland, USA

N. Georgiev
T. Dekorsy
M. Helm
M. Semtsiv[1]
W.T. Masselink[1]

Intersubband transitions in strain compensated InGaAs/AlAs quantum well structures grown on InP

Pseudomorphic InxGa1-xAs/AlAs heterostructures on InP or GaAs have emerged as excellent candidates for short-wavelength intersubband transitions because of their large conduction band offset. However, the growth of appropriate structures on both GaAs or InP substrates requires to grow highly strained well and/or barrier layers. The increased strain accommodation in the InGaAs/AlAs system considerably affects the band offsets of these QW structures and the performance of the appropriate devices. We have investigated the intersubband optical absorption of $InxGa_{1-x}As/AlAs/In_yAl_{1-y}As$ (x~0.7, y~0.55) QW structures grown on InP substrates. In these structures, we utilise the high barrier provided by thin AlAs layers. An increased In content in the well and in the $In_yAl_{1-y}As$ barrier layers helps to compensate the large AlAs tensile strain. Additionally, it provides a smaller InGaAs band gap that results in a shift of the first Γ-like well subband to lower energies relative to the X-minimum in the barrier layers even in very narrow wells. Intersubband absorption at wavelengths shorter than 3.0 μm is observed in thin symmetric and asymmetric multiquantum well structures as well as short-period superlattices.
Supported by DFG
Collaboration: [1]Humboldt-University Berlin, Department of Physics

N. Georgiev
T. Dekorsy
M. Helm
K. Biermann[1]
H. Künzel[1]

Short-wavelength intersubband transitions in InGaAs/AlAsSb multiple quantum well structures

InGaAs/AlAsSb quantum wells (QWs) are very attractive for development of new devices based on intersubband transitions, such as near-infrared detectors, ultra-fast switches and light emitters that operate at the communication wavelength of 1.55 μm. The structures are also of great interest for investigating the properties of strongly confined systems due to large conduction-band offset in these heterosystems. However, realizing intersubband transitions at wavelengths shorter than 2.0 μm requires an extremely narrow well thickness, placing stringent demands on the structural quality of the As/Sb heterointer-

face. We have studied the structural and optical properties of InGaAs/AlAsSb multiple QW structures grown lattice matched on InP substrates. Although growth terminations at interfaces under As overpressure were used during the growth of the structures, Raman spectra show presence of specific interface related InSb and GaSb modes that indicate some As/Sb intermixing at the heterointerfaces. Absorption wavelengths down to ~2.0 μm are observed in the samples with 7 and 8 monolayers thick QWs. Further optimisation of the growth conditions is needed in order to get below 2.0 μm.

Supported by DFG
Collaboration: [1]Fraunhofer Institut Nachrichtentechnik, Heinrich-Hertz-Institut, Berlin

N. Georgiev
F. Eichhorn
A. Bauer
T. Dekorsy
M. Helm
M. Semtsiv[1]
W. T. Masselink[1]

XRD characterization of strain compensated InGaAs/AlAs quantum well structures

The growth of strain-compensated quantum well structures has appeared as a promising technique for band-structure modifications. InGaAs/AlAs quantum well structures are interesting for the development of novel optoelectronic devices. Strain effects and the structural quality of the structures considerably influence the optical properties of the structures. We performed detailed X-ray diffraction and X-ray reflectivity analysis of $In_xGa_{1-x}As/AlAs$ (x~0.7) multi-quantum well structures grown on InP substrates. We found that in order to compensate the larger tensile strain of the AlAs layers additional compressively strained $In_yAl_{1-y}As$ (y~0.55) should be grown as a buffer and additional barrier layers in addition to the also compressively strained InGaAs. In spite of the large misfit of the AlAs layers the average mismatch in the MQW is small, because the AlAs layers are much thinner than the InGaAs and InAlAs layers in the MQW. Growth of the suitably thick and compressively strained InAlAs layers is of crucial importance for obtaining high quality samples. If we grow these layers lattice matched we observe both a broadening and a reduced number of the satellite peaks. This is an indication for the deterioration of the crystalline and interfacial quality in the MQW due to the increased strain from strongly mismatched AlAs layers.

Supported by DFG
Collaboration: [1]Humboldt-University Berlin, Department of Physics

H.-J. Fitting[1]
T. Barfels[1]
A.N. Trukhin[2]
B. Schmidt
A. Gulans[2]
A. von Czarnowski[1]

Cathodoluminescence of Ge^+, Si^+, and O^+ implanted SiO_2 layers and the role of mobile oxygen in defect transformation

Thermally grown SiO_2 layers of thickness d = 500 nm were implanted by Ge^+, Si^+, and O^+ ions of energy 350, 150, and 100 keV, respectively, and a uniform implantation dose of $D = 5x10^{16}$ cm^{-2}. Thus implantation profiles with a concentration maximum of nearly 4 at% at the half-depth d_m = 250 nm of the SiO_2 layers are expected. After thermal annealing to 900°C for 1 h in dry nitrogen or vacuum the typical violet luminescence band (at 400 nm) of the Ge^+ implanted centers is increased more than 200-fold and the Ge luminescent center depth profile is shifted from about 250 to 170 nm towards the surface as determined by cathodoluminescence (CL) depth profiling. Implanting oxygen increases the red band (at 650 nm) but does not affect the blue band (at 460 nm). Silicon surplus increases the amplitude of the blue (B) luminescence, but reduces the amplitude of the red (R) one. Studying the irradiation dose dependence of these blue and red bands we have established defect kinetics in SiO_2 including six main defects and precursors, including the non-bridging oxygen hole center for the red luminescence, the twofold-coordinated silicon as the oxygen deficient center ODC(2) for the blue luminescence and the mobile oxygen as the main transmitter between precursors and the radiation induced defects. The kinetics is described by a set of eight differential equations which predict the dose dependence of the CL.

Collaboration: [1]Universität Rostock; [2]University of Latvia, Riga, Latvia

J. Seidel[1]
S. Grafström[1]
L. Eng[1]
L. Bischoff

Surface plasmon transmission across narrow grooves in thin silver films

Propagation of optical-frequency surface plasmons at metal / dielectric interfaces and their interaction with defined surface structures are of interest for applications in integrated optics. We report on the direct measurement of surface plasmon transmissivity of narrow grooves, fabricated by focused ion beam sputtering in thin silver films using near-field optical microscopy in an attenuated total-reflection-setup. Characteristic changes in transmissivity are observed for different groove widths of 250, 420 and 500 nm, respectively. One big advantage of the experimental method employed here is the direct mapping of the plasmon field on the metal surface. The aquired results show a strong variation of transmissivity with surface groove width, which was attributed to resonant plasmon mode coupling across the groove. The results are in good agreement with existing theoretical predictions. Furthermore, elastic scattering of surface plasmons by irregularities of the groove edge was observed.

Collaboration: [1]Institut für Angewandte Photophysik, TU Dresden

Others

W. Leitenberger[1]
H. Wendrock[2]
L. Bischoff
T. Panzner[1]
U. Pietsch[1]
J. Grenzer[1]
A. Pucher[1]

Double pinhole diffraction of white synchrotron radiation

The characterization of X-ray beams, in particular their coherence properties, is of large interest for quantitative interpretation of experimental data. The spatial coherence of hard X-rays provided by a bending magnet of the storage ring BESSY II was investigated performing Young's interference experiment. The interference pattern was created by the diffraction of two 2 µm pinholes drilled into a thin tantalum foil by focused ion beam sputtering. The aspect ratio of the micromachined holes was in the order of 10. Using an energy-dispersive detector with an energy resolution of 200 eV the interference pattern were detected simultaneously between $5\ \mathrm{keV} < E < 16\ \mathrm{keV}$ scanning a 5 µm pinhole through the detector window. The set-up is suitable to characterize the coherence properties of the beamline in a simple manner, i.e. to deduce parameters such as the effective source size, the coherence length and the visibility. For the present case the visibility is near 100% at 5 keV and decreases to 20% at 16 keV.

Collaboration: [1]Institut für Physik, Universität Potsdam; [2]Institut für Festkörper- und Werkstoffforschung Dresden

T. Wang[1]
F. Eichhorn
N. Schell
D. Grambole
F. Wunderlich[2]
B. Wunderlich[2]

In-situ study of the thermal stability of a new TiH_2 phase

A new TiH_2 phase has been found in Ti after H implantation or mechanical polishing. An in-situ analysis of its thermal stability and transition has been carried out at the ROBL facility. Various samples were measured under gracing incidence in a high-temperature chamber at Cu-Kα wavelength. A thermal phase transition from the TiH_2 to Ti/H (α) was found at a critical temperature of 48±2°C. The transition rate was temperature-dependent. A constant transition rate was obtained at a fixed temperature of 65°C. The Ti/H layer was inhomogeneous before heating and totally dehydrogenated after heating to 200°C in two hours. This Ti/H phase transformation can also be induced by mechanical stress. Therefore, it has a potential to be used as an alternative phase for H-storage and to dehydrogenate the titanium surface.

Supported by MPG

Collaboration: [1]Institute of Modern Physics, Chinese Academy of Sciences, Lanzhou, China; [2]Friedrich-Schiller-Universität Jena, Institut für Optik und Quantenelektronik

D. Grambole
T. Wang[1]
F. Herrmann
F. Eichhorn

Bending stress related diffusion of hydrogen in titanium studied by micro ERDA

The influence of bending stress on the hydrogen behaviour in titanium was investigated by ERDA with a heavy ion microbeam, and by XRD. The samples were prepared by H^+ implantation into polished pure Ti disks. Three dimensional H distributions were obtained by scanning the microbeam over the sample using the depth information of ERDA. Inhomogeneous H distributions were observed which vary with the depth. With mechanical bending of the samples these inhomogeneities increase differently. The H on the surface loaded by surface polishing is stable, while the implanted H located inside of the sample is mobile under bending. These different H behaviors are relevant to the chemical states of H. Different titanium hydrides are formed by the different loading methods. The less common Ti/H phase (TiH_2(x)) with a tetragonal texture in the depth region of implanted H is less stable than the normal TiH_2 observed in the surface region. The change of H distribution is related to the dehydrogenation of the TiH_2(x) and TiH(γ) under bending.

Supported by MPG

Collaboration: [1]Institute of Modern Physics, Chinese Academy of Sciences, Lanzhou, P.R. China

J. Cizek[1]
I. Prochazka[1]
R. Kuzel[1]

Microstructure of ultra-fine grained copper

Ultra-fine grained (UFG) materials exhibit a number of unusual properties which are known to be connected with a significant volume fraction of grain

R.K. Islamgaliev[2]
W. Anwand
G. Brauer

boundaries. The microstructure of UFG copper (99.99% purity), prepared by equal-channel angular pressing (ECAP) for severe plastic deformation at room temperature, was investigated by TEM and SPIS after different passes of pressing. After 1 pass, prolonged grains are formed. The grains contain dislocation cells with a mean size of about 300 nm separated by low-angle boundaries. Positrons annihilate after trapping at dislocations in distorted regions along grain boundaries and at microvoids situated inside grains. The size of microvoids after 1 ECAP pass is about 3-4 vacancies and decreases with increasing number of passes. The decrease is accompanied by an increase of the concentration of microvoids. The most pronounced change is observed between 1 and 2 ECAP passes.

Supported by BMBF

Collaboration: [1]Charles University, Prague, Czech Republic; [2]Ufa State Aviation Technical University, Ufa, Russia

Equipment

M. Friedrich
W. Bürger
S. Turuc

Operation and development of the electrostatic accelerators

The ***2 MV VdG accelerator*** has been used mainly for RBS analysis. After changing the belt charging system in the last year to an arrangement with tungsten foil pieces as charge emitter, we operate this system now with a new current stabilizer adapted to the considerably lower charging voltage.

The ***5 MV Tandem*** has been applied mainly for ion beam analysis and high-energy implantation. The power supply of the analysing magnet was replaced by a Danfysik System 8000 model 853 unit (400 A/ 95 V). After its installation a significant improvement of the stability of the magnetic field has been obtained. Encouraging progress was achieved in the reconstruction of the vacuum control system on basis of PLC SIEMENS S7-200 components including the use of the so-called A/S-Interface (a simply to implement serial actor/ sensor - bus system). For the purpose of efficient boron acceleration, a DANFYSIK CHORDIS ion source was purchased. First experiments with this device showed some problems of the optical adaptation of the charge-exchange canal in the present injector configuration. The beam line from the tandem to the ultrahigh resolution magnetic spectrometer has been completed and tested.

The ***3 MV Tandetron*** has been applied mainly for high-energy implantation and ion beam analysis. In the beginning of 2002, the defective high voltage resonance coil in the power transformer had to be replaced. For more efficient helium acceleration, the RF He ion source was removed, and a HVEE Model 358 duoplasmatron was put into operation. The lifetime of the Cs sputter ion source 860-C has been improved by an additional internal screening electrode. The last test version of the modified ion source is still in operation since August 2002.

In 2002 the ***total operating hours*** of the high-energy accelerators were 1364 h (VdG), 2227 h (Tandetron, note however about 2 month's down time for resonance coil replacement) and 2223 h (Tandem).

L. Bischoff
Ch. Akhmadaliev
L. Roussel[1]

Installation of a new high resolution focused ion beam column

After a 12 year period of operation the ion optical column of the IMSA-100 FIB instrument was replaced by the modern type CANION 31Z from Orsay Physics. For this purpose, the vacuum chamber had to be redesigned to provide space for the installation of additional features such as a gas injection system (GIS) for FIB-aided etching and metal deposition, and also for a IR-CCD camera for controlling of the GIS and stage movements. The ion beam column contains a mass separator and allows to achieve spot sizes smaller than 20 nm. The ion energy ranges from 10 to 30 keV for single charged ions. Options such as target heating or cooling, electrical measurements during irradiation, ion acoustic detection as well as the precise laser interferometer controlled stage for up to 6 inch wafers are still available.

Collaboration: [1]Orsay Physics, France

Ch. Akhmadaliev
L. Bischoff
G. L. R. Mair[1]
C.J. Aidinis[1]

Frequency spectra of emission instabilities of liquid metal alloy ion sources

Detailed investigations of the emission instabilities and their frequency spectra for Liquid Metal Alloy Ion Sources (LMAIS) wetted with Ga, AuGeSi and AuGe, were carried out. Ion sources with extracting electrode (triode scheme) as well as without extractor (diode scheme) were applied. The ion current coming from a collector electrode was amplified and converted into a voltage. Frequency spectra from 0 to 100 MHz were measured using a HP8591 spectrum analyzer with a resolution of 300 kHz. Simultaneously the corresponding oscilloscope traces of the emission current were obtained and correlated with the spectra. The pulses are believed to be the result of a droplet emission, and

their terminal frequency appears to coincide with the frequency of vibrations of the sides of the liquid cone at high currents. The emitted droplets screen the source tip, which leads to a decrease of the effective electric field and to fluctuations of the emission process. The following disintegration of the droplets into smaller ones aggravates the noise, which depends nonlinearly on the emission current. This dependence shows an "S" shape, at low emission current the noise is negligible, at 40-60 µA the fluctuations increase rapidly and above 70 µA they saturate. At 100 µA emission current the fluctuations are about 5 µA (rms). With increasing LMAIS temperature up to 1100°C stronger fluctuations were registered. A better understanding of the instabilities at the liquid anodes is useful for deposition purposes.

Collaboration: [1]University of Athens, Department of Physics, Section of Solid State Physics, Athens, Greece

T. Dekorsy
S. Winnerl
W. Seidel[1]
A. Poppe[2]

Synchronization of a femtosecond oscillator to a reference clock with timing jitter below 400 fs

In order to perform two color pump-probe experiments with a free-electron laser and solid-state mode-locked femtosecond lasers, both lasers have to be synchronized to each other with high precision. The achievable time resolution is limited by the pulse duration of the involved lasers and the timing jitter of the synchronization. We have synchronized a femtosecond Kerr-lens mode-locked Ti:sapphire oscillator delivering 12 fs pulses at a repetition rate of 78 MHz. This frequency equals six times the anticipated repetition rate of the free-electron laser (FEL) of 13 MHz, which was derived from a quartz oscillator. The phase-locked loop of the synchronization is stabilized at the 30th harmonics of the FEL repetition rate (390 MHz). The timing jitter of the femtosecond oscillator is determined from measuring and integrating the noise spectral density with a fast photo diode and a spectrum analyzer. We derive a timing jitter below 400 fs, which is better than values reported up to date in the literature.

Collaboration: [1]Institute for Nuclear and Hadron Physics, FZR; [2]Femtolasers GmbH, Vienna, Austria

Glossary

AES	Auger electron spectroscopy
AFM	Atomic force microscopy
AMS	Atomic mass spectrometry
CEMS	Conversion electron Mössbauer spectroscopy
CMOS	Complementary metal-oxide-semiconductor
CV	Capacitance-voltage-characteristics
CVD	Chemical vapor deposition
DLC	Diamond-like carbon
ECR	Electron-cyclotron-resonance
EL	Electroluminescence
ERDA	Elastic recoil detection analysis
ESRF	European Synchrotron Radiation Facility, Grenoble
FEG	Field emission gun (at the TEM)
FIB	Focused ion beam
FIR	Far infrared
FTIR	Fourier transformed infrared spectroscopy
FWHM	Full width at half maximum
GDOS	Glow discharge optical spectroscopy
GIXRD	Gracing incidence X-ray diffraction
GMR	Giant magnetoresistance
GRID	Gammy-ray induced Doppler-broadening
IBA	Ion beam analysis
IBIC	Ion beam induced crystallization
IBAD	Ion beam assisted deposition
HSS	High speed steel
IBS	Ion beam synthesis
IV	Current-voltage-characteristics
MBE	Molecular beam epitaxy
MOS	Metal-oxide-semiconductor
NIR	Near infrared
NRA	Nuclear reaction analysis
PAS	Positron annihilation spectroscopy
PECVD	Plasma enhanced chemical vapor deposition
PIGE	Proton-induced Gamma-ray emission
PIII	Plasma immersion ion implantation
PIIIAD	Plasma immersion ion implantation assisted deposition
PIXE	Proton-induces X-ray emission

PL	Photoluminescence
PSD	Position sensitive detector
PVD	Physical vapor deposition
ROBL	**RO**ssendorf Synchrotron **B**eam**L**ine (at the ESRF)
RBS	Rutherford backscattering spectroscopy
RBS/C	Rutherford backscattering spectroscopy under channelling conditions
RF	Radio frequency
RTA	Rapid thermal annealing
SE	Spectroscopic ellipsometry
SEM	Scanning electron microscopy
SIMS	Secondary ion mass spectrometry
SPIS	Slow positron implantation spectroscopy
SQUID	Superconducting quantum interferometer device
SRIM (TRIM)	Computer program “Stopping and Ranges of Ions in Matter”
STM	Scanning tunnel microscope
TEM	Transmission electron microscopy
XANES	X-ray absorption near-edge spectroscopy
XPS	X-ray photoelectron spectroscopy
XRD	X-ray diffraction
XRF	X-ray fluorescence analysis
XTEM	Cross-section transmission electron microscopy

Supporting Institutions

AiF	Arbeitsgemeinschaft Industrieller Forschungsvereinigungen e.V.
AvH	Alexander-von-Humboldt Stiftung
BMBF	Bundesministerium für Bildung und Forschung
BMWi	Bundesministerium für Wirtschaft
DAAD	Deutscher Akademischer Austauschdienst
DFG	Deutsche Forschungsgemeinschaft
EU	European Union
MPG	Max-Planck-Gesellschaft
SMWK	Sächsisches Staatsministerium für Wissenschaft und Kunst
SMWA	Sächsisches Staatsministerium für Wirtschaft und Arbeit
WTZ	Programs of „Scientific-Technical-Cooperation”

Editorships

Brauer, G., Anwand, W. (Guest Editors)
Proceedings of the Ninth International Workshop on Slow Positron Beam Techniques for Solids and Surfaces (Dresden, Sep 16-22, 2001),
Appl. Surf. Sci. **194** (2002)

Publications

Akhmadaliev, Ch., Bischoff, L., Teichert, J., Kazbekov, K.,
Ion acoustic microscopy based on IMSA-100 focused ion beam system,
Vacuum **69** (2002) 431

Akhmadaliev, Ch., Mair, G.L.R., Aidinis, C.J., Bischoff, L.,
Frequency spectra and electrohydrodynamic phenomena in a liquid gallium field ion emission source,
J. Appl. Phys. **35** (2002) L91

Alonso, F.A., Gago, R., Jiménez, I., Gómez-Aleixandre, C., Albella, J.M.,
On the bonding structure of hydrogenated carbon nitrides grown by electron cyclotron chemical vapour deposition: towards the synthesis of non-graphitic carbon nitride,
Diam. Rel. Mat. **11** (2002) 1161

Alves, E., Barradas, N.P., Monteiro, T., Correia, R., Kreissig, U.,
Ion beam studies of MBE grown GaN films on (111) silicon substrates,
Nucl. Instr. Meth. B **188** (2002) 73

Anwand, W., Brauer, G., Skorupa, W.,
Vacancy-type defects in 6H-SiC caused by N^+ and Al^+ high fluence co-implantation,
Appl. Surf. Sci. **194** (2002) 131

Anwand, W., Brauer, G., Wirth, H., Skorupa, W., Coleman, P.G.,
The influence of substrate temperature on the evolution of ion implantation induced defects in epitaxial 6H-SiC,
Appl. Surf. Sci. **194** (2002) 127

Arazi, A., Faestermann, T., Fernandez Niello, J., Knie, K., Korschinek, G., Richter, E., Rugel, G., Wallner, A.,
Measurement of the $^{25}Mg(p,\gamma)^{26}Al$ reaction at stellar energies,
New Astron. Rev. **46** (2002) 525

Auger, M.A., Gago, R., Fernández, M., Sánchez, O., Albella, J. M.,
Deposition of TiN/AlN bilayers on a rotating substrate holder by reactive sputtering,
Surf. Coat. Technol. **157** (2002) 26

Barfels, T., Schmidt, B., Czarnowski, A. von, Fitting, H.-J.,
Catohodoluminescence depth profiling in SiO_2:Ge layers
Microchim. Acta **139** (2002) 11

Beloto, A.F., Ueda, M., Abramof, E., Senna, J.R., da Silva, M.D., Kuranaga, C., Reuther, H., Ferreira da Silva, A., Pepe, I.,
Sponge-like and columnar porous silicon implanted with nitrogen by plasma immersion ion implantation (PIII),
Surf. Coat. Technol. **156** (2002) 267

Belov, A.Yu., Jäger, H.U.,
Elastic constants of tetrahedral amorphous carbon: the effect of intrinsic stresses,
Surf. Coat. Technol. **151-152** (2002) 128

Belov, A.Yu., Jäger, H.U.,
Calculation of intrinsic stresses in amorphous carbon films grown by molecular dynamics simulation: from atomic to macroscopic scale,
Comp. Mat. Sci. **24** (2002) 154

Bischoff, L., Mair, G.L.R., Aidinis, C.J., Ganetsos, Th.,
Fundamental properties of erbium-ions-producing liquid metal alloy ion sources,
Nucl. Instr. Meth. B **197** (2002) 282

Bischoff, L., Teichert, J., Kitova, S., Tsvetkova, T.,
Optical pattern formation in a-SiC:H films by Ga^+ ion implantation,
Vacuum **69** (2002) 73

Borany, J. von, Gebel, T., Stegemann, K.-H., Thees, H.-J., Wittmaack, M.,
Memory properties of Si^+ implanted gate oxides: From MOS to nv-SRAM,
Solid State Electron. **46** (2002) 1729

Bøttiger, J., Chevallier, J., Petersen, J. H., Schell, N., Matz, W., Mücklich, A.,
Observation of the growth mode of TiN during magnetron sputtering using synchrotron radiation,
J. Appl. Phys. **91** (2002) 5429

Brauer, G., Anwand, W., Skorupa, W., Revesz, A.G., Kuriplach, J.,
Characterization of the SiO_2/Si interface by positron annihilation spectroscopy,
Phys. Rev. B **66** (2002) 195331

Cizek, J., Prochazka, I., Melikhova, O., Brauer, G., Anwand, W., Kuzel, R., Cieslar, M., Islamgaliev, R.K.,
Investigation of spatial distribution of defects in ultra-fine grained copper,
Appl. Surf. Sci. **194** (2002) 140

Deshkovskaya, A., Richter, E., Komar, V.,
Ion beam-stimulated phase formation in fused silica,
Surf. Coat. Technol. **158-159** (2002) 508

Donchev, T., Tsaneva, V., Nurgaliev, T., Gravier, L., Ansermet, J.Ph., Petrov, I., Petrova, V., Matz, W., Grötzschel, R., Pignard, S., Vincent, H.,
YBCO/LSMO and LSMO/YBCO double-layer deposition by off-axis magnetron sputtering and strain effects,
Vacuum **69** (2002) 243

Eichhorn, F., Schell, N., Mücklich, A., Metzger, H., Matz, W., Kögler, R.,
Structural relation between Si and SiC formed by carbon ion implantation,
J. Appl. Phys. **91** (2002) 1287

Facsko S., Bobek T., Kurz H., Dekorsy T., Kyrsta S., Cremer R.,
Ion-induced formation of regular nanostructures on amorphous GaSb surfaces,
Appl. Phys. Lett. **80** (2002) 130

Fitz, C., Kolitsch, A., Fukarek, W., Möller, W.,
Growth of low stress cubic boron nitride films by simultaneous medium energy ion implantation,
Appl. Phys. Lett. **80** (2002) 55

Fitting, H.-J., Barfels, T., Trukhin, A.N., Schmidt, B., Gulans, A., Czarnowski, A. von,
Cathodoluminescence of Ge^+, Si^+, and O^+ implanted SiO_2 layers and the role of mobile oxygen in defect transformation,
J. Non-Crystalline Solids **303** (2002) 218

Fitting, H. J., Barfels, T., Schmidt, B., Czarnowsky, A. von,
CL and EDX depth profiling in Ge-implanted SiO_2 layers,
Proc. of the 15th Int. Congress on Electron Microscopy, Vol. 1: Physical, Materials and Earth Sciences, Sept 1-6, 2002, Durban, South Africa, pp. 797-798

Fitz, C., Fukarek, W., Möller, W.,
Stress relaxation and phase stability of cubic boron nitride films during ion post implantation and annealing,
Thin Solid Films **408** (2002) 155

Fitz, T., Möller, W.,
AlN growth kinetics during ion nitriding of aluminum,
J. Appl. Phys. **92** (2002) 6862

Friedrich, M., Bürger, W., Turuc, S., Tyrroff, H.,
New developments at the Rossendorf electrostatic accelerators,
in: Symposium of the North Eastern Accelerator Personnel SNEAP XXXIV, Lund University, Sweden, Oct. 22-25, 2001, Eds.: R. Hellborg, M. Faarinen, C.E. Magnusson, P. Persson, G. Skog, K. Stenström, Dept of Physics, Lund University, 2002, p. 257

Fritsche, B., Chevolleau, T., Kourtev, J., Kolitsch, A., Möller, W.,
Plasma diagnostic of an RF magnetron Ar/N_2 discharge,
Vacuum **69** (2002) 139

Gago, R., Jiménez, I., Albella, J.M., García, I.,
Growth and characterisation of boron-carbon-nitrogen coatings obtained by ion beam assisted evaporation,
Vacuum **64** (2002) 199

Gago, R., Jiménez, I., Kreissig, U., Albella, J.M.,
X-Ray absorption study of the bonding structure of BCN compounds enriched in carbon by CH_4 ion assistance,
Diam. Rel. Mat. **11** (2002) 1295

Gago, R., Vázquez, L., Cuerno, R., Albella, J.M.,
Production of nanoscale patterning on silicon surfaces by ion beam sputtering,
Nanotechnology **13** (2002) 304

Gago, R., Jiménez, I., Agulló-Rueda, F., Albella, J.M., Czigány, Zs., Hultman, L.,
Transition from amorphous boron carbide to hexagonal boron carbon nitride thin films induced by nitrogen ion assistance,
J. Appl. Phys. **92** (2002) 5177

Gammer, K., Gritsch, M., Peeva, A., Kögler, R., Hutter, H.,
SIMS investigations of gettering centers in ion-implanted and annealed silicon,
J. Trace Microprobe Tech. **20** (2002) 47

Gebel, T., Rebohle, L., Skorupa, W., Nazarov, A.N., Osiyuk, I.N., Lysenko, V.S.,
Charge trapping in light-emitting SiO_2 layers implanted with Ge^+ ions,
Appl. Phys. Lett. **81** (2002) 1575

Gebel, T., Voelskow, M., Skorupa, W., Mannino, G., Privitera, V., Priolo, F., Napolitani, E., Carnera, A.,
Flash lamp annealing with millisecond pulses for ultra shallow boron profiles in silicon,
Nucl. Instr. Meth. B **186** (2002) 287

Gopal A.V., Yoshida H., Neogi A., Georgiev N., Mozume T., Simoyama T., Wada O., Ishikawa H.,
Intersubband Absorption Saturation in InGaAs-AlAsSb quantum wells,
IEEE J. Quant. Electron. **38** (2002) 1515

Grigorov, K., Tsaneva, V., Spasov, A., Matz, W., Grötzschel, R., Reuther, H.,
RBS and ion channelling study of YBCO/STO and YBCO/LSMO/STO structures. Oxygen content estimated by X-ray diffraction,
Vacuum **69** (2002) 315

Günzel, R., Rogozin, A.I., Astrelin, V.T.,
Fast, uniform, and large-scale heat treatment by plasma-based electrons,
Vacuum **65** (2002) 59

Heera, V., Madhusoodanan, K.N., Mücklich, A., Panknin, D., Skorupa, W.,
Low-resistivity, p-type SiC layers produced by Al implantation and ion-beam-induced crystallization,
Appl. Phys. Lett. **81** (2002) 70

Iacopi, F., Tökei, Zs., Le, Q.T., Shamiryan, D., Conard, T., Brijs, B., Kreissig, U., Van Hove, M., Maex, K.,
Factors affecting an efficient sealing of porous low-k dielectrics by physical vapor deposition Ta(N) thin films,
J. Appl. Phys. **92** (2002) 1548

Ivanov, Yu., Matz, W., Rotshtein, V., Günzel, R., Shevchenko. N.,
Pulsed electron-beam melting of high-speed steel: structural phase transformations and wear resistance,
Surf. Coat. Technol. **150** (2002) 188

Jagielski, J., Kopcewicz, M., Gawlik, G., Matz, W., Thomé, L.,
Thickness dependent phase transformations in implanted iron layers,
J. Appl. Phys. **91** (2002) 6465

Jembrih-Simbürger, D., Neelmeijer, C., Schalm, O., Fredrichx, P., Schreiner, M., Vis, K. de, Mäder, M., Schryvers, D., Caen, J.,
The colour of silver stained glass - analytical investigations carried out with XRF, SEM/EDX, TEM, and IBA,
J. Anal. At. Spectrom. **17** (2002) 321

Jiraskova, Y., Brauer, G., Schneeweiss, O., Blawert, C., Anwand, W., Coleman, P.G.,
The migration of defects and nitrogen atoms in nitrided surface layers of austenitic stainless steel followed by microscopic methods,
Appl. Surf. Sci. **194** (2002) 145

Klemm, R., Thiele, E., Holste, C., Eckert, J., Schell, N.,
Thermal stability of grain structure and defects in submicrocrystalline and nanocrystalline nickel,
Scripta Materialia **46** (2002) 685

Klimenkov, M., Borany, J. von, Matz, W., Grötzschel, R., Herrmann, F.,
Formation of a single interface-near, δ-like Ge nanocluster band in thin SiO_2 films using ion-beam synthesis,

J. Appl. Phys. **91** (2002) 10062

Klimenkov, M., Borany, J. von, Matz, W., Eckert, D., Wolf, M., Müller, K.-H.,
Structure and magnetic properties of Co nanoclusters fabricated by ion beam synthesis in SiO_2 films,
Appl. Phys. **A 74** (2002) 571

Knapp, W., Bischoff, L., Teichert, J.,
Solidified Liquid Metal Ion Source – Formation of a Nanoemitter,
Vacuum **69** (2002) 345

Kögler, R., Peeva, A., Kaschny, J., Skorupa, W., Hutter, H.,
Defect engineering and prevention of impurity gettering at $R_P/2$ in ion - implanted silicon,
Solid State Phenom. **82-84** (2002) 399

Kögler, R., Peeva, A., Kaschny, J., Skorupa, W., Hutter, H.,
Prevention of impurity gettering in the $R_P/2$ region of ion-implanted silicon by defect engineering,
Nucl. Instr. Meth, **B 186** (2002) 298

Kokkoris, M., Kossionides, S., Vlastou, R., Aslanoglou, X.A., Grötzschel, R., Nsouli, B., Kuznetsov, A., Petrovic S., Paradellis, T.,
Determination of parameters for channeling of protons in SiC polytype crystals in the backscattering geometry,
Nucl. Instr. Meth. B **184** (2002) 319

Kokkoris, M., Trapalis, C.C., Kossionides, S., Vlastou, R., Nsouli, B., Grötzschel, R., Spartalis, S., Kordas, G., Paradellis, T.,
RBS and HIRBS studies of nanostructured $AgSiO_2$ sol–gel thin coatings,
Nucl. Instr. Meth. B **188** (2002) 67

Kolitsch, A., Ujvari, T., Toth, A. Mohai, M., Bertoti, I.,
XPS characterisation of the composition and bonding states of elements in CN_x layers prepared by ion beam assisted deposition,
Diam. Rel. Mat. **11** (2002) 1149

Kopcewicz, M., Jagielski, J., Matz, W.,
Thickness dependent phase transformations in implanted iron,
Hyperfine Interactions **139-140** (2002) 369

Kowalczyk, A., Jagoda, A., Mücklich, A., Matz, W., Pawlowska, M., Ratajczak, R., Turos, A.,
Electron microscopy and X-ray diffraction study of AIN layers,
Acta Phys. Pol. **102** (2002) 221

Kuriplach, J., Anwand, W., Brauer, G., Skorupa, W.,
Positron characteristics of various SiO_2 polymorphs,
Appl. Surf. Sci. **194** (2002) 84

Mair, G.L.R., Bischoff, L., Mair, A.W.R., Aidinis, C.J., Ganetsos, Th., Akhmadaliev, Ch.,
An in-depth investigation of the energy distribution of doubly-charged ions emitted from a Liquid Metal Alloy Ion Source,
J. Phys. D: Appl. Phys. **35** (2002) L 33

Mair, G.L.R., Aidinis, C.J., Bischoff, L., Ganetsos, Th.,
On the dynamics of liquid metal ion sources,
J. Phys. D: Appl. Phys. **35** (2002) 1392

Maitz, M.F., Pham, M.T., Matz, W., Reuther, H., Steiner, G.,

Promoted calcium-phosphate precipitation from solution on titanium for improved biocompatibility by ion implantation,
Surf. Coat. Techn. **158-159C** (2002) 151

Maitz, M.F., Pham, M.T., Matz, W., Reuther, H., Steiner, G., Richter, E.,
Ion beam treatment of titanium surfaces for enhancing deposition of hydroxyapatite from solution,
Biomol. Engineer. **19** (2002) 271

Markwitz, A., Matz, W., Short, K., Waldschmidt, M.,
Surface structuring and phase formation in thin metallic layers deposited at various temperatures,
Surf. Inter. Anal. **33** (2002) 1

Misochko, O.V., Georgiev, N., Dekorsy, T., Helm, M.,
Two crossovers in the pseudogap regime of $YBa_2Cu_3O_{7-x}$ superconductors observed by ultrafast spectroscopy,
Phys. Rev. Lett. **89** (2002) 067002

Misochko, O.V., Georgiev, N., Dekorsy, T., Helm, M.,
Characteristic features of the pseudogap and superconducting states of $YBa_2Cu_3O_{7-x}$,
JETP Letters **75** (2002) 642

Mukherjee, S., Reuther, H., Prokert, F., Richter, E., Möller, W.,
Substrate bias effects in plasma immersion ion implantation assisted deposition from a TiAl cathodic arc,
Surf. Coat. Technol. **160** (2002) 93

Mukherjee, S., Pham, M.-T., Maitz, M.F.,
Ti based coatings on stainless steel for bone integrated implants,
in: Siwei, Z., Zhongrong, Z., Liajun, L., Minhao, Z. (Eds.), Contributions of Surface Engineering to Modern Manufacturing and Remanufacturing, Southwest Jiaotong University Press, Chengdu, China 2002, pp. 465-468

Müller, T., Heinig, K.-H., Möller, W.,
Size and location control of Si nanocrystals at ion beam synthesis in thin SiO_2 films,
Appl. Phys. Lett. **81** (2002) 3049

Müller, T., Heinig, K.-H., Schmidt, B.,
Template-directed self-assembly of buried nanowires and the pearling instability,
Mat. Sci. Eng. C **19** (2002) 209

Nangia, A., Kim, J.H., Weiss, A.H., Brauer, G.,
Experimental determination of positron-related surface characteristics of 6H-SiC,
J. Appl. Phys. **91** (2002) 2818

Neelmeijer, C., Mäder, M.,
The merits of PIXE in revealing painting techniques,
Nucl. Instr. Meth. B **189** (2002) 293

Peeva, A., Fichtner, P.F.P., da Silva, D.L., Behar, M., Kögler, R., Skorupa, W.,
Gettering of copper in silicon at half of the projected ion range induced by helium implantation,
J. Appl. Phys. **91** (2002) 69

Peikert, M., Wieser, E., Reuter, H.,Wenzel, C.,
Enhanced thermal stability of Ta-based thin diffusion barriers by ion implantation,
Vacuum **69** (2002) 91

Persson, P.O.Å., Hultman, L., Janson, M.S., Hallén, A., Yakimova, R., Panknin, D., Skorupa, W.,
On the nature of ion implantation induced dislocation loops in 4H-silicon carbide,
J. Appl. Phys. **92** (2002) 2501

Pham, M.T., Matz, W., Reuther, H., Richter, E., Steiner, G., Oswald, S.,
Interface-mediated synthesis of hydroxyapatite,
J. Biomed. Mater. Res. **59** (2002) 254

Pham, M.T., Matz, W., Grambole, D., Herrmann, F., Reuther, H., Richter, E., Steiner, G.,
Solution deposition of hydroxyapatite on titanium pretreated with a sodium ion implantation,
J. Biomed. Mater. Res. **59** (2002) 716

Piekoszewski, J., Stanisławski, J., Grötzschel, R., Matz, W., Jagielski, J., Szymczyk, W.,
Electrode erosion mechanism in the rod plasma injector type of generator as deduced from the structure of irradiated substrates
Nukleonika **47** (2002) 113

Posselt, M., Bischoff, L., Teichert, J., Ster, A.,
Dose rate and temperature dependence of ion-beam-induced defect evolution in Si and SiC,
MRS Symp. Proc. **719** (2002) F11.2.1

Prokert, F., Noetzel, J., Schell, N., Wieser, E., Gorbunov, A.,
Effect of annealing on the interface structure of cross-beam pulsed laser deposited Co/Cu multilayers,
Thin Solid Films **416** (2002) 114

Prokert, F., Kravtsov, E., Milyaev, M., Romashev, L., Ustinov, V., Schell, N.,
Reflektivitätsuntersuchungen mittels Synchrotronstrahlung an durch MBE erzeugten Fe/Cr-Multischichten,
Zeitschrift für Kristallographie, Suppl. Issue No. **19** (2002) 58

Rebohle, L., Gebel, T., Zhao, J., Borany, J. von, Fröb, H., Borchert, D., Skorupa, W.,
Strong visible electroluminescence from Ge- and Sn-nanoclusters rich SiO_2 layers,
Mat. Sci. Eng. C **19** (2002) 373

Rebohle, L., Gebel, T., Borany, J. von, Skorupa, W., Helm, M., Pacifici, D., Franzo, G., Priolo, F.,
Transient behaviour of the strong violet electroluminescence of Ge-implanted SiO_2 layers,
Appl. Phys. B **74** (2002) 53

Rebohle, L., Borany, J. von, Fröb, H., Gebel, T., Helm, M., Skorupa, W.,
Ion beam synthesized nanoclusters for silicon-based light emission,
Nucl. Instr. Meth. B **188** (2002) 28

Revesz, A.G., Anwand, W., Brauer, G., Hughes, H.L., Skorupa, W.,
Density gradient in SiO_2 films on silicon as revealed by positron annihilation spectroscopy,
Appl. Surf. Sci. **194** (2002) 101

Reuther, H.,
Annealing behavior of magnesium and aluminum implanted with iron ions,
J. Appl. Phys. **92** (2002) 7056

Reuther, H., Behr, G.,
Determination of the hyperfine parameters of iron silicides by angle dependent conversion electron Mössbauer spectroscopy on single crystals,
Hyperfine Interactions **141-142** (2002) 435

Richter, E., Piekoszewski, J., Wieser, E., Prokert, F., Stanislawski, J., Walis, L., Reuther, H.,

Modification of titanium surface by its alloying with silicon using intense pulsed plasma beams,
Surf. Coat. Technol. **158-159** (2002) 324

Rinderknecht, J., Prinz, H., Kammler, T., Berberich, F., Zschech, E.,
In situ high temperature synchrotron radiation diffraction studies of Ni and Co-Ni silicidation processes,
Microelectr. Engineering **64** (2002) 143

Romanova, V., Begishev, V., Karmanov, V., Kondyurin, A., Maitz, M.F.,
FT-Raman and FT-IR spectra of crosslinked polyurethaneurea films synthesised from solutions,
J. Raman. Spectr. **33** (2002) 769

Safran, G., Kolitsch, A., Malhouitre, S., Trasobares, S., Kovacs, I., Geszti, O., Menyhard, M., Colliex, C., Radnoczi, G.,
Modulated CN_x films prepared by IBAD,
Diam. Rel. Mat. **11** (2002) 1552

Scheerschmidt, K., Conrad, D., Belov, A.,
Atomic processes at bonded Si-interfaces studied by molecular dynamics: tailoring densities and band gaps?
Comp. Mat. Sci. **24** (2002) 35

Schell, N., Matz, W., Bøttiger, Chevallier, J., Kringhøj, P.,
Development of texture in TiN films by use of in situ synchrotron x-ray scattering,
J. Appl. Phys. **91** (2002) 2037

Schell, N., Bøttiger, J., Matz, W., Chevallier, J., Petersen, J., Andreasen, K.P., Jensen, T.,
New possibilities of characterizing growing sputter-deposited thin films,
Proc. 9th Annual International Conference on Composite Engineering (ICCE/9) in San Diego, CA, July 1-6, 2002, ed. Hui, D., p. 697-698

Schmidt, B., Grambole, D., Herrmann, F.,
Impact of ambient atmosphere on as-implanted amorphous insulating layers,
Nucl. Instr. Meth. B **191** (2002) 482

Schütze, M., Schumacher, G., Dettenwanger, F., Hornauer, U., Richter, E., Wieser, E., Möller, W.,
The halogen effect in the oxidation of intermetallic titanium aluminides,
Corrosion Science **44** (2002) 303

Sendezera, E.J., Davidson, A.T., Jili, P.T., Chithambo, M.L., Anwand, W., Brauer, G., Nicht, E.-M.,
Characterisation of defects in LiF implanted with Ar^+ using variable energy positron beam,
Nucl. Instr. Meth. B **192** (2002) 202

Shevchenko, N., Rogozin, A., Matz, W., Günzel, R.,
Features of structure formation of TiN coatings obtained by Plasma Immersion Ion Implantation assisted deposition,
Proc. 6th Intern. Conf. on Modification of Materials with Particle Beams and Plasma Flows, Tomsk, Russia, September 23-28, 2002, pp. 540-543

Silva, D.L. da, Fichtner, P.F.P., Behar, M., Peeva, A., Kögler, R., Skorupa, W.,
Implantation temperature dependence of He bubble formation in Si,
Nucl. Instr. Meth. B **190** (2002) 756

Stanislawski, J., Piekoszewski, J., Richter, E., Werner, Z.,
An apparatus for sequential pulsed plasma beam treatment in combination with Arc PVC deposition,
Nukleonika **47** (2002) 119

Theodossiu, E., Baumann, H., Matz, W., Mücklich, A.,
Ion beam synthesis and characterization of crystalline Si_3N_4 surface layers,
Phys. Stat. Sol. (a) **194** (2002) 47

Thiele, E., Bretschneider, J., Buque. C., Schell, N., Schwab, A., Holste, C.,
Internal strains in single grains of fatigued polycrystalline nickel,
Mat. Sci. Forum **404-407** (2002) 823

Travlos, A., Boukos, N., Apostolopoulos, G., Aidinis C.J., Bischoff, L.,
Epitaxial erbium silicide on Ge^+ implanted silicon,
Nucl. Instr. Meth. B **196** (2002) 174

Tsyganov, I., Wieser, E., Matz, W., Reuther, H., Richter, E.,
Modification of the Ti-6Al-4V alloy by ion implantation of calcium and/or phosphorus,
Surf. Coat. Technol. **158-159** (2002) 318

Ulyashin, A., Job, R., Fahrner, W.R., Grambole, D., Herrmann, F.,
Hydrogen redistribution and void formation in hydrogen plasma treated Czochralski silicon,
Solid State Phenom. **82-84** (2002) 315

Ulyashin, A., Job, R., Fahrner, W. R., Richard, O., Bender, H., Claeys, C., Simoen, E., Grambole, D.,
Substrate orientation, doping and plasma frequency dependencies of structural defect formation in hydrogen plasma treated silicon,
J. Phys. Cond. Matter **14** (2002) 13037

Vinnichenko, M., Chevolleau, T., Pham, M.T., Poperenko, L., Maitz, M.F.,
Spectroellipsometric, AFM and XPS probing of stainless steel surface subjected to biological influences,
Appl. Surf. Sci. **201** (2002) 41

Wang, T., Eichhorn, F., Grambole, D., Grötzschel, R., Herrmann, F., Kreissig, U., Möller, W.,
A new Ti/H phase transformation in the H_2^+ implanted titanium alloy studied by X-ray diffraction, nuclear reaction analysis, elastic recoil detection analysis and scanning electron microscopy,
J. Phys. Cond. Matter **14** (2002) 11605

Wang, T., Grambole, D., Grötzschel, R., Herrmann, F., Kreißig, U., Eichhorn, F., Brauer, G., Möller, W.,
Mobility and retention of implanted hydrogen in Ti225 titanium alloy,
Surf. Coat Technol. **158-159** (2002) 139

Warchoł, S., Rzewuski, H., Krynicki, J., Grötzschel, R.,
Angular dependence of post-implantation damage recovery under 1 MeV electron irradiation in GaAs,
Nukleonika **47** (2002) 19

Wei, P., Barradas, N.P., Soares, J.C., da Silva, M.F., Kreissig, U., Cardoso, S., Freitas, P.P.,
Composition analysis of the insulating barrier in magnetic tunnel junctions by grazing angle of incidence RBS,
Nucl. Instr. Meth. B **190** (2002) 684

Weima, J.A., Borany, J. von, Grötzschel, R., Fahrner, W.R.,
Investigating contaminants on thermochemically refined surfaces of chemical vapor deposited diamond films,
J. Electrochem. Soc. **149** (2002) G30

Weima, J.A., Borany, J. von, Meusingen, K., Horstmann, J., Fahrner, W.R.,
Double injection of charge carriers in chemical vapor deposited diamond-based diodes,

J. Appl. Phys. **92** (2002) 4047

Werner, Z., Piekoszewski, J., Szymczyk, W., Bonilla, F.A., Ong, T.S., Skeldon, P., Thompson, S.G., Zielinski, E., Chmielewski, A., Grötzschel, R., Stanisławski, J.,
Palladium profiles in titanium treated by high-intensity plasma pulses,
Surf. Coat. Technol. **158-159** (2002) 21

Wielunski, L.S., Grambole, D., Kreissig, U., Grötzschel, R., Harding, G., Szilagyi, E.,
Hydrogen depth resolution in multilayer metal structures, comparison of elastic recoil detection and resonant nuclear reaction method,
Nucl. Instr. Meth. B **190** (2002) 693

Wieser, E., Peikert, M., Wenzel, C., Schreiber, J., Bartha, J.W., Bendjus, B., Melov, V.V., Reuther, H., Mücklich, A., Adolphi, B., Fischer, D.,
Improvement of Ta-based thin film barriers on copper by ion implantation of nitrogen and oxygen,
Thin Solid Films **410** (2002) 121

Wieser, E., Reuther, H., Prokert, F., Gorbunov, A., Tselev, A., Pompe, W., Levin, A.A., Meyer, D.C., Paufler, P.,
Structural and magnetic phase transformation in metastable Fe-Cr alloys induced by ion irradiation,
J. Appl. Phys. **92** (2002) 572

Zechner, C., Matveev, D., Erlebach, A., Simeonov, S., Menialenko, V., Mickevicius, R., Foad, M., Al-Bayati, A., Lebedev, A., Posselt, M.,
TCAD calibration of USJ profiles for advanced deep sub-µm CMOS processes,
Nucl. Instr. Meth. B **186** (2002) 303

Zhao, J., Rebohle, L., Gebel, T., Borany, J. von, Skorupa, W.,
Bulk-limited conduction of Ge-implanted thermally grown SiO_2 layers,
Solid State Electron. **46** (2002) 661

Zolnai, Z., Khánh, N.Q., Szilágyi, E., Kótai, E., Ster, A., Posselt, M., Lohner, T., Gyulai, J.,
Investigation of ion implantation induced damage in the carbon and silicon sublattices of 6H-SiC,
Diam. Rel. Mat. **11** (2002) 1239

Invited Talks

Belov, A.Yu., Jäger, H.U.,
Simulation of the non-equilibrium processes for tetrahedral amorphous carbon: deposition and structural relaxation,
6th Int. Conf. on Computer Simulation of Radiation Effects in Solids (COSIRES 2002), Dresden, Germany, July 23-27, 2002

Bischoff, L.,
Alternative Liquid Metal Ion Sources,
Workshop „Focused Ion Beam Technique and Cross Beam System Leo XB 1540“, IFW Dresden, May 13–16, 2002

Bischoff, L.,
Application of mass separated focused ion beams,
IV Int. Symp.on Ion Implantation and other Applications of Ions and Electrons, ION 2002, Kazimierz Dolny, Poland, June 10 – 13, 2002

Brauer, G., Anwand, W., Skorupa, W., Revesz, A.G., Kuriplach, J.,

Int. Workshop on the Effect of Ions in Layer Growth, Balatonvilagos, Hungary, Sept 9-12, 2002

Schell, N., Bøttiger, J., Matz, W., Chevallier, J., Petersen, J., Andreasen, K.P., Jensen, T.,
New possibilities of characterizing growing sputter-deposited thin films,
9th Annual Int. Conf. on Composite Engineering (ICCE/9), San Diego, CA, USA, July 1-6, 2002

Skorupa, W.,
Defect engineering and gettering by ion implantation,
Workshop on „Semiconductor Defect Engineering: Progress and Prospects“, Orleans, France, March 14-15, 2002

Skorupa, W.,
Ion beam synthesis of nanocluster-rich SiO_2-layers: from microstructure to electrooptical applications,
IV. Int. Symp. on Ion Implantation and Other Application of Ions and Electrons "ION 2002", Kazimierz Dolny, Poland, June 10-13, 2002

Skorupa, W., Gebel, T., Rebohle, L., Helm, M.,
Nanocluster-rich SiO_2-layers produced by ion beam synthesis: electrical and optical properties,
Int. Workshop on "Effect of ions in layer growth", Balatonvilágos, Hungary, Sept 9-11, 2002

Conference Contributions

Abendroth, B., Gago, R., Kolitsch, A., Möller, W.,
In situ stress measurement and relaxation during magnetron deposition of cBN,
9. cBN Expertentreffen, Bonn, Oct 9-11, 2002

Akhmadaliev, Ch., Bischoff, L.,
Investigation of elastic wave generation in a solid target by a pulsed ion beam,
DPG Tagung, Regensburg, March 11 – 15, 2002

Akhmadaliev, Ch., Bischoff, L.,
Analysis of microstructures using the ion-acoustic effect,
E-MRS Spring Meeting, Strasbourg, France, June 18 – 21, 2002

Anwand, W., Brauer, G., Skorupa, W.,
Al^+ implantation into epitaxial 6H-SiC: evolution of vacancy-type damage influenced by the substrate temperature,
Europ. Conf. on Silicon Carbide and Related Materials (ECSCRM2002), Linköping, Sweden, Sept 1-5, 2002

Arazi, A., Faestermann, T., Fenandez Niello, J., Knie, K., Korschinek, G., Richter, E., Rugel, G., Wallner, A.,
AMS measurements of the $^{25}Mg(p,\gamma)^{26}Al$ reaction at stellar energies,
XXIV Brazilian Workshop on Nuclear Physics, Sao Pablo, Brasil, Aug 31 – Sept 4, 2002,
Int. Conf. on Applications of High Precision Atomic & Nuclear Methods, Neptun, Romania, Sept 2-5, 2002,
9th Accelerator Mass Spectroscopy Conference, Nagoya, Japan, Sept 9-13, 2002

Ayache, R., Bouabellou, A., Richter, E.,Möller, W.,
Synthesis of ß-$FeSi_2$ by ion beam implantation,
Cinquieme Congres National de la Physique et de ses Application, Batna, Algerie, Oct 28-30, 2002

Azzaroni, O., Schilardi, P.L., Gago, R., Vázquez, L., Salvarezza, R.C.,

Direct fabrication of ordered polymer nanocavity arrays from surface-modified ion-nanostructured silicon templates,
35th IUVSTA Workshop on Pattern Formation and Atomic Processes in Epitaxial Growth and Ion Erosion, Trofaiach, Austria, June 9-13,2002

Beckers, M., Schell, N., Möller, W.,
In-situ growth characterization of magnetron sputtered thin films by synchrotron radiation,
36th IUVSTA Workshop on the Mechanisms of Formation and Applications of Hard Nanostructured Coatings, Plzen, Czech Republic, Oct 20-24, 2002

Belko, V., Posselt, M., Chagarov, E.,
Improvement of the repulsive part of the classical interatomic potential for SiC,
6th Int. Conf. on Computer Simulation of Radiation Effects in Solids (COSIRES 2002), Dresden, Germany, June 23-27, 2002

Belov, A.Yu., Jäger, H.U.,
Atomistic study of ion beam deposition conditions for hard amorphous carbon,
E-MRS Spring Meeting, Strasbourg, France, June 18-21, 2002

Belov, A.Yu.,
Atomic scale simulation of the stress relief in tetrahedral amorphous carbon,
E-MRS Spring Meeting, Strasbourg, France, June 18-21, 2002

Berberich, F., Matz, W., Kreißig, U., Schell, N., Mücklich, A.,
Mechanism of degradation of surface hardening at elevated temperature in TiAlV-alloys by in situ synchrotron radiation diffraction,
3rd Int. Conf. on Synchrotron Radiation in Materials Science (SRMS-3), Singapore, Jan 21-24, 2002

Bernas, H., Halley, D., Heinig, K.-H., Attané, J.P., Marty, A., Auric, P., Ravelosona, D., Chappert, C., Samson, Y.,
Tailoring magnetic nanostructures by ion irradiation,
Int. Workshop on Nanostructures for Electronics and Optics (NEOP), Dresden, Germany, Oct 6–9, 2002

Beyer, R., Beyreuther, E., Borany, J. von, Weber, J.,
A study of the charge storage in Si-implanted oxide layers using scanning probe techniques,
Int. Workshop on Nanostructures for Electronics and Optics (NEOP), Dresden, Germany, Oct 6-9, 2002

Beyer, V., Müller, T., Borany, J. von, Heinig, K.-H.,
Ion beam sythesized Au nanocrystals in ultra-thin SiO_2,
E-MRS Spring Meeting, Strasbourg, France, June 18-21, 2002

Beyer, V., Müller, T., Borany, J. von, Heinig, K.-H.,
Charge storage behavior of ion beam synthesized Au nanocrystals,
Intern. Workshop on Nanostructures for Electronics and Optics (NEOP), Dresden, Germany, Oct 6-9, 2002

Bischoff, L., Schmidt, B., Heinig, K.-H., Müller, T., Hellwig, S.,
Plasmonic structures fabricated by focused ion beams,
Int. Workshop on Nanostructures for Electronics and Optics (NEOP), Dresden, Germany, Oct 6-9, 2002

Borany, J. von, Beyer, D., Beyer, V., Schmidt, B., Schnabel, B.,
A novel silicon detector for energetic electrons with improved linearity characteristics,
Int. Conf. on Micro- and Nanoengineering 2002 (MNE 2002), Lugano, Switzerland, Sept 26-19, 2002

Borany, J. von, Schmidt, B., Heinig, K.-H., Mücklich, A., Grambole, D.,
Technological challenges for the ion beam synthesis of semiconductor nanoclusters in thin gate dielectrics,
14th Int. Conf. on Ion Implantation Technology (IIT 2002), Taos, NM, USA, Sept 22-27, 2002

Borodin, V.A., Heinig, K.-H.,
Thermally activated nanocluster evolution in reactive environment,
Int. Workshop on Nanostructures for Electronics and Optics (NEOP), Dresden, Germany, Oct 6–9, 2002

Camero, M., Gago, R., Gómez-Aleixandre, C., Albella, J.M.,
Hydrogen incorporation on CNx films deposited by ECR Chemical Vapor Deposition,
13th Europ. Conf. on Diamond, Diamond-like Materials, Carbon Nanotubes, Nitrides and Silicon Carbide, Granada, Spain, Sept 8-13, 2002

Cieslak, J., Dubiel, S.M., Zukrowski, J., Reuther, H.,
CEMS evidence on the presurface zone enhancement of the spin-density in chromium,
5nd Seeheim Workshop on Mössbauer Spectroscopy, Seeheim, May 21-26, 2002

Cizek, J., Kirchheim, R., Pundt, A., Brauer, G., Anwand, W.,
Use of slow positron implantation spectroscopy as a tool for investigation of hydrogen loaded Nb films,
9th TMR Workshop Switchable Metal-hydride Films, Mallorca, Spain, Feb 16-22, 2002

Cizek, J., Prochazka, I., Kuzel, R., Cieslar, M., Stulikova, I., Brauer, G., Anwand, W., Islamgaliev, R.K.,
Defect studies of ultra fine grained metals, prepared by severe plastic deformation, by means of positron annihilation spectroscopy,
National Conference „Nano 02“, Brno, Czech Republic, Nov 19-21, 2002

Cizek, J., Prochazka, I., Brauer, G., Anwand, W., Kuzel, R., Cieslar, M., Islamgaliev, R.K.,
Ultra-fine grained copper prepared by high pressure torsion: spatial distribution of defects,
2nd Int. Conf.on Nanomaterials by Severe Plastic Deformation: Fundamentals - Processing - Applications, Vienna, Austria, Dec 9-13, 2002

Cizek, J., Prochazka, I., Brauer, G., Anwand, W., Kuzel, R., Cieslar, M., Islamgaliev, R.K.,
Lateral and depth distribution of defects in ultra fine grained copper prepared by high pressure torsion,
2nd Workshop on Nanomaterials: Fundamentals and Applications, Sevilla, Spain, Oct 3-4, 2002

Dekorsy T., Georgiev N., Helm M., Misochko O.V.,
Observation of a hysteretic pseudogap behavior via coherent phonons in high temperature superconductors,
13th Conference on Ultrafast Phenomena, Vancouver, Canada, May 12-17, 2002

Dekorsy, T.,
IR spectroscopic possibilities with the Rossendorf free-electron laser,
1st Workshop on High Magnetic Fields, Dresden, June 21-22, 2002

Dvurechenskii, A.V. Grötzschel, R., Smagina, Zh., Zinovev, V.A., Novikov, P., Tyes, S.A.,
Ge/Si nanostructures with quantum dots grown by ion-beam assisted heteroepitaxy,
2nd Int. Workshop on Nucleation and Non-Linear Problems in First-Order Phase Transitions, St. Petersburg, Russia, July 1-5, 2002

Eichhorn, F., Schell, N., Mücklich, A., Kögler, R., Matz, W.,

Structural studies of heteroepitaxial SiC formed by ion beam synthesis in Si,
3rd Int. Conf. on Synchrotron Radiation in Materials Science (SRMS-3), Singapore, Jan 21-24, 2002

Eichhorn, F., Heera, V., Weishart, H., Schell, N.,
Structural studies of ion beam synthesized nanocrystals: diamond in SiC and SiC in diamond,
6th Biennial Conf. on High-Resolution X-Ray Diffraction and Imaging (X-TOP 2002), Grenoble – Aussois, Frankreich, Sept 10-14, 2002

Facsko, S., Bobek, T., Teichert, C., Dekorsy, T., Kurz, H.,
Evolution of nanostructures during low-energy ion-sputtering of semiconductors,
35th IUVSTA Workshop on Pattern Formation and Atomic Processes in Epitaxial Growth and Ion Erosion, Trofaiach, Austria, June 9-13, 2002

Facsko, S., Bobek, T., Teichert, C., Dekorsy, T., Kurz, H.,
Evolution of nanostructures during low-energy ion-sputtering,
Int. Workshop on Nanostructures for Electronics and Optics (NEOP), Dresden, Germany, Oct 6-9, 2002

Fitting, H.-J., Trukhin, A. N., Barfels, T., Schmidt, B., Czarnowski, A. von,
Radiation induced defects in SiO_2*,*
9th Europhysical Conference on Defects in Insulating Materials EURODIM 2002, Wroclaw, Poland, June 30 - July 5, 2002

Först, M., Kurz, H., Dekorsy, T., Leavitt, R. P.,
Coupled Bloch-phonon oscillations in biased InGaAs/InAlAs superlattices,
Quantum Electronics and Laser Sciences Conference (QELS) 2002, Long Beach, California, USA, May 19-24, 2002

Friedrich, M., Pilz, W., Bekris, N., Glugla, M., Kiisk, M., Liechtenstein, V.,
A small and compact AMS facility for tritium depth profiling,
9th Int. Conference on Heavy Ion Accelerator Technology (HIAT-9), New Delhi, India, Jan. 14-18, 2002
9th Int. Conf. on Accelerator Mass Spectrometry (AMS-9), Nagoya, Japan, Sept. 9-13, 2002

Fritsche, B., Kolitsch, A., Möller, W.,
The role of hydrogen incorporation into hBN/cBN layered thin films,
13th Europ. Conf. on Diamond, Diamond-like Materials, Carbon Nanotubes, Nitrides and Silicon Carbide, Granada, Spain, Sept 8-13, 2002

Fritsche, B., Chevolleau, T., Kolitsch, A., Möller, W.,
Charakterisierung einer RF Ar/N_2 *Magnetron Entladung zur Abscheidung von cBN,*
X. Erfahrungsaustausch Oberflächentechnologie mit Plasma- und Ionenstrahlprozessen, Mühlleiten, March 18-21, 2002

Fromknecht, R., Linker, G., Wang, L. M., Zhu, S., Sun, K., van Veen, A., van Hius, M., Niemeyer, J., Weimann, T., Wang, J., Eichhorn, F., Wang, T.,
Forming of Au-nanocrystals and diffusion effects in ion implanted TiO_2 *single crystals,*
German-Chinese Workshop 2002 "Nanoscience", Karlsruhe, Germany, July 1-4, 2002

Gago, R., Kolitsch, A., Möller, W.,
Deposition of thick cubic boron nitride thin films by dual ion beam deposition,
13th Europ. Conf. on Diamond, Diamond-like Materials, Carbon Nanotubes, Nitrides and Silicon Carbide, Granada, Spain, Sept 8-13, 2002

Gago, R., Vázquez, L., Varela, M., Ballesteros, C., Cuerno, R., Albella, J.M.,
Temperature studies on the formation of silicon nanodots by low energy ion beam sputtering,

35th IUVSTA Workshop on Pattern Formation and Atomic Processes in Epitaxial Growth and Ion Erosion, Trofaiach, Austria, June 9-13, 2002

Gago, R., Kolitsch, A., Möller, W.,
On the production of fullerene-like carbon nitride thin films by Ion Beam Assisted Deposition,
MRS Fall Meeting, Boston, USA, Dec 2-6, 2002

Gebel, T., Voelskow, M., Skorupa, W., Mannino, G., Privitera, V., Priolo, F., Napolitani, E., Carnera, A.,
Millisecond pulse annealing of ultra-shallow boron profiles in silicon by flash lamp annealing,
MRS Spring Meeting, San Francisco, USA, April 1-5, 2002

Gebel, T., Rebohle, L., Skorupa, W.,
Lichtemitter-Arrays in Si-Technologie für Lab-on-Chip Anwendungen,
FUTOUR Gründerkongress, Berlin, April 24-25, 2002

Gebel, T., Rebohle, L., Skorupa, W.,
Anwendung nanoclusterreicher SiO_2 Schichten in der Optoelektronik,
BMBF Fachkongress "NanoDE", Bonn, Germany, May 6-7, 2002

Gebel, T., Rebohle, L., Sun, J., Skorupa, W., Nazarov, A.N., Osiyuk, I.N.,
Correlation of charge trapping and electroluminescence in highly efficient Si-based light emitters,
E-MRS Spring Meeting, Strasbourg, France, June 17-21, 2002

Gebel, T., Voelskow, M., Eichhorn, F., Skorupa, W., Mannino, G., Privitera, V., Priolo, F., Napolitani, E., Carnera, A.,
Flash-lamp processing with millisecond pulses for ultra-shallow boron implants in silicon,
14th Int. Conf. on Ion Implantation Technology (IIT 2002), Taos, USA, Sept 22-27, 2002

Gebel, T., Sun, J., Skorupa, W., Rebohle, L., Nazarov, A.N., Osiyuk, I.,
Ion beam synthesized nanostructures in SiO_2 layers: Effects of charge trapping and electroluminescence,
Int. Workshop on Nanostructures for Electronics and Optics (NEOP), Dresden, Germany, Oct 6-9, 2002

Gebel, T., Rebohle, L., Skorupa, W.,
Optoelectronic properties of group-IV-ion implanted SiO_2 layers,
EUREKA Meeting, Kiev (Ukaine), Nov 5-6, 2002

Gebel, T., Trautmann, T., Skorupa, W., Privitera, V., Priolo, F., Napolitani, E.,
Flash-lamp annealing with millisecond pulses for the treatment of ultra-shallow junctions and heteroepitaxial layers,
Deutsche RTP-Nutzertagung, Erlangen, Germany, Nov 7, 2002

Georgiev N., Mozume T., Asakawa A., Yoshida H., Neogi A., Wada O., Akiyama T.,
Structural and optical characterization of MBE-grown InGaAs/AlAsSb quantum wells with large intersubband energies,
Int. Workshop on Light Emitters Based on Intersubband Transitions, Berlin, Feb 15-18, 2002

Georgiev N., Semtsiv M., Dekorsy T., Eichhorn F., Bauer A., Helm M., Masselink, T.,
Intersubband transitions in strain compensated $In_xGa_{1-x}As/AlAs$ quantum well structures grown on InP substrates,
29th Int. Symp. on Compound Semiconductors 2002, Lausanne, Switzerland, Oct 7-10, 2002

Gorbunov, A., Levin, A.A., Wieser, E., Bischoff, L., Eckert, D., Mensch, A., Mertig, M., Meyer, D.C., Reuther, H., Paufler, P., Pompe, W.,

Formation and decomposition of laser-deposited metastable Fe-Cr phases,
IQEC/LAT 2002, Int. Quantum Electronics Conference 2002/Conf. on Lasers, Applications and Technologies 2002, Moscow, Russia, June 22-28, 2002

Grambole, D., Wang, T., Herrmann, F., Eichhorn, F.,
Diffusion of hydrogen in titanium due to bending stress studied by micro ERDA,
8th Int. Conf. on Nuclear Microprobe Technology and Applications (ICNMTA2002), Takasaki, Japan, Sept 8-13, 2002

Guo, B. N., Variam, N., Jeong, U., Mehta, S., Posselt, M., Lebedev, A.,
Experimental and simulation studies of the channeling phenomena for high-energy implantation,
14th Int. Conf. on Ion Implantation Technology (IIT2002), Taos, USA, Sept 22-27, 2002

Guo, B.N., Variam, N., Jeong, U., Mehta, S., Posselt, M., Lebedev, A.,
Channeling doping profiles studies for small incident angle implantation into silicon wafers,
17th Int. Conf. on the Application of Accelerators in Research and Industry (CAARI 2002), Denton, USA, Nov 12-16, 2002

Heera, V.,
Elektrische Eigenschaften von nanokristallinem SiC,
1. Deutsches Arbeitskreistreffen Siliziumkarbid, Paderborn, June 24-25, 2002

Heera, V., Madhusoodanan, K.N., Mücklich, A., Skorupa, W.,
Nanocrystalline SiC layers produced by ion beam induced crystallisation-morphology and resistivity,
13th Europ.Conf. on Diamond, Diamond-Like Materials, Carbon Nanotubes, Nitrides and Silicon Carbide, Granada, Spain, Sept 8-13, 2002

Heera, V., Madhusoodanan, K.N., Mücklich, A., Skorupa, W.,
Nanocrystalline SiC layers produced by ion-beam-induced crystallization - morphology and resistivity
Europ. Conf. on Silicon Carbide and Related Materials (ECSCRM 2002), Linköping, Sweden, Sept 1-5, 2002

Heera, V., Madhusoodanan, K.N. Mücklich, A., Panknin, D., Skorupa, W.,
Improved p-type conductivity in heavily, Al-doped SiC by ion beam induced nano-crystallization,
Europ. Conf. on Silicon Carbide and Related Materials (ECSCRM 2002), Linköping, Sweden, Sept 1-5, 2002

Heinig, K.-H., Schmidt, B., Borany, J. von, Stegemann, K.-H., Müller, T.,
Nanocrystals in gate oxides by ion beam synthesis – Fundamentals and applications in non-volatile memories,
E-MRS Spring Meeting, Strasbourg, France, June 18-21, 2002

Heitmann, J., Kovalev, D., Schmidt, M., Yi, L. X., Scholz, R., Eichhorn, F., Zacharias, M.,
Synthesis and size-control of Si nanocrystals by SiO/SiO_2 superlattices and Er doping,
MRS Fall Meeting, Boston, USA, Dec 2-6, 2002

Jäger, H.U.,
a-C growth simulations by molecular dynamics,
Linköping - Rossendorf Thin Film Meeting, Dresden, Germany, June 11, 2002

Jiménez, I., Gago, R., Albella, J.M.,
Fine structure at the x-ray absorption p and s* bands of amorphous carbon: distorted trigonal and tetragonal bonding?*
4th Specialist Meeting on Amorphous Carbon (SMAC 2002), Barcelona (Spain), Sept 5-6, 2002

Jiménez, I., Gago, R., Caretti, I., Albella, J.M.,

X-ray absorption studies of the bonding structure of B-C-N compounds,
13th Europ. Conf. on Diamond, Diamond-like Materials, Carbon Nanotubes, Nitrides and Silicon Carbide, Granada, Spain, Sept 8-13, 2002

Kiryanov, S.A., Sidorenko, A.F., Babanov, Yu.A., Ryazhkin, A.V, Romashev, L.N., Patselov, A.M., Reich, T., Funke, H., Prokert, F., Schell, N.,
Anomalous X-ray scattering and EXAFS study in the determination of the short range order of the solid state solution $Fe_{78.4}Cr_{21.6}$*,*
XIV. Russian Synchrotron Radiation Conference, SR-2002, Novosibirsk, Russia, July 15-19, 2002

Kögler, R., Eichhorn, F., Kaschny, J.R., Mücklich, A., Reuther, H., Skorupa, W.,
Synthesis of nano-sized SiC precipitates in Si by simultaneous dual ion implantation of C^+ *and* Si^+ *ions,*
Workshop on „Semiconductor Defect Engineering: Progress and Prospects“, Orleans, France, March 14-15, 2002

Kögler, R., Eichhorn, F., Kaschny, J.R., Mücklich, A., Reuther, H., Skorupa, W., Lindner, J.K.N.,
Synthesis of SiC by simultaneous dual ion implantation into silicon,
13th Int. Conf. on Ion Beam Modification of Materials (IBMM 2002), Kobe, Japan, Sept 1-6, 2002

Kolitsch, A., Möller, W.,
AIM - An European Large-Scale Facility of Ion Beam Technologies,
12th General Conference of the European Physical Society (EPS-12), "Trends in Physics", Budapest, Hungary, Aug 26-30, 2002

Leitenberger, W., Wendrock, H., Bischoff, L., Panzer, T., Pietsch, U., Grenzer J., Pucher, A.,
Double pinhole diffraction of white synchrotron radiation,
7th Int. Conf. on Surface X-Ray and Neutron Scattering, Lake Tahoe, California, USA, Sept 23-27, 2002

Leitenberger, W., Wendrock, H., Bischoff, L., Pietsch, U., Panzer, T., Grenzer, J.,
Hard X-ray spatial coherence measurements using a double slit interference,
Workshop on Exploiting the Coherence of X-rays, Motzen, Germany, Sept 23 – 24, 2002

Mäder, M., Neelmeijer, C.,
Ionenstrahlanalyse - ideal zur Charakterisierung historischer Gläser,
DPG Frühjahrstagung, Regensburg, March 11-15, 2002

Maitz, M.F., Mukherjee, S., Pham, M.T., Richter, E.,
Deposition of Ti based coatings with different surface structure and chemistry for medical devices,
EMRS Spring Meeting, Strasbourg, France, June 18–21, 2002

Mazur, K., Sass, J., Kowalik, A., Eichhorn, F., Gladki, A.,
Characterization of lateral surface nanostructures on GaAs by X-ray diffraction,
2nd Seminar of Bruker axs and Bruker-Nonius, Krynica Gorska, Poland, Sept 22-24, 2002

Mukherjee, S., Pham, M.-T., Maitz, M.F.,
Ti based coatings on stainless steel for bone integrated implants,
ICSE, 3rd Int. Conf. on Surface Engineering, Chengdu, China, Oct 10-13, 2002

Müller, T., Heinig, K.-H., Möller, W.,
Nanocluster formation by phase separation in ultra-thin ion implanted gate oxides,
E-MRS Spring Meeting, Strasbourg, France, June 18–21, 2002

Müller, T., Heinig, K.-H.,

Regular chains of nanocrystals fabricated from nanowires – predictions based on kinetic MC simulations,
E-MRS Spring Meeting, Strasbourg, France, June 18–21, 2002

Müller, T., Heinig, K.-H., Möller, W.,
Nanocluster synthesis by high-fluence ion implantation in thin films studied by MC simulations,
6th Int. Conf. on Computer Simulation of Radiation Effects in Solids (COSIRES 2002), Dresden, Germany, June 23-27, 2002

Müller, T., Heinig, K.-H., Möller, W.,
Size and location control of Si nanocrystals at ion beam synthesis in thin gate oxides,
Int. Workshop on Nanostructures for Electronics and Optics (NEOP), Dresden, Germany, Oct 6–9, 2002

Nageswara Rao, S. V. S., Lakshmi, G. B. V. S., Pathak, A. P., Srivastava, S. K., Siddiqui, A. M., Avasthi, D. K., Srinivasan, T., Tiwari, U., Mehta, S. K., Muralidharan, R., Jain, R. K., Eichhorn, F., Grötzschel, R., Schell, N.,
Ion beam irradiation effects on the strains in GaAs/InGaAs layers,
Int. Conf. on Physics of Solids and Surfaces, Puri, India, March, 2002

Neelmeijer, C., Mäder, M.,
Endangered glass objects identified by ion beam analysis,
7th Int. Conf. on Non-destructive Testing and Microanalysis for the Diagnostics and Conservation of the Cultural and Environmental Heritage (Art2002), Antwerpen, Belgien, June 2-6, 2002

Neidhardt, J., Hultman, L., Fritsche, B., Gago, R., Möller, W.,
Plasma analysis of a DC sputtering discharge in an N_2/Ar atmosphere for the deposition of fullerene like carbon nitride,
Int. Conf. on Metallurgical Coatings and Thin Films - ICMCTF 2002, San Diego, USA, April 22-26, 2002

Neumaier, P., Dollinger, G., Bergmaier, A., Ronning, C., Hofsäss, H., Jäger, H.U.,
Range distributions of low-energy carbon ions in tetrahedral amorphous carbon thin films,
13th Europ. Conf. on Diamond, Diamond-Like Materials, Carbon Nanotubes, Nitrides and Silicon Carbide (DIAMOND 2002), Granada, Spain, Sept 8-13, 2002

Novikov, P., Heinig, K.-H., Larsen, A.N., Dvurechenskii, A.,
Tunnel oxide morphology in Ge nanocluster-based non-volatile memories,
Int. Workshop on Nanostructures for Electronics and Optics (NEOP), Dresden, Germany, Oct 6–9, 2002

Ovchinnikov, V.V., Goloborodski, B.Yu., Gushchina, N.V., Chemerinskaya, L.S., Semionkin, V.A., Wieser, E., Möller, W.,
Investigation of the effect of irradiation with gaseous and metallic ions on the atomic structure of the alloy Fe+15 at.% Cr,
III Int. Scientific Conf. “Radiation Thermal Effects and Processing in Inorganic Materials”, Tomsk, Russia, July 29 – Aug 3, 2002

Pathak, A.P., Siddiqui, A.M., Srivastava, S.K., Avasthi, D.K., Eichhorn, F., Grötzschel, R., Schell, N., Turos, A.,
Ion beam studies of strains/defects in semiconductor multilayers,
17th Int. Conf. on the Application of Accelerators in Research and Industry (CAARI 2002), Denton, Texas, USA, Nov 12-16, 2002

Peeva, A., Kaschny, J., Kögler, R., Skorupa, W.,
Interaction between Si-Interstitial and Helium-implantation related defects for cavity stabilisation,

MRS Spring Meeting, San Francisco, USA, April 1-5, 2002

Peeva, A., Kögler, R., Skorupa, W.,
Visualisation of vacancy type defects in the $R_P/2$ region of ion implanted and annealed silicon,
13th Int. Conf. on Ion Beam Modification of Materials (IBMM 2002), Kobe, Japan, Sept 1-6, 2002

Piekoszewski, J., Krajewski, A., Prokert, F., Stanislawski, J., Walis, L., Werner, Z., Wlosilski, W.,
Brazing of alumina ceramics modified by pulsed plasma beams combined with Arc PVD treatment,
IV Int. Symp. on Ion Implantation and other Application of Ions and Electrons (ION 2002), Kazimierz Dolny, June 10-13, 2002

Posselt, M., Belko, V.,
Molecular dynamics study of atomic displacements and subsequent lattice relaxation in 3C- and 4H-SiC,
Europ. Conf. on Silicon Carbide and Related Materials (ECSCRM 2002), Linköping, Sweden, Sept 1-5, 2002

Posselt, M., Bischoff, L., Teichert, J., Ster, A.,
Dose rate and temperature dependence of ion-beam-induced defect evolution in Si and SiC studied by channeling implantation,
MRS Spring Meeting, San Francisco, California, USA, April 1-5, 2002

Posselt, M., Gao, F., Belko, V., Weber, W. J.,
Structure and energetics of elementary defects in 4H-SiC,
6th Int. Conf. on Computer Simulation of Radiation Effects in Solids (COSIRES 2002), Dresden, Germany, June 23-27, 2002

Prokert, F., Kravtsov, E., Milyaev, M., Romashev, L., Ustinov, V., Schell, N.,
Reflektivitätsuntersuchungen mittels Synchrotronstrahlung an durch MBE erzeugten Fe/Cr-Multischichten,
DGK-Tagung, March 4-7, 2002

Prokert, F., Schell, N., Gorbunov, A.,
Use of anomalous scattering for synchrotron x-ray reflectivity studies of Fe-Cr and Co-Cu double layers,
3rd Int. Conf. on Synchrotron Radiation in Materials Science (SRMS-3), Singapore, Jan 21-24, 2002

Rebohle, L., Gebel. T., Skorupa, W., Helm, M.,
Si based light emission from ion beam synthesized nanostructures in thin SiO_2 layers,
Int. Workshop on Nanostructures for Electronics and Optics (NEOP), Dresden, Germany, Oct 6-9, 2002

Renger, J., Grafström, S., Eng, L., Schmidt, B., Bischoff, L.,
Investigation of aperture SNOM levers fabricated by FIB patterning and wet chemical etching,
7th Int. Conf. on Near Field Optics and Related Techniques, Rochester, NY, USA, Aug 11-15, 2002

Rinderknecht, J., Prinz, H., Kammler, T., Berberich, F., Zschech, E.,
In situ high temperature synchrotron-radiation diffraction studies of Ni and Co-Ni silicidation processes,
Europ. Workshop on "Materials for Advanced Metallization", Vaals, The Netherlands, March 3-5, 2002

Rogozin, A.I., Astrelin, V.T.,
Focusing of an electron beam extracted from the plasma to a metallic anode,
6th Int. Conf. on Modification of Materials with Particle Beams and Plasma Flows, Tomsk, Russia, Sept 23-28, 2002

Romanova, V.A., Begishev, V.P., Guenzel, R., Maitz, M., Kondyurin, A.V., Kondyurina, I.V.,
Synthesis of polyurethane coating with drug compounds on metal stents,
Conference "Oligomers 2002", Chernogolovka, Russia, Sept 9-14, 2002

Sass, J., Mazur, K., Eichhorn, F., Turos, A., Gladki, A., Jasik, A.,
Study of 60° misfit dislocations in semiconductor epi-layers,
2nd Seminar of Bruker axs and Bruker-Nonius, Krynica Gorska, Poland, Sept 22-24, 2002

Schell, N., Bøttiger, J., Matz, W., Chevallier, J., Mücklich, A., Petersen, J.H.,
Microstructural development of wear-protective coatings studied by in situ synchrotron x-ray scattering,
12th ESRF Users Meeting, Grenoble, Feb 13, 2002
ESRF Workshop: Surfaces and Interfaces on the Atomic- and Nano-Scale: Semiconductors, Magnetic Materials and Oxides, Grenoble, Feb 14-15, 2002

Schell, N.,
Growth mode and texture development in TiN films during magnetron sputtering – an in situ synchrotron radiation study,
3rd Int. Conf. on Synchrotron Radiation in Materials Science (SRMS-3), Singapore, Jan 21-24, 2002

Schell, N., Bøttiger, J., Matz, W., Chevallier, Mücklich, A., Petersen, J.H.,
New possibilities of characterizing growing sputter-deposited thin films,
Experimental Division Science Days, Aussois, France, May 22-24, 2002

Schmidt, B., Heinig, K.-H., Grambole, D., Herrmann, F., Perego, M.,
Impact of moisture from ambient on ion beam synthesis of nanocrystals in thin SiO_2 layers,
Int. Workshop on Nanostructures for Electronics and Optics (NEOP), Dresden, Germany,
Oct 6-9, 2002

Schmidt, B., Heinig, K.-H., Müller, T., Stegemann, K.-H.,
Self-organized NC-layers by conventional ion implantation,
NEON Meeting, Athens, Greece, Jan 17-18, 2002

Schmidt, J. U., Schmidt, B.,
Investigation of Si nanocluster formation in sputter deposited silicon suboxides and application to nanocluster memory structures,
E-MRS Spring Meeting, Strasbourg, France, June 18-21, 2002

Schmidt, J. U., Schmidt, B.,
Si-nanocluster layers embedded in SiO_2, preparation by sputtering and annealing of SiO_2/SiO_X stacks-electrical and optical characterization,
Int. Workshop on Nanostructures for Electronics and Optics (NEOP), Dresden, Germany,
Oct 6-9, 2002

Schmidt, J. U., Schmidt, B.,
Si-nanocrystal memory devices prepared by r.f. magnetron sputtering,
MRS Fall Meeting, Boston, USA, Nov 24-29, 2002

Schmidt, J., Tritschler, H., Bischoff, L.,
Improvement of micro end milling tools through variation of tool manufacturing method and geometry,
Int. Conf. on Micro and Nano Systems, ICMNS2002, Kumning, China, August 11-14, 2002

Schultrich, B., Jäger, H.U.,
Simulation of growth of tetrahedrally bonded amorphous carbon films by high energy ions,

8th Conference on Plasma Surface Engineering (PSE 2002), Garmisch-Partenkirchen, Germany, Sept 9-13, 2002

Shevchenko, N., Prokert, F., Borany, J. von,
Structural studies of oxygen implanted buried layers in titanium,
6th Int. Conf. on Modification of Materials with Particle Beams and Plasma Flows, Tomsk, Russia, Sept 23-28, 2002

Shevchenko, N., Rogozin, A., Matz, W., Günzel, R.,
Features of structure formation of TiN coatings obtained by plasma immersion ion implantation assisted deposition,
6th Int. Conf. on Modification of Materials with Particle Beams and Plasma Flows, Tomsk, Russia, Sept 23-28, 2002

Sinning S., Dekorsy T., Helm, M.,
Optical properties of N - implanted GaAs,
56th Scottish Universities Summer School in Physics "Ultrafast-Photonics", St. Andrews, Scotland, Sept 1-14, 2002

Skorupa, W., Gebel, T., Rebohle, L., Sun, J.,
Electroluminescence from thin SiO_2 layers after Si-and C-coimplantation,
E-MRS Spring Meeting, Strasbourg, France, June 17-21, 2002

Skorupa, W.,
FLASiC- ein europäisches GROWTH-Projekt für die verbesserte SiC-Si-Heteroepitaxie
1. Deutsches Arbeitskreistreffen Siliziumkarbid, Paderborn, June 24-25, 2002

Skorupa, W., Rebohle, L., Gebel, T., Helm, M.,
Strong blue light emission from ion implanted Si/SiO_2 structures,
NATO Advanced Research Workshop: Towards the First Silicon Laser, Trento, Italy, Sept 21-26, 2002

Skorupa, W., Gebel, T., Panknin, D., Priolo, F.,
Flash-lamp annealing at millisecond pulses: a new approach to optimize ultra-shallow junctions and heteroepitaxial layers,
EUREKA Meeting, Kiev, Ukraine, Nov 5-6, 2002

Späth, D., Tritschler, H., Bischoff, L., Schulz, W.,
Micromilling – high potential technology for micromechanical parts,
6th Int. Conf. on Advanced Manufacturing Systems and Technology, AMST 02, Udine, Italy, June 20-21, 2002

Spiga, S., Franciulli, M., Ferretti, N., Boscherini, F., Schmidt, B.,
Formation and structure of Sn nanoclusters in thin SiO_2 films,
E-MRS Spring Meeting, Strasbourg, France, June 18-21, 2002

Spiga, S., Franciulli, M., Montavan, R., Boscherini, F., Ferretti, N., Schmidt, B., Grötzschel, R., Mücklich, A.,
EXAFS and CEMS investigation of the local structure of Sn implanted SiO_2,
Silicon Workshop, INFM, Sede Genova, Italy, Feb 6-8, 2002

Sztucki, M., Metzger, T.H., Milita, S., Berberich, F., Schell, N., Rouvière, J.L., Patel, J.,
Depth resolved investigations of boron implanted silicon,
E-MRS Spring Meeting, Strasbourg, France, June 18-21, 2002

Tsyganov I., Wieser E., Maitz M., Prokert F., Richter E., Rogozin A

Structure and properties of TiO_{2-X} layers prepared by metal plasma immersion ion implantation and deposition (MPIIID),
8th Int. Conf. on Plasma Surface Engineering (PSE-2002), Garmisch-Partenkirchen, Sept 9-13, 2002

Vinnichenko, M.V., Pham, M.T., Chevolleau, T., Poperenko, L.V., Maitz, M.F.,
In situ ellipsometric investigation of the stainless steel corrosion behavior in biological media,
1st Materials Science Forum on Future Sustainable Technologies, Augsburg, Sept 17-20, 2002

Vlakhov, E.S., Wieser, E., Nenkov, K.A., Grötzschel, R.,
Effet of Fe- and Ni- ion implantation on the magnetoresistance of $La_{0.7}$ $Sr_{0.3}$ MnO_3 thin films,
Europ. Conf. Physics of Magnetism ' 02, Poznan, Poland, July 1-5, 2002

Volkov, A.E., Heinig, K.-H., Strobel, M., and Ryazanov, A.J.,
Nanocluster nucleation under continuous supply by monomers - new quality from comparison between kinetic MC and analytical results,
6th Int. Conf. on Computer Simulation of Radiation Effects in Solids (COSIRES 2002), Dresden, Germany, June 23-27, 2002

Walterfang, M., Keune, W., Reuther, H.,
Mössbauer-Effect studies of metastable c-FeSi synthesized by molecular beam epitaxy (MBE) and by ion implantation,
5th Seeheim Workshop on Mössbauer Spectroscopy, Seeheim, May 21-26, 2002

Wang, T., Kreissig, U., Grambole, D., Grötzschel, R., Eichhorn, F., Herrmann, F.,
Anti-oxidation effect of the TiH_2-rich layer on Ti225 alloy formed by H_2^+ implantation,
13th Int. Conf. on Ion Beam Modification of Materials (IBMM 2002), Kobe, Japan, Sept 1-6, 2002

Weishart, H., Heera, V., Eichhorn, F., Pecz, B., Barna A., Skorupa, W.,
Ion beam synthesis of diamond-SiC-heterostructures,
13th Europ.Conf. on Diamond, Diamond-Like Materials, Carbon Nanotubes, Nitrides and Silicon Carbide, Granada, Spain, Sept 8-13, 2002

Wellner, A., Pillard, V., Bonafos, C., Carrada, M., Claverie, A., Stegemann, K. H., Schmidt, B.,
Raman spectroscopy of germanium nanoparticles in amorphous silicon oxide films,
Int. Conf. on Superlattices, Nano-Structures and Nano-Devices, Toulouse, France, July 22-26, 2002

Lectures

Bischoff, L.,
Focused ion beams from alloy liquid metal ion sources,
Institute of Solid State Physics and Institute of Electronics, Sofia, April 19, 2002

Brauer, G.,
Positron annihilation spectroscopy studies of the SiO_2/Si interface,
Karls-Universität Prag, Prague, Czech Republic, May 28, 2002

Brauer, G.,
Untersuchungen an SiO_2 mittels Positronen-Annihilationsspektroskopie,
Geoforschungszentrum Potsdam, Aug 13, 2002

Brauer, G.,
Vacancy-type damage in ion implanted SiC characterized by positron annihilation spectroscopy,
University of Texas at Arlington, USA, Nov 11, 2002

Structure and properties of TiO_{2-X} layers prepared by metal plasma immersion ion implantation and deposition (MPIIID),
8th Int. Conf. on Plasma Surface Engineering (PSE-2002), Garmisch-Partenkirchen, Sept 9-13, 2002

Vinnichenko, M.V., Pham, M.T., Chevolleau, T., Poperenko, L.V., Maitz, M.F.,
In situ ellipsometric investigation of the stainless steel corrosion behavior in biological media,
1st Materials Science Forum on Future Sustainable Technologies, Augsburg, Sept 17-20, 2002

Vlakhov, E.S., Wieser, E., Nenkov, K.A., Grötzschel, R.,
Effet of Fe- and Ni- ion implantation on the magnetoresistance of $La_{0.7}\,Sr_{0.3}\,MnO_3$ thin films,
Europ. Conf. Physics of Magnetism ' 02, Poznan, Poland, July 1-5, 2002

Volkov, A.E., Heinig, K.-H., Strobel, M., and Ryazanov, A.J.,
Nanocluster nucleation under continuous supply by monomers - new quality from comparison between kinetic MC and analytical results,
6th Int. Conf. on Computer Simulation of Radiation Effects in Solids (COSIRES 2002), Dresden, Germany, June 23-27, 2002

Walterfang, M., Keune, W., Reuther, H.,
Mössbauer-Effect studies of metastable c-FeSi synthesized by molecular beam epitaxy (MBE) and by ion implantation,
5th Seeheim Workshop on Mössbauer Spectroscopy, Seeheim, May 21-26, 2002

Wang, T., Kreissig, U., Grambole, D., Grötzschel, R., Eichhorn, F., Herrmann, F.,
Anti-oxidation effect of the TiH_2-rich layer on Ti225 alloy formed by H_2^+ implantation,
13th Int. Conf. on Ion Beam Modification of Materials (IBMM 2002), Kobe, Japan, Sept 1-6, 2002

Weishart, H., Heera, V., Eichhorn, F., Pecz, B., Barna A., Skorupa, W.,
Ion beam synthesis of diamond-SiC-heterostructures,
13th Europ.Conf. on Diamond, Diamond-Like Materials, Carbon Nanotubes, Nitrides and Silicon Carbide, Granada, Spain, Sept 8-13, 2002

Wellner, A., Pillard, V., Bonafos, C., Carrada, M., Claverie, A., Stegemann, K. H., Schmidt, B.,
Raman spectroscopy of germanium nanoparticles in amorphous silicon oxide films,
Int. Conf. on Superlattices, Nano-Structures and Nano-Devices, Toulouse, France, July 22-26, 2002

Lectures

Bischoff, L.,
Focused ion beams from alloy liquid metal ion sources,
Institute of Solid State Physics and Institute of Electronics, Sofia, April 19, 2002

Brauer, G.,
Positron annihilation spectroscopy studies of the SiO_2/Si interface,
Karls-Universität Prag, Prague, Czech Republic, May 28, 2002

Brauer, G.,
Untersuchungen an SiO_2 mittels Positronen-Annihilationsspektroskopie,
Geoforschungszentrum Potsdam, Aug 13, 2002

Brauer, G.,
Vacancy-type damage in ion implanted SiC characterized by positron annihilation spectroscopy,
University of Texas at Arlington, USA, Nov 11, 2002

Eichhorn, F.,
Ionenstrahlsynthese von Nanokristallen im System (Si,C),
Institutsseminar des Institutes für Festkörper- und Werkstoffforschung Dresden, Nov 27, 2002

Grambole, D.,
Mikrostrahl am Tandetron des FZR,
TU Dresden, Institut für Strahlenschutzphysik, April 18, 2002

Grambole, D.,
Micro-ERDA,
AIM Round Table Meeting and Int. User Selection Panel Meeting, Dresden, April 15, 2002

Heinig, K.-H.,
Process simulations of nanocluster synthesis for nonvolatile semiconductor memories,
Meeting of the European Growth Project NEON, Athens, Greece, Jan 17–18, 2002

Heinig, K.-H.,
Search for advanced nanometric materials – examples of predictive atomistic simulations,
Meeting of the European Growth Project NEON, CEMES/CNRS, Toulouse, France,
Dec 3–6, 2002

Heinig, K.-H.,
Predictive computer simulations and data base improvement,
STMicroelectronics, Milano, Italy, July 1–2, 2002

Helm, M.,
The electron accelerator facility ELBE at Rossendorf/Dresden and its applications,
Karls-Universität Prague, Czech Republic, May 27, 2002

Helm, M.,
Bloch-Oszillationen: ein Faszinosum der Festkörperphysik seit 70 Jahren,
Universität Würzburg, Deutschland, Physikkolloquium, July 15, 2002

Kögler, R.,
The Rossendorf Double Implantation Chamber (DIC),
AIM Round Table Meeting and Int. User Selection Panel Meeting, Dresden, April 15, 2002

Kolitsch, A.,
AIM - An European Large-Scale Facility of Ion Beam Technologies,
Institute of Electronics, Sofia, Bulgaria, Sept 10, 2002

Mäder, M.,
Zerstörungsfreie Charakterisierung historischer Glasobjekte mittels Ionenstrahlen,
Ionenstrahl-Meeting, Universität Stuttgart, Nov 24-26, 2002

Maitz, M.F. ,
Ion beam induced formation of blood compatible layers based on titanium oxide,
Boston Scientific SCIMED, Minneapolis, USA, April 29, 2002

Maitz, M.F.,
Biomaterials-Body Interaction
- Principles of biomaterials testing
- Biomaterials in bone
- Biomaterials in blood
- The complement system

Seminars for undergraduate students and PhD students at Biomaterials Department, Southwest Jiaotong University, Chengdu, China, Oct 14 - Nov 8, 2002

Möller, W.,
Nanostrukturen durch Ionenimplantation: Computersimulation, Experiment und Anwendung,
Institut für Strahlenphysik der Universität Stuttgart, Jan 24, 2002

Möller, W.,
Selbstorganisierte Nanostrukturen durch Ionenimplantation,
Universität Giessen, May 23, 2002

Möller, W.,
Grundlagen der Ionen-Festkörper-Wechselwirkung,
W.E. Heraeus-Ferienkurs für Physik, TU Dresden, Sept 16-17, 2002

Möller, W.
Ionenimplantation, Plasma-Immersions-Ionenimplantation und ionengestützte Schichtabscheidung,
Course "Surface Engineering and Nanotechnology", Oct 15, 2002

Möller, W.,
Nanodesign durch Ionenstrahlen: Computersimulation, Experiment und Anwendung,
Institut für Allgemeine Physik, TU Wien, Austria, Nov 5, 2002

Müller, T.,
Nanocluster formation by low energy Si^+ implantation – basic mechanisms II,
Meeting of the European Growth Project NEON, Athens, Greece, Jan 17-21, 2002

Müller, T., Heinig, K.-H., Schmidt, B.,
Partial oxidation of implanted Si by humidity penetrated into damaged SiO_2 substrates,
Meeting of the European Growth Project NEON, Toulouse, France, Dec 3-6, 2002

Reuther, H.,
Surface investigations by Auger electron and X-ray induced photoelectron spectroscopy,
Phase analysis on ion treated surfaces by conversion electron Mössbauer spectroscopy,
Alloying by high dose ion implantation of iron into magnesium and aluminium,
Electron microscopy in the Research Center Rossendorf,
Instituto Nacional de Pesquisas Espaciais (The National Institute for Space Research) INPE, São José dos Campos, Brasilien, Oct 3-9, 2002

Richter, E.,
Surface modification of magnesium by ion beams,
Hannover Messe, April 19, 2002

Schell, N., Bøttiger, J., Matz, W., Chevallier, J., Mücklich, A., Petersen, J.H.,
Microstructural development of wear-protective coatings studied by in situ synchrotron X-ray scattering,
ESRF User Meeting, Feb 2002

Schell, N., Hennig, Ch.,
ROBL – the Rossendorf CRG Beamline for Radiochemistry and Materials Research, Environmental Studies and Characterization of New Materials,
ESRF Science Advisory Committee Evaluation Hearing, Grenoble, France, Nov 8, 2002

Schmidt, B.,
Erzeugung von Nanostrukturen durch Ionenbestrahlung,
Frühjahrssitzung des AK Plasmaoberflächentechnologie, Universität Kassel, May 13-14, 2002

Schmidt, J. U.,
Gateoxides with embedded Si-nanoclusters for memory applications - preparation by magnetron sputtering, electrical and optical characterization,
Institut für Tieftemperaturphysik der TU Dresden, Germany, May 23, 2002

Schmidt, J. U.,
Si-nanocluster based memory structures - preparation by thermal annealing of sputtered silicon suboxides, optical and electrical characterization,
Woollam Seminar "Spectroscopic Ellipsometry", Darmstadt, Germany, Oct 15-16, 2002

Skorupa, W.,
Ion beam synthesized nanoclusters for silicon-based light emission,
Marie-Curie-Sklodowska-University, Lublin, Poland, June 6, 2002

Voelskow, M., Panknin, D., Skorupa, W.,
Marker studies of the heteroepitaxial SiC-on-Si growth supported by flash lamp processing,
Meeting of the European GROWTH Project FLASiC, Univ. of Cambridge, UK, Sept 26-28, 2002

Wieser, E.,
Structural and magnetic phase transformations in metastable Fe-Cr alloys induced by ion irradiation,
Institute of Electrophysics, Yekaterinburg, Russia, Sept 11, 2002

Reports

Fitz, C.
Entwicklung und Relaxation mechanischer Spannungen in Bornitrid-Schichten,
Wissenschaftlich Technische Berichte, FZR-337, ISSN 1437-322X, July 2002

Fitz, T.
Ion nitriding of aluminium,
Wissenschaftlich Technische Berichte, FZR-354, ISSN 1437-322X, July 2002

Gebel, T.,
Nanocluster-rich SiO_2 layers produced by ion beam synthesis: electrical and optoelectronic properties,
Wissenschaftlich Technische Berichte, FZR-350, ISSN 1437-322X, July 2002

Patents

Friedrich, M., Tyrroff, H.,
Vorrichtung zur Erhöhung der Lebensdauer einer Sputterionenquelle,
Patent application DE 10241252.9., 06.09.2002

Heera, V., Skorupa, W.,
Verfahren zur gezielten Herstellung von n-leitenden Bereichen in Diamantschichten mittels Ionenimplantation,
Patent EP 0 996 972 B1, 29.05.2002

Heera, V.,
Verfahren zur Dotierung von Siliziumkarbid-Halbleiterbereichen,
Patent DE 100 62 212 C 1, 21.11.2002

Schmidt, B., Bischoff, L., Eng, L.,

Schmidt, J. U.,
Gateoxides with embedded Si-nanoclusters for memory applications - preparation by magnetron sputtering, electrical and optical characterization,
Institut für Tieftemperaturphysik der TU Dresden, Germany, May 23, 2002

Schmidt, J. U.,
Si-nanocluster based memory structures - preparation by thermal annealing of sputtered silicon suboxides, optical and electrical characterization,
Woollam Seminar "Spectroscopic Ellipsometry", Darmstadt, Germany, Oct 15-16, 2002

Skorupa, W.,
Ion beam synthesized nanoclusters for silicon-based light emission,
Marie-Curie-Sklodowska-University, Lublin, Poland, June 6, 2002

Voelskow, M., Panknin, D., Skorupa, W.,
Marker studies of the heteroepitaxial SiC-on-Si growth supported by flash lamp processing,
Meeting of the European GROWTH Project FLASiC, Univ. of Cambridge, UK, Sept 26-28, 2002

Wieser, E.,
Structural and magnetic phase transformations in metastable Fe-Cr alloys induced by ion irradiation,
Institute of Electrophysics, Yekaterinburg, Russia, Sept 11, 2002

Reports

Fitz, C.
Entwicklung und Relaxation mechanischer Spannungen in Bornitrid-Schichten,
Wissenschaftlich Technische Berichte, FZR-337, ISSN 1437-322X, July 2002

Fitz, T.
Ion nitriding of aluminium,
Wissenschaftlich Technische Berichte, FZR-354, ISSN 1437-322X, July 2002

Gebel, T.,
Nanocluster-rich SiO_2 layers produced by ion beam synthesis: electrical and optoelectronic properties,
Wissenschaftlich Technische Berichte, FZR-350, ISSN 1437-322X, July 2002

Patents

Friedrich, M., Tyrroff, H.,
Vorrichtung zur Erhöhung der Lebensdauer einer Sputterionenquelle,
Patent application DE 10241252.9., 06.09.2002

Heera, V., Skorupa, W.,
Verfahren zur gezielten Herstellung von n-leitenden Bereichen in Diamantschichten mittels Ionenimplantation,
Patent EP 0 996 972 B1, 29.05.2002

Heera, V.,
Verfahren zur Dotierung von Siliziumkarbid-Halbleiterbereichen,
Patent DE 100 62 212 C 1, 21.11.2002

Schmidt, B., Bischoff, L., Eng, L.,

Schmidt, J. U.,
Gateoxides with embedded Si-nanoclusters for memory applications - preparation by magnetron sputtering, electrical and optical characterization,
Institut für Tieftemperaturphysik der TU Dresden, Germany, May 23, 2002

Schmidt, J. U.,
Si-nanocluster based memory structures - preparation by thermal annealing of sputtered silicon suboxides, optical and electrical characterization,
Woollam Seminar "Spectroscopic Ellipsometry", Darmstadt, Germany, Oct 15-16, 2002

Skorupa, W.,
Ion beam synthesized nanoclusters for silicon-based light emission,
Marie-Curie-Sklodowska-University, Lublin, Poland, June 6, 2002

Voelskow, M., Panknin, D., Skorupa, W.,
Marker studies of the heteroepitaxial SiC-on-Si growth supported by flash lamp processing,
Meeting of the European GROWTH Project FLASiC, Univ. of Cambridge, UK, Sept 26-28, 2002

Wieser, E.,
Structural and magnetic phase transformations in metastable Fe-Cr alloys induced by ion irradiation,
Institute of Electrophysics, Yekaterinburg, Russia, Sept 11, 2002

Reports

Fitz, C.
Entwicklung und Relaxation mechanischer Spannungen in Bornitrid-Schichten,
Wissenschaftlich Technische Berichte, FZR-337, ISSN 1437-322X, July 2002

Fitz, T.
Ion nitriding of aluminium,
Wissenschaftlich Technische Berichte, FZR-354, ISSN 1437-322X, July 2002

Gebel, T.,
Nanocluster-rich SiO_2 layers produced by ion beam synthesis: electrical and optoelectronic properties,
Wissenschaftlich Technische Berichte, FZR-350, ISSN 1437-322X, July 2002

Patents

Friedrich, M., Tyrroff, H.,
Vorrichtung zur Erhöhung der Lebensdauer einer Sputterionenquelle,
Patent application DE 10241252.9., 06.09.2002

Heera, V., Skorupa, W.,
Verfahren zur gezielten Herstellung von n-leitenden Bereichen in Diamantschichten mittels Ionenimplantation,
Patent EP 0 996 972 B1, 29.05.2002

Heera, V.,
Verfahren zur Dotierung von Siliziumkarbid-Halbleiterbereichen,
Patent DE 100 62 212 C 1, 21.11.2002

Schmidt, B., Bischoff, L., Eng, L.,

Verfahren zur Herstellung von integrierten Abtastnadeln,
Patent application EP 1 209 689 A, 20.05.2002

Schmidt, B., Heinig, K.-H.,
Verfahren zur Herstellung von Monolagen aus Silizium-Nanoclustern in Siliziumdioxid,
Patent DE 199 33 632 C2, 21.11.2002

Diploma Thesis

Laudien, G.,
Plasmadiagnostics on Ar/Cl-plasma,
TU Dresden, April 2002

PhD Theses

Berberich, F.,
In situ Untersuchungen der Phasentransformation und der mechanischen Eigenschaften stickstoffimplantierter Ti-6Al-4V Legierungen,
TU Dresden, Nov 8, 2002

Fitz, T.,
Ion nitriding of aluminium,
TU Dresden, July 2002
Gebel, T.,
Nanocluster-rich SiO_2 layers produced by ion beam synthesis: electrical and optoelectronic properties,
TU Dresden, July 17, 2002

Mäder, M.,
Zerstörungsfreie Charakterisierung historischer Glasobjekte mittels Ionenstrahlen,
TU Dresden, Nov 1, 2002

Awards

Borany; J. von, Gebel, T., Heinig, K.-H., Schmidt, B., Müller, T.,
Entwicklung eines neuartigen nichtflüchtigen Halbleiterspeichers,
Technologiepreis des FZR, Dec 19, 2002

Gebel, T.
EMRS – Young Scientist Award, Strasbourg, France, June 2002

Organization of Meetings

4th Meeting of the International Users Selection Panel and Round Table Meeting of AIM Large-scale facility,
Organization: W. Möller, A. Kolitsch
Rossendorf, April 14 –15, 2002

FLASiC-Meeting (Kick-off for an European GROWTH Project),
Organization: W. Skorupa
Rossendorf, April 21-23, 2002

Verfahren zur Herstellung von integrierten Abtastnadeln,
Patent application EP 1 209 689 A, 20.05.2002

Schmidt, B., Heinig, K.-H.,
Verfahren zur Herstellung von Monolagen aus Silizium-Nanoclustern in Siliziumdioxid,
Patent DE 199 33 632 C2, 21.11.2002

Diploma Thesis

Laudien, G.,
Plasmadiagnostics on Ar/Cl-plasma,
TU Dresden, April 2002

PhD Theses

Berberich, F.,
In situ Untersuchungen der Phasentransformation und der mechanischen Eigenschaften stickstoffimplantierter Ti-6Al-4V Legierungen,
TU Dresden, Nov 8, 2002

Fitz, T.,
Ion nitriding of aluminium,
TU Dresden, July 2002
Gebel, T.,
Nanocluster-rich SiO_2 layers produced by ion beam synthesis: electrical and optoelectronic properties,
TU Dresden, July 17, 2002

Mäder, M.,
Zerstörungsfreie Charakterisierung historischer Glasobjekte mittels Ionenstrahlen,
TU Dresden, Nov 1, 2002

Awards

Borany; J. von, Gebel, T., Heinig, K.-H., Schmidt, B., Müller, T.,
Entwicklung eines neuartigen nichtflüchtigen Halbleiterspeichers,
Technologiepreis des FZR, Dec 19, 2002

Gebel, T.
EMRS – Young Scientist Award, Strasbourg, France, June 2002

Organization of Meetings

4th Meeting of the International Users Selection Panel and Round Table Meeting of AIM Large-scale facility,
Organization: W. Möller, A. Kolitsch
Rossendorf, April 14 –15, 2002

FLASiC-Meeting (Kick-off for an European GROWTH Project),
Organization: W. Skorupa
Rossendorf, April 21-23, 2002

Verfahren zur Herstellung von integrierten Abtastnadeln,
Patent application EP 1 209 689 A, 20.05.2002

Schmidt, B., Heinig, K.-H.,
Verfahren zur Herstellung von Monolagen aus Silizium-Nanoclustern in Siliziumdioxid,
Patent DE 199 33 632 C2, 21.11.2002

Diploma Thesis

Laudien, G.,
Plasmadiagnostics on Ar/Cl-plasma,
TU Dresden, April 2002

PhD Theses

Berberich, F.,
In situ Untersuchungen der Phasentransformation und der mechanischen Eigenschaften stickstoffimplantierter Ti-6Al-4V Legierungen,
TU Dresden, Nov 8, 2002

Fitz, T.,
Ion nitriding of aluminium,
TU Dresden, July 2002
Gebel, T.,
Nanocluster-rich SiO_2 layers produced by ion beam synthesis: electrical and optoelectronic properties,
TU Dresden, July 17, 2002

Mäder, M.,
Zerstörungsfreie Charakterisierung historischer Glasobjekte mittels Ionenstrahlen,
TU Dresden, Nov 1, 2002

Awards

Borany; J. von, Gebel, T., Heinig, K.-H., Schmidt, B., Müller, T.,
Entwicklung eines neuartigen nichtflüchtigen Halbleiterspeichers,
Technologiepreis des FZR, Dec 19, 2002

Gebel, T.
EMRS – Young Scientist Award, Strasbourg, France, June 2002

Organization of Meetings

4th Meeting of the International Users Selection Panel and Round Table Meeting of AIM Large-scale facility,
Organization: W. Möller, A. Kolitsch
Rossendorf, April 14 –15, 2002

FLASiC-Meeting (Kick-off for an European GROWTH Project),
Organization: W. Skorupa
Rossendorf, April 21-23, 2002

Verfahren zur Herstellung von integrierten Abtastnadeln,
Patent application EP 1 209 689 A, 20.05.2002

Schmidt, B., Heinig, K.-H.,
Verfahren zur Herstellung von Monolagen aus Silizium-Nanoclustern in Siliziumdioxid,
Patent DE 199 33 632 C2, 21.11.2002

Diploma Thesis

Laudien, G.,
Plasmadiagnostics on Ar/Cl-plasma,
TU Dresden, April 2002

PhD Theses

Berberich, F.,
In situ Untersuchungen der Phasentransformation und der mechanischen Eigenschaften stickstoffimplantierter Ti-6Al-4V Legierungen,
TU Dresden, Nov 8, 2002

Fitz, T.,
Ion nitriding of aluminium,
TU Dresden, July 2002
Gebel, T.,
Nanocluster-rich SiO_2 layers produced by ion beam synthesis: electrical and optoelectronic properties,
TU Dresden, July 17, 2002

Mäder, M.,
Zerstörungsfreie Charakterisierung historischer Glasobjekte mittels Ionenstrahlen,
TU Dresden, Nov 1, 2002

Awards

Borany; J. von, Gebel, T., Heinig, K.-H., Schmidt, B., Müller, T.,
Entwicklung eines neuartigen nichtflüchtigen Halbleiterspeichers,
Technologiepreis des FZR, Dec 19, 2002

Gebel, T.
EMRS – Young Scientist Award, Strasbourg, France, June 2002

Organization of Meetings

4th Meeting of the International Users Selection Panel and Round Table Meeting of AIM Large-scale facility,
Organization: W. Möller, A. Kolitsch
Rossendorf, April 14 –15, 2002

FLASiC-Meeting (Kick-off for an European GROWTH Project),
Organization: W. Skorupa
Rossendorf, April 21-23, 2002

Linköping - Rossendorf Thin Film Meeting,
Organization: W. Möller, A. Kolitsch
Rossendorf, June 10-11, 2002

6th Int. Conf. on Computer Simulation of Radiation Effects in Solids (COSIRES),
Chairmen: W. Möller, M. Posselt, Dresden, June 23 - 27, 2002
International Tutorial "Fundamentals and Trends in Plasma Processing" in connection with 8th Int. Conf. on Plasma Surface Engineering,
Organization: W. Möller
Garmisch-Partenkirchen, Sept. 7 - 8, 2002

International Workshop on Nanostructures for Electronics and Optics (NEOP),
Co-Chairman: K.-H. Heinig
Dresden, Oct 6 - 9, 2002

Laboratory visits

Abendroth, B.,
LURE (Laboratoire pour l' utilization de rayonnement electromaqnetique) Sychrotron facillity, Orsay, France, Nov 17-30, 2002

Beckers, M.
European Synchrotron Radiation Facility, Grenoble, France, Oct 6-13; Nov 27 - Dec 5, 2002

Bischoff, L.,
Institute of Solid State Physics and Institute of Electronics, Sofia, April 15 - 21, 2002

Brauer, G.,
Charles University Prague, Czech Republic, May 22-29, 2002

Brauer, G.,
DGA-CTA-LOT Arcueil, France, June 29 – July 1, 2002

Brauer, G.,
Geoforschungszentrum Potsdam, Germany, Aug 12-13, 2002

Dekorsy T.,
Free-Electron Laser Facility FELIX, Rijnhuizen, Netherlands, July 21-26, 2002

Dekorsy T.,
RWTH Aachen, Nov 18-19, 2002

Eichhorn, F.,
European Synchrotron Radiation Facility, Grenoble, France, March 5-10; May 14-22; July 2-9, Sept 8-11, 2002

Gago, R.,
LURE (Laboratoire pour l' utilization de rayonnement electromaqnetique) Sychrotron facillity, Orsay, France, Nov 17-30, 2002

Gebel, T.,
Mattson GmbH, Dornstadt bei Ulm, Oct 14-15, 2002

Gebel, T.

Linköping - Rossendorf Thin Film Meeting,
Organization: W. Möller, A. Kolitsch
Rossendorf, June 10-11, 2002

6th Int. Conf. on Computer Simulation of Radiation Effects in Solids (COSIRES),
Chairmen: W. Möller, M. Posselt, Dresden, June 23 - 27, 2002
International Tutorial "Fundamentals and Trends in Plasma Processing" in connection with 8th Int. Conf. on Plasma Surface Engineering,
Organization: W. Möller
Garmisch-Partenkirchen, Sept. 7 - 8, 2002

International Workshop on Nanostructures for Electronics and Optics (NEOP),
Co-Chairman: K.-H. Heinig
Dresden, Oct 6 - 9, 2002

Laboratory visits

Abendroth, B.,
LURE (Laboratoire pour l' utilization de rayonnement electromaqnetique) Sychrotron facillity, Orsay, France, Nov 17-30, 2002

Beckers, M.
European Synchrotron Radiation Facility, Grenoble, France, Oct 6-13; Nov 27 - Dec 5, 2002

Bischoff, L.,
Institute of Solid State Physics and Institute of Electronics, Sofia, April 15 - 21, 2002

Brauer, G.,
Charles University Prague, Czech Republic, May 22-29, 2002

Brauer, G.,
DGA-CTA-LOT Arcueil, France, June 29 – July 1, 2002

Brauer, G.,
Geoforschungszentrum Potsdam, Germany, Aug 12-13, 2002

Dekorsy T.,
Free-Electron Laser Facility FELIX, Rijnhuizen, Netherlands, July 21-26, 2002

Dekorsy T.,
RWTH Aachen, Nov 18-19, 2002

Eichhorn, F.,
European Synchrotron Radiation Facility, Grenoble, France, March 5-10; May 14-22; July 2-9, Sept 8-11, 2002

Gago, R.,
LURE (Laboratoire pour l' utilization de rayonnement electromaqnetique) Sychrotron facillity, Orsay, France, Nov 17-30, 2002

Gebel, T.,
Mattson GmbH, Dornstadt bei Ulm, Oct 14-15, 2002

Gebel, T.

Inst. of Semiconductor Physics, Kiev, Ukraine, Nov 2-6, 2002

Georgiev N.
European Synchrotron Radiation Facility, Grenoble, France: May 14-19; July 5-9,2002

Heinig, K.-H.,
NCSR „Demokritos“, Athens, Greece, Jan 17-18, 2002

Heinig, K.-H.,
STMicroelectronics Agrate/Milano, Italy, July 1-2, 2002

Heinig, K.-H.,
CEMES/CNRS, Toulouse, France, Dec 3-6, 2002

Kolitsch, A.,
Institute of Electronics, Institute of Solid State Physics, Sofia, Bulgaria, Sept 8-11, 2002

Maitz, M.F.,
University of Perm and Russian Academy of Science, Perm, Russia, July 2-10, 2002,

Maitz, M.F.,
Biomaterials Department, Southwest Jiaotong University, Chengdu, China, Oct 9 - Nov 8, 2002

Panknin, D.,
Dept. of Engineering, Univ. of Cambridge, Sept 26-28, 2002

Reuther, H.,
Instituto Nacional de Pesquisas Espaciais (The National Institute for Space Research) INPE,
São José dos Campos, Brasil, Oct 1-16, 2002

Schell, N.,
University of Aarhus, Denmark, Feb 21-27; Aug 17-22, 2002

Schmidt, B.,
National Center for Scientific Research 'Demokritos', Institute of Microelectronics, Athene, Greece,
Jan 17-18, 2002

Schmidt, B.,
Universität Kassel, Institut für Mikrostrukturtechnologie and Analytik, May 13-14, 2002

Skorupa, W.,
Dept. of Engineering, Univ. of Cambridge, Sept 26-28, 2002

Skorupa, W.,
Mattson GmbH, Dornstadt bei Ulm, Oct 14-15, 2002

Skorupa, W.,
Inst. of Semiconductor Physics, Kiev, Ukraine, Nov 2-6, 2002

Skorupa, W.,
Dept. of Microelectronics and Information Technology, Kungl Tekniska Högskolan (Royal Institute of
Technology), Stockholm, Sweden, Nov 21-23, 2002

Voelskow, M.,
Dept. of Engineering, Univ. of Cambridge, Sept 26-28, 2002

Winnerl, S.,
BESSY, Berlin, Nov 18 – 19, 2002

Guests

Abdel-Rahman, A.M.,
South Valley University, Egypt., Oct 1 - Dec 31, 2002

Ayache, R.,
University of Batna, Algeria, March 3 - April 3, 2002

Bankov, P.,
Institute of Electronics, Sofia, Bulgaria, May 26 - June 10, 2002

Beck, A.,
NRCN Beer-Sheva, Israel, Aug 14-16, 2002

Belko, V.I.,
Belorussian State University, Minsk, Belarus, Oct 1 - Dec 31, 2002

Bonafos, C.,
CEMES-CNRS, Toulouse, France, April 24-28, 2002

Borodin, V.,
Russian Research Centre "Kurchatov Institute", Moscow, Russia, Aug 15 - Oct 8, 2002

Chan Hay Yee, S.,
National University of Singapore and Chartered Semiconductor Manufacturing Ltd., Singapore, July 1-7, 2002

Chen, J.,
University of Antwerp, Belgium, Oct 14-18, 2002

Cizek, J.,
Charles University, Prague, Czech Republic, Jan 14-27, May 15 - Jun 15, 2002

Devanathan, R.,
Indian Institute of Technology, Chennai (Madras), India, June 3 - July 5, 2002

Förster, C. E.,
Universidade Estadual de Ponta Grossa, Brazil, Jan 1 - Dec 27, 2002

Gaca, J., (at ROBL)
Institute of Electronic Materials Research, Warschau, Polen, Nov 9-15, 2002

Gammer, K.,
TU Wien, Austria, July 1-4, 2002

Gao, F.,
Pacific Northwest National Laboratory, Richland, USA, Dec 9-20, 2002

Grenzer, J.,
Universität Potsdam, Institut für Physik, Oct 24-25, 2002

Winnerl, S.,
BESSY, Berlin, Nov 18 – 19, 2002

Guests

Abdel-Rahman, A.M.,
South Valley University, Egypt., Oct 1 - Dec 31, 2002

Ayache, R.,
University of Batna, Algeria, March 3 - April 3, 2002

Bankov, P.,
Institute of Electronics, Sofia, Bulgaria, May 26 - June 10, 2002

Beck, A.,
NRCN Beer-Sheva, Israel, Aug 14-16, 2002

Belko, V.I.,
Belorussian State University, Minsk, Belarus, Oct 1 - Dec 31, 2002

Bonafos, C.,
CEMES-CNRS, Toulouse, France, April 24-28, 2002

Borodin, V.,
Russian Research Centre “Kurchatov Institute”, Moscow, Russia, Aug 15 - Oct 8, 2002

Chan Hay Yee, S.,
National University of Singapore and Chartered Semiconductor Manufacturing Ltd.,
Singapore, July 1-7, 2002

Chen, J.,
University of Antwerp, Belgium, Oct 14-18, 2002

Cizek, J.,
Charles University, Prague, Czech Republic, Jan 14-27, May 15 - Jun 15, 2002

Devanathan, R.,
Indian Institute of Technology, Chennai (Madras), India, June 3 - July 5, 2002

Förster, C. E.,
Universidade Estadual de Ponta Grossa, Brazil, Jan 1 - Dec 27, 2002

Gaca, J., (at ROBL)
Institute of Electronic Materials Research, Warschau, Polen, Nov 9-15, 2002

Gammer, K.,
TU Wien, Austria, July 1-4, 2002

Gao, F.,
Pacific Northwest National Laboratory, Richland, USA, Dec 9-20, 2002

Grenzer, J.,
Universität Potsdam, Institut für Physik, Oct 24-25, 2002

Guschtschina, N.,
Institute of Electrophysics, Yekaterinburg, Russia, Nov 2 - Dec 3, 2002

Ignatova, V.,
University of Antwerp, Belgium, Oct 14-18, 2002

Khalfaoui, R.,
University of Boumerdes, Algeria, Oct 13-15, 2002

Kido, A.,
Nara Medical University, Nara, Japan, Dec 16-17, 2002

Kondyurin, A.,
University of Perm, Russia, Jan 1 - Dec 31, 2002

Kondyurina, I.,
University of Perm, Russia, Jan 1 - Dec 31, 2002

Krzyżanowska, H.,
Inst. of Physics, Marie-Curie-Sklodowska-University, Lublin, Poland, Sept 16-22, 2002

Kuriplach, J.,
Charles University, Prague, Czech Republic, Nov 6-20, Nov 26 - Dec 10, 2002

Kuzmin, V.,
Joint Institute for Nuclear Research, Dubna, Russia, Nov 18 - Dec 14, 2002

Lebedev, M.,
Institute for Solid State Physics, Chernogolovka, Russia, Aug 26 - Sep 27, 2002

Macková, A.,
Nuclear Physics Institute, Rez near Prague, Czech Republic, Sept 16 - Nov 30, 2002

Madhusoodanan, K.N.,
Cochin University of Science and Technology, Cochin March 2, 2001 - Feb 24, 2002

Malyshko, E.,
University of Lipetsk, Russia, Nov 24 - Dec 21, 2002

Martin de Palma, R.J. ,
Universitad Autonoma de Madrid, Spain, Sept 21-25, 2002

May-Tal Beck, S.,
NRCN Beer-Sheva, Israel, Aug 14 - 16, 2002

Migunova, T.,
University of Lipetsk, Russia, Nov 24 - Dec 21, 2002

Misochko, O.V.,
Institute for Solid State Physics, Chernogolovka, Russia, Nov 11 - Dec 10, 2002

Mukherjee, S.,
Institute for Plasma Research, Gandhinagar, India, Jan 1 - May 29, 2002

Nechitailo, G.,
Institute of Biochemical Physics, Moscow, Russia, Jan 1-31, 2002

Nekvindová, P.,
VSCHT, Prague, Czech Republic, Sept 16-27, 2002

Novikov, P.,
Institute of Semiconductor Physics, Novosibirsk, Russia, Aug 12 - Nov 11, 2002

Otano, W.,
University of Puerto Rico at Cayey, USA, Sept 14-17, 2002

Pathak, A.P.,
School of Physics, University of Hyderabad, India, May 9 - Aug 3, 2002

Paul, S.,
Mattson Thermal Products GmbH Dornstadt, Germany, May 28-29; Oct 30, 2002

Pécz, B.,
MTA MFA, Res. Inst. Techn. Phys.& Mater. Sci., Budapest, June 2 - July 30, 2002

Peev, N.,
Institute for Solid State Physics, Sofia, Bulgaria, March 4 - April 6, 2002

Piekoszewski, J.,
Soltan Institute for Nuclear Studies, Otwock, Poland, March 11-20; Aug 26 - Sept 5;
Nov 25 - Dec 6, 2002

Prochazka, I.,
Charles University, Prague, Czech Republic, March 11-18; April 2-9, 2002

Properenko, L.,
Taras Shevchenko University Kiev, Ukraina, July 20 - Sept 20, 2002

Ram Mohan Rao, K.,
Indian Institute of Technology, Kharagpur, India, Oct 7 - Dec 31, 2002

Revesz, A.G.,
Revesz Associates, Bethesda/MD, USA, April 8-18, 2002

Sass, J.,
Institute of Electronic Materials Research, Warschau, Polen, Oct 3-6, 2002

Saude, S.,
DGA-CTA-LOT Arcueil, France, Aug 19 - Sep 7; Oct 24 - Nov 24, 2002

Stangl, J.,
Universität Linz, Institut für Halbleiter- und Festkörperphysik, Österreich, Oct 24-25, 2002

Ster, A.,
Research Institute for Technical and Materials Science, Budapest, Hungary, Nov 26 - Dec 7, 2002

Sukhodub, L.,
Institute of Applied Physics, Sumy, Ukraina, March 20-21, 2002

Sulkio-Cleff, B.,
Institut für Kernphysik, University of Münster, March 20-21, 2002

Tsyganov, I.,
University of Lipetsk, Russia, Jan 15 - April 30; July 20 - Dec 21, 2002

Turos, A.,
Institute of Electronic Materials Research, Warschau, Polen, Oct 3-6, 2002

Vinnichenko, M.,
Taras Shevchenko University Kiev, Ukraina, July 1 - Dec 31, 2002

Volkov, A.,
Russian Research Centre “Kurchatov Institute”, Moscow, Russia, Oct 6-19, 2002

Walther, K. (at ROBL),
Geoforschungszentrum Potsdam, Nov 26 - Dec 3, 2002

Werner, Z.,
Soltan Institute for Nuclear Studies, Otwock, Poland, March 11-20; Aug 31 - Sept 5;
Nov 25 - Dec 6, 2002

Wojcik, M. (at ROBL),
Institute of Electronic Materials Research, Warschau, Polen, Nov 9-15, 2002

Zhuravlev, K.S.,
Institute of Semiconductor Physics, Novosibirsk, March 12-31, 2002

Zuk, J.,
Inst. of Physics, Marie-Curie-Sklodowska-University, Lublin, Poland, Sept 16-22, 2002

List of EC supported users of AIM-LSF

Abrasonis, G.,
Laboratoire de Metallurgie Physique, University of Poitiers, France, Dec 16-19, 2002

Baede, L.,
Eindhoven University, The Netherlands, May 12-17; June 23-27, 2002

Bardeleben, H.-J. von,
Universite Paris, France, March 16-20, 2002

Brijs, B.,
IMEC Leuven, Belgium, Feb 5-6; July 1-3, 2002

Bugoi, R.-N.,
Institute of Atomic Physics Bucharest, Romania, March 10-29, Nov 24 - Dec 7, 2002

Cantin, J. L.,
Universite Paris, France, March 16-20, 2002

Cigal, J.-C.,
Eindhoven University, The Netherlands, June 23-27, 2002

Constantinescu, B.,
Institute of Atomic Physics Bucharest, Romania, March 10-29, Nov 24 - Dec 7, 2002

Mentesse, S.,
Johannes Kepler Universität, Institut für Halbleiterphysik, Linz, Austria, June 12-18, 2002

Pelka, J.,
Institute of Physics, Polish Academy of Sciences, Warsaw, Poland, Nov 6-10, 2002

Reniewicz, H.,
University at Bialystok, Institute of Experimental Physics, Bialystok, Poland, Nov 6-10, 2002

Sass, J.,
Institute of Electronic Materials Technology, Warsaw, Poland, May 19-22, 2002

Stangl, J.,
Johannes Kepler Universität, Institut für Halbleiterphysik, Linz, Austria, June 12-18, 2002

Marie Curie Training Site

Kiisk, M.,
Lund University, Sweden, Jan 1 - Sept 28, 2002

Pecheva, E.,
Institut of Solid State Physics Sofia, Bulgaria, June 24 - Aug 16, Oct 1 - Dec 31, 2002

Razpet, A.,
University of Ljubljana, Slowenia, June 1-30, 2002

Romanek, J.,
Marie Curie-Sklodowska University Lublin, Poland, June 14-30, Sept 15 - Dec 31, 2002

Ruzicka, M.,
University of West Bohemia, Plzen, Czech Republic, Feb 1 - Aug 31, Oct 13 - Dec 31, 2002

Institute Seminars

J. R. Abelson - University of Illinois at Urbana-Champaign/USA
Medium-range order in amorphous silicon measured by fluctuation electron microscopy
Dec 9, 2002

J. Birch - Linköping University, Sweden
Recent advances in ion-assisted growth of multilayer X-ray mirrors for the water window
Jan 17, 2002

D. O. Boerma - University of Groningen, Netherlands
Growth and characterization of magnetic iron nitride layers
Jan 23, 2002

C. Bonafos - CEMES/CNRS Toulouse, France
Nucleation and growth of semiconductor nanoparticles in SiO2: experiments, modelling and applications
April 25, 2002

U. Diebold - Fritz-Haber-Institut Berlin

Oberflächen von oxidischen Materialien
Nov 14, 2002

L. Eng - TU Dresden
Near-Field Optics: The challenge for future nanodevices
Nov 28, 2002
(Gemeinsames Institutskolloquium FWI/FWK)

M. Grundmann - Universität Leipzig
Intersubniveau-Übergänge in Quantenpunkten
Feb 7, 2002

M. Grunze - Universität Heidelberg
Chemische Nanolithographie
Feb 14, 2002

H. Hilgers - IBM Mainz
Neuere Entwicklungen für die Speichertechnologie
Feb 21, 2002

L. Hultman - Linköping University, Sweden
Wear-resistant nitride coatings and superlattices: Thin film research at Linköping
June 11, 2002

U. Kaiser - Friedrich- Schiller-Universität Jena
Transmissionselektronenmikroskopie zur Beurteilung des Wachstums von niedrigdimensionalen Strukturen in und auf SiC
Jan 31, 2002

H. Lebius - CIRIL/GANIL Caen, France
Einfluss potentieller und kinetischer Energie auf den Sputteryield von UO_2
April 18, 2002

H. Lichte - TU Dresden
Electron holography - a powerful tool for nano-analysis
May 16, 2002

K.-H. Müller - Institut für Festkörper- und Werkstofforschung Dresden
MgB_2 *- ein neuer Supraleiter*
May 30, 2002

G. Seifert - TU Dresden
Nanotubes - Struktur und Eigenschaften
May 2, 2002

H.-J. Spies - TU Bergakademie Freiberg
Untersuchungen zum Plasmanitrieren von Aluminium-Legierungen
Feb 22, 2002

J. Strümpfel - von Ardenne Anlagentechnik Dresden
Großflächige Abscheidung von Oxidschichten mittels Magentronsputtern und EB-Verdampfung
Jan 10, 2002

C. Teichert - Montanuniversität Leoben, Austria
Selbstorganisation von Halbleiternanostrukturen bei heteroepitaktischem Wachstum

und Ionenbeschuss
Dec 5, 2002

W. Witthuhn - Friedrich-Schiller-Universität Jena
Störstellen und Defektkomplexe in Siliziumkarbid
Aug 7, 2002

Other Seminars

H. Amekura - National Institute for Materials Science, Tsukuba, Japan
Some research topics in the ion accelerator laboratory in NIMS - Cu nanoparticles in SiO_2,
- Radiation-induced conductivity in Si and a-Si:H
Feb 6, 2002

M. Aziz - Harvard University, Cambridge, USA
Nanoscale morphology control using ion beams
March 15, 2002

H.J. von Bardeleben - Université Paris, France
EPR analysis of ion implantation induced defects in SiC
March 20, 2002

M.M. Bilek - University of Sydney, Australia
Control of stress and microstructure in thin film materials
June 21, 2002

R. Devanathan - Indian Institute of Technology, Chennai (Madras), India
Computer simulation of radiation damage in SiC and $ZrSiO_4$
July 1, 2002

H. Feick - Department of Materials Science and Engineering, University of California, USA
Defects of GaN after electron and proton irradiation
Dec 6, 2002

J. Grenzer - Universität Potsdam, Institut für Physik
Beugung an Halbleiter-Hetero und Nanostrukturen mit Röntgenstrahlen
Oct 24, 2002

J. Heber - Bell Labs, Lucent Technologies, Murray Hill, USA
Vergleich ultraschneller Intersubband-Übergänge bei 1.55 µm Wellenlänge in GaN/AlGaN Heterostrukturen
April 4, 2002

V. Ignatova - University of Antwerp, Belgium
Possibilities and limitations of TOF-SIMS in microanalysis and ultra shallow depth profiling
Oct 15, 2002

G. Kroesen - Eindhoven University, Netherlands
Overview of the research activities within the group "Elementary Processes in Gas Discharges"
May 15, 2002

H. Krzyzanowska - University of Lublin, Poland
Ge and Si nanoclusters in SiO_2 studied by XPS and Brilloin scattering
Sept 19, 2002

A. Kuznetsov – University of Oslo, Norway and KTH Stockholm, Sweden
Interstitial and vacancy depth profile separation proven by DLTS filling pulse technique
Nov 29, 2002

J. Musil - West Bohemian University, Plzen, Czech Republic
Recent progress in sputtered nanostructured films
June 5, 2002

K. Nakamura - Chubu University, Aichi, Japan
In-situ secondary electron measurements and its application to process monitoring in plasma immersion ion implantation
July 23, 2002

W. Otano - University of Puerto Rico at Cayey
The role of aluminium contents in BN films
Sept 17, 2002

A. Pronin - Universität Augsburg
Coherent source spectroscopy in the terahertz region: principles and application to investigations in superconductivity
May 22, 2002

A. G. Revesz - Revesz Associates, Bethesda, USA
Concentration dependence of the dielectric constant in mixed oxides $M_xO_yM'_pO_q$
April 16, 2002

J. Stangl - Universität Linz, Institut für Halbleiter- und Festkörperphysik, Austria
Investigation of hetero- and nanostructures by X-ray diffraction and reflectivity
Oct 24, 2002

H. Sugai - Nagoya University, Japan
Application of surface waves to plasma production and diagnostics
July 19, 2002

I. Tsyganov - University of Lipetsk, Russia
Ion beam induced formation of blood compatible layers based on titanium oxide for medical implants
March 28, 2002

J. Zuk - University of Lublin, Poland
Ionoluminescence study of porous silicon
Sept 19, 2002

Projects

11/1997 - 10/2002 European Union, within TMR Network EU
"Synthesis, structure and properties of new carbon based hard materials"
Dr. A. Kolitsch Tel.: 0351 260-3348 a.kolitsch@fz-rossendorf.de

03/1998 - 02/2002 European Union, within TMR Network EU
"European Network on defect engineering of advanced semiconductor devices"
Dr. K.-H. Heinig Tel.: 0351 260-3288 k.h.heinig@fz-rossendorf.de

07/1999 - 06/2002 WTZ with Bulgaria WTZ
"Investigation of the cluster emission characteristics of liquid metal ion source with the aim to produce focused cluster beams"
Dr. L. Bischoff Tel.: 0351 260-2963 l.bischoff@fz-rossendorf.de

11/1998 -07/2002 Deutsche Forschungsgemeinschaft DFG
„Amorphe Kohlenstoffschichten"
Dr. H.-U. Jäger Tel.: 0351 260-3373 h.u.jaeger@fz-rossendorf.de

11/1999 -12/2002 Deutsche Forschungsgemeinschaft DFG
„Erzeugung von gestapelten Monolagen aus Halbleiter-Nanoclustern"
Dr. B. Schmidt Tel: 0351 260-2726 bernd.schmidt@fz-rossendorf.de

02/2000 - 01/2003 European Union, within EU
"Transnational Access to Major Research Infrastructures" as a Large-Scale Facility
"Center for Application of Ion Beams in Materials Research"
Dr. A. Kolitsch Tel. 0351 260-3348 a.kolitsch@fz-rossendorf.de

02/2000 - 01/2003 European Union, within EU
"Transnational Access to Major Research Infrastructures" as a Large-Scale Facility
"ROBL (Rossendorf synchrotron radiation beamline for radiochemistry and material research) at the ESRF"
Dr. N. Schell Tel.: 0033 476 88 2367 schell@esrf.fr

03/2000 – 03/2003 Bilateral agreement BAS – FZR SMWK
"Applications of focused ion beam systems for optical data storage and other uses in optoelectronics and photonics"
Dr. L. Bischoff Tel.: 0351 260-2963 l.bischoff@fz-rossendorf.de

04/2000 – 03/2002 Deutsche Forschungsgemeinschaft DFG
"Investigation of vacancy-type defects in ion beam treated silicon carbide by means of positron annihilation spectroscopy"
Dr. G. Brauer Tel.: 0351 260-2117 g.brauer@fz-rossendorf.de

04/2000-04/2003 Deutsche Forschungsgemeinschaft DFG
"Ion beam synthesis of doped diamond-SiC-heterostructures"
Dr. V. Heera Tel.: 0351 260-3343 v.heera@fz-rossendorf.de

06/2000-03/2002 Deutsche Forschungsgemeinschaft DFG
"Modification of SiC-layers by ion beam stimulated recrystallization and phase formation"
Dr. V. Heera Tel.: 0351 260-3343 v.heera@fz-rossendorf.de

06/2000 – 05/2002 WTZ with Czech Republic WTZ
"Positron annihilation spectroscopy of metals with a complex structure"
Dr. G. Brauer Tel.: 0351 260-2117 g.brauer@fz-rossendorf.de

09/2000 - 08/2003 Deutsche Forschungsgemeinschaft DFG
"Dynamische in situ Untersuchung der Entstehung von kompressiven Spannungen in Bornitrid-Schichten und des Einflusses von Verunreinigungen und Wachstumsparametern"
Prof. W. Möller Tel. 0351260-2245 w.moeller@fz-rossendorf.de

10/2000 - 11/2002 Bundesministerium für Wirtschaft BMWi
„Enhanced oxidation resistance of new light construction materials for high-temperature application by ion implantation"
Prof. E. Wieser Tel. 0351 260-3096 e.wieser@fz-rossendorf.de

10/2000 - 12/2003 Sächsisches Staatsministerium für Wirtschaft und Arbeit SMWA
„Aufsticken von Edelstahl, Teilthema Plasma-Immersions-Implantation"
Dr. E. Richter Tel.: 0351 260-3326 e.richter@fz-rossendorf.de

10/2000 - 09/2004 European Union within Marie-Curie Program, EU
"Stays at Marie-Curie Training Site"
Dr. A. Kolitsch Tel.: 0351 260-3348 a.kolitsch@fz-rossendorf.de

01/2001 - 12/2003 WTZ with Ukraine WTZ
"Luminescence and memory effects in SiO_2 layers ccontaining Si/Ge nanoclusters"
Dr. W. Skorupa Tel.: 0351 260-3612 w.skorupa@fz-rossendorf.de

01/2001- 01/2004 European Union, within Growth Project EU
"Nanoclusters for Electronics (NEON)"
Dr. K.-H. Heinig Tel.: 0351 260-3288 k.h.heinig@fz-rossendorf.de

03/2001 - 03/2003 Deutsche Forschungsgemeinschaft DFG
"Defektengineering in Silizium, Implantationsdefekte und ihr Getterverhalten"
Dr. R. Kögler Tel.: 0351 260-3613 r.koegler@fz-rossendorf.de

04/2001 - 03/2004 Bundesministerium für Bildung und Forschung BMBF
"Zusammenhang zwischen Plasmaparametern und Schichteigenschaften beim MF-Puls-Magnetronsputtern"
Dr. A. Kolitsch Tel. 0351 260-3348 a.kolitsch@fz-rossendorf.de

04/2001 - 03/2004 Sächsisches Staatsministerium für Wirtschaft und Arbeit SMWA
„Erhöhung der Funktionssicherheit dünner Barrieren auf Ta-Basis für Kupfer-Metallisierungssysteme, Teilthema: Plasma-Immersions-Ionenimplantation"
Dr. E. Richter Tel.: 0351 260-3326 e.richter@fz-rossendorf.de

04/2001 - 03/2004 Bundesministerium für Bildung und Forschung BMBF
"Charakterisierung von Struktur und Morphologie vergrabener Übergangsmetalloxide"
Dr. F. Prokert Tel.: 0351 260-3389 f.prokert@fz-rossendorf.de

04/2001 - 03/2004 Bundesministerium für Bildung und Forschung BMBF
„Nutzung der Rossendorfer Beschleuniger für ionenstrahlphysikalische Verbund-forschungsprojekte"
Prof. W. Möller Tel. 0351260-2245 w.moeller@fz-rossendorf.de

07/2001 - 06/2003 Bundesministerium für Bildung und Forschung BMBF
"Ionenstrahlmodifizierung und Synthese von Halbleiter-Nanoclustern in dünnen Gatedielektrika für Flash- und EEPROM- Anwendungen"
Dr. J. von Borany Tel.: 0351 260-3378 j.v.borany@fz-rossendorf.de

07/2001 - 12/2002 WTZ with Russia WTZ
"Entwicklung eines Polymers mit Drug Release Eigenschaften"

Dr. Manfred Maitz Tel.: 0351 260 2014 m.maitz@fz-rossendorf.de

10/2001 - 9/2003 Bundesministerium für Bildung und Forschung BMBF
"Hochenergie-Ionenimplantation in Si-Wafer für Bauelemente der Leistungselektronik"
Dr. J. von Borany Tel.: 0351 260-3378 j.v.borany@fz-rossendorf.de

11/2001 - 10/2002 Bundesministerium für Bildung und Forschung BMBF
"Ausgründung der nanoparc GmbH"
Dr. T. Gebel Tel: 0351 269 5350 gebel@nanoparc.de

04/2002 - 03/2005 European Union EU
"Flash lamp supported deposition of 3C-SiC films"
Dr. W. Skorupa Tel.: 0351 260-3612 w.skorupa@fz-rossendorf.de

07/2002 - 06/2004 North Atlantic Treaty Organization NATO
"Combined Time- and Frequency-domain Study of Superconductors and Manganites"
Dr. T. Dekorsy Tel.: 0351 260-2880 t.dekorsy@fz-rossendorf.de

07/2002 - 05/2004 Deutsche Forschungsgemeinschaft DFG
"Infrarotspektroskopie an Quantenkaskadenstrukturen"
Prof. M. Helm Tel.: 0351 260-2260 m.helm@fz-rossendorf.de

08/2002 - 09/2004 Deutsche Forschungsgemeinschaft DFG
"Phasen- und Strukturdesign von Ti-Al-N-Schichten durch Echtzeit-in-situ-Röntgendiffraktion“
Dr. N. Schell Tel.: 0033 476 88 2367 schell@esrf.fr

09/2002 - 08/2005 WTZ with Russia WTZ
"Dynamische Bestrahlungseffekte in metastabilen Legierungen unter Ionenbeschuss"
Prof. E. Wieser Tel.: 0351 260-3096 e.wieser@fz-rossendorf.de

10/2002 - 09/2005 Bundesministerium für Bildung und Forschung BMBF
"Strukturelle Charakterisierung von Heterostrukturen für die Opto- und Mikroelektronik"
Dr. F. Eichhorn Tel.: 0351 260-3534 f.eichhorn@fz-rossendorf.de

10/2002 - 09/2006 European Union EU
"Synthesis, structure and properties of new fullerene like materials"
Dr. A. Kolitsch Tel.: 0351 260-3348 a.kolitsch@fz-rossendorf.de